Microfluidic Devices for High-Resolution Whole Brain Imaging of *Drosophila* Larvae using Light-Sheet Fluorescence Microscopy (LSFM)

Microfluidic Devices for High-Resolution Whole Brain Imaging of *Drosophila* Larvae using Light-Sheet Fluorescence Microscopy (LSFM)

By

DEVON EMILY JONES

H.B.Sc. Biology (Physiology Specialization) (McMaster University, Ontario, Canada)

A Thesis

Submitted to the School of Graduate Studies

In Partial Fulfillment of the Requirements

For the Degree

Master of Applied Science

McMaster University

MASTER OF APPLIED SCIENCE (2019) McMaster University

(School of Biomedical Engineering) Hamilton, Ontario, Canada

TITLE MICROFLUIDIC DEVICES FOR HIGH-RESOLUTION WHOLE BRAIN IMAGING OF *DROSOPHILA* LARVAE USING LIGHT-SHEET FLUORESCENCE MICROSCOPY (LSFM)

AUTHOR DEVON EMILY JONES, H.B.Sc.

SUPERVISOR Professor P.R. Selvaganapathy

Department of Mechanical Engineering

NUMBER OF PAGES (xvii), (141)

Abstract

Improving the understanding of the way neurons interact at the whole-brain level is of great interest to neuroscientists. These “circuit diagrams” of the human brain could revolutionize the way neurological diseases are treated, but before this level of study can be conducted, neuroimaging technology must be improved. Using the model organism *Drosophila melanogaster*, improvements in spatiotemporal resolution of microscopy techniques are being made. Microfluidic devices have been created to improve the spatial resolution of live neuroimaging in *Drosophila* 3rd instar larva using confocal microscopy, but the desired high temporal resolution has not yet been demonstrated in a live organism. In this research, the high spatial resolution possible using an immobilization device for live larvae is combined with the high temporal resolution of the light-sheet microscope. A microfluidic device was designed to be compatible with the physical constraints of the light-sheet microscope while simultaneously incorporating a 3D-segmental pinning immobilization channel to ensure minimized motion of the CNS of the larvae. The device achieved single-cell resolution (< 5 μm) of the whole brain of a live, intact larva. Z-stack images and time-series captures demonstrated the capability of the microscope to record volumetric images and high image acquisition rates of the live, intact larval CNS respectively.

Acknowledgments

Many incredible individuals have assisted me in completing this project over the last two years.

First, my primary supervisor, Professor Ponnambalam Ravi Selvaganapathy, has been an amazing guide through this entire degree. Beyond helping my biology brain understand the engineering concepts to which I was introduced, he has a very special way of keeping me focused on moving forward. In countless meetings, I learned so much more about myself and my goals not just within this degree, but in my career and the rest of my future. He always knew the right way to push me to solve each and every obstacle I encountered, and I truly appreciate how his teaching style has helped me to grow so much.

Second, Louise Brown from the Lunefeld-Tanenbaum Institute has been an incredible mentor and friend. I began this project with minimal microscopy experience and suddenly found myself working with an extremely complicated machine. Louise taught me to speak the same language as the microscope, and in addition to helping with any technical issues encountered over these two years, she spent hours helping me brainstorm new directions for my fabrication process, found laboratories in the Institute where I could perform my dissections, and was a wonderful, bright light through all of my trials and errors. I could not have accomplished any of this without her support.

Dr. Roger Jacobs was my fly-guy throughout this project, and had the answer to every single one of my *Drosophila* questions. He provided any materials or tools I ever needed to maintain my fly stocks, and any time I needed help performing crosses or dissections, he or one of his students was available almost immediately. To Roger, Rachel, and Dugyu, thank you so much for helping this fish-and-mouse biologist-turned engineer to appreciate these invertebrates for the powerful tool that they are.

Thank you to my wonderful lab mates who welcomed me in and tolerated my funny noises and strange sentences while working. I am sure I was an unusual colleague to get used to, but you all accepted me quickly and helped make the lab a working environment I could feel totally comfortable in. I also truly appreciate all the brainstorming help, especially from Alireza Shahin-Shamsabadi, Sreekant Damodara and Mohammadhossein Dabaghi. You guys made me think like an engineer and your unending patience was appreciated. Vinay, Celine, Nidhi, Rong, Neda, Parker, Shadi and Fathalla, thanks for being such great people throughout this experience, and always supporting me no matter what.

Finally, to all the friends and family who stuck with me through this journey, both the new and old. Amanda and Colleen, for all the late-night chats about everything from lobsters to societal constructs. Julia, Sam, and my friends from the EGS for keeping me fun when I was stuck.

Marisa, for always being there for absolutely anything. And to all the friends who had no idea what I was saying when I started talking about this project but listened anyway: Shayen, Kirsti, Clare, Caitlin and Andrew. I know you've got my back whenever I need you. Most importantly, to my parents, Michael and Shauna, and to my amazing sister Rowan: you guys rode this emotional roller coaster the entire time with me, and I appreciate you putting up with me through all of it. I hope you're ready for whatever I put you through next!

Table of Contents

List of Figures

List of Tables

List of Acronyms

ATP – Adenosine triphosphate

BL's – Brain Lobes

Ca2+ - Calcium ion

CaM – Calmodulin

CCD – Charge coupled device

Cha – Choline acetyltransferase

CNS – Central Nervous System

CPS – Cephalopharyngeal Skeleton

DI – Distilled (water)

DRG – Dorsal Root Ganglion

dsRNA – double-stranded RNA

FFT – Fast Fourier Transform

FRET – Förster resonance energy transfer

GAL4 – protein used in the GAL4-UAS based gene expression system

GECI – Genetically Encoded Calcium Indicator

LITE – Lateral interference tilted excitation

LSFM – Light Sheet Fluorescence Microscopy

M13 – myosin light chain kinase component of the GCAMP5 molecule

PDMS – Polydimethylsiloxane

RNAi – RNA interference

ROI – Region of Interest

sCMOS – Scientific complementary metal-oxide-semiconductor

SLM – Spatial Light Modulator

SNR – Signal-to-noise Ratio

SPIM – Selective plane illumination microscopy

TOR – Target of Rapamycin

UAS – Upstream activating sequence

VNC – Ventral Nerve Cord

1 Introduction

1.1 Motivation

Through years of scientific discovery and research, the human brain has remained poorly understood by researchers. While molecular and cellular physiology within neurons has been elucidated, and a great deal of mapping of regions of activity through the use of fMRI has helped scientists to understand the role structures like the occipital lobe or hippocampus play in processing the world around an individual, there remains the question of how these areas interact together. Beyond the monitoring of global activity, there is interest in creating circuit diagrams representing the innervation of neurons throughout the brain, and interpreting how these areas interact in time and space. This technique is being sought after by the BRAIN (Brain Research through Advancing Innovative Neurotechnologies) Initiative in the United States. The current neurotechnology is not capable of answering these questions, however, and development of the neuroimaging field is a crucial next step to achieving these goals. For example, before being able to monitor signal transduction from a sensory organ like the eyes all the way to a motor response for that stimulus, the detection technology must be able to perform at the speed of thought while maintaining the spatial resolution required to view individual neurons. To develop these technologies, it is useful to begin with a smaller scale brain than the human brain, such as observing the nervous system of a model organism like *Drosophila melanogaster*.

The *Drosophila* is a model organism already used throughout human disease research and drug discovery testing [1]–[9]. The advantages to working with this organism include their smaller, simplified organ systems, genomic similarity to humans, and large population size. The shorter generational periods of these animals allow for a more rapid development of desired mutant strains that can be used to model a specific human disease condition, such as Alzheimer's or Huntington's Disease. The *Drosophila* is especially useful for neurological imaging due to the optical transparency of the larval life stages. Genetically encoded calcium indicators (GECIs) can be inserted transgenically and allow for visualization of certain groups of neurons based on the expression pattern of the inserted gene [1], [8], [10]. In order to obtain high spatial resolution in any live organism, it is important that the organism is not moving around. The *Drosophila* larva is extremely mobile, and muscle contractions result in movement of the internal organs within the body cavity, impeding imaging of the central nervous system. To solve this problem, scientists have used various methods, such as dissecting the brain away from the body, anaesthetizing live larva, or even gluing the larva to a substrate. However, it is desired to image a larva that is intact and shows true physiological responses to a stimulus, unaltered by drug influence on the central nervous system. Additionally, while this level of spatial resolution, obtained using a microfluidic device to immobilize the larva, has been performed using confocal microscopy, the temporal resolution desired is not yet achieved in this application. The primary goal of this project is to achieve single-neuron level resolution during whole-brain imaging of 3rd instar *Drosophila melanogaster* larvae with high temporal resolution, using a novel microfluidic device design. This tool will allow researchers to hold a model organism's nervous system extremely still for development of high temporal resolution imaging technologies in the future.

1.2 Organization

The organization of the chapters in this thesis is as follows:

Chapter 2 presents an introduction to the use of *Drosophila* as a model organism, genetic manipulation of this model, and their application for neuronal study in connection to human disease research. It also discusses existing work using microfluidic devices for *Drosophila* study and work to date using microfluidics to enhance neuronal imaging.

Chapter 3 establishes the conceptual design of the proposed device and the experimental setup involved in applying the use of this device to the field of neuronal imaging. It describes the functionality and operation of the successful, Iteration III device, and describes the operation protocols critical for proper use. It also highlights the required design criteria that must be met for successful operation.

Chapter 4 describes the fabrication techniques and materials used in the microfabrication and assembly of the three primary iterations of the immobilization device tested. It briefly outlines why some iterations did not meet the design criteria and thus justifies successive device iterations.

Chapter 5 outlines the results of the device characterization testing and the results of imaging using the device in a light-sheet fluorescent microscope. It presents evidence showing the immobilization device can meet the design criteria to allow high-resolution, whole-brain imaging

of *Drosophila* and presents both z-stack and time series images. It also demonstrates the ability to conduct stimulus-response assays using this microscope.

Chapter 6 concludes this thesis by highlighting the contributions of this research to the field of invertebrate neuronal imaging, including: the creation of a novel microfluidic device for use in a light-sheet fluorescent microscope, a new sacrificial-template based microfabrication technique, and the demonstration of the ability to capture high-resolution, whole-brain images of the *Drosophila* 3rd instar larva. The chapter then provides suggestions for future development of the device.

1.3 Contributions

The main contributions for this research are listed below:

- Recent microfluidic devices for immobilizing *Drosophila* larva have been effective, but are not compatible with imaging technologies with high temporal resolution, such as a light-sheet microscope. *Drosophila* research using light-sheet fluorescent microscopy has previously been conducted with dissected, fixed specimens only, not live, intact organisms. This device developed in this thesis represents the first microfluidic immobilization tool for live, intact *Drosophila* larvae imaging using light-sheet microscopy.
- A novel fabrication technique is introduced as the use of paraffin wax to create formed, solid channels to act as a sacrificial template for casting small PDMS devices. This

method allows for a channel to be created within a solid PDMS shape, eliminating the need for bonding two pieces of a device today. A novel application of another fabrication technique was demonstrated in this work as well. Partially-cured bonding of two pieces of PDMS was used to facilitate bonding of devices where the surface area of the two pieces being attached is too small to allow strong bonding using conventional plasma-bonding techniques.

- A preliminary experiment of altering the ambient temperature surrounding an organism expressing a GCaMP calcium indicator in the central nervous system was conducted. Previous research using GCaMP indicators has always been conducted in live organisms at normal body temperature for that organism, such as room temperature for invertebrates like *Drosophila*, or 37 °C for mammals. This study investigated the response of the fluorescent molecules in a chilled, 12 °C environment, demonstrating a decreased signal which may be as a result of denaturation of the GCaMP5 molecules in response to the temperature, something not shown before.

2 Literature Review

2.1 Introduction

The brain has always been of great interest to scientists. It has been vastly studied from the biochemical and cellular levels, building an understanding of the way individual molecules interact to send signals between cells, and at the whole-brain level through MRI or CT scanning to investigate the regions of the brain responsible for different actions. However, it is still unknown how exactly these two levels of physiology are related. The next step is to develop a method of examining the activation of all brain neurons and the time sequenced manner of response to external stimuli. This technique is being sought after by the BRAIN (Brain Research through Advancing Innovative Neurotechnologies) Initiative in the United States. This requires advances in the field of imaging technology and appropriate models to perform this research at a smaller scale before human brain research can be conducted. Model organisms like the *Drosophila* becomes essential to not just this example, but to nearly every area of biomedical research, due to their smaller size, shorter generational periods, ability to be readily observed and genetically modified, genomic similarity to humans, and large population size. These organisms are an ideal model in developing technology for neurological imaging specifically due to the optical transparency of the larval life stages and the readily manipulated genome. Genetically encoded calcium indicators (GECIs) can be inserted transgenically, and as a result, fluorescent imaging of the activity in the *Drosophila* central nervous system (CNS) has become common using genes like GCaMP5. However, the larvae exhibit robust digging and burrowing behaviour,

which in turn generates motion of the internal organs within the hemolymph-filled body cavity and impedes image clarity. While anaesthesia, glue, and dissection have been used in the past, more recent immobilization methods have been developed that allow for live, unaltered neurological imaging of responses to sensory stimuli. This is performed primarily through the development and use of microfluidic devices, which can minimize motion artifacts. The primary goal of this project is to achieve single-neuron level resolution during whole-brain imaging of 3rd instar *Drosophila melanogaster* larvae with high temporal resolution, something not yet possible in this organism.

2.2 Model Organisms

Biological and medical research has long been linked to the use of model organisms. Whether a novel method for drug delivery, a biocompatible surface treatment, or a new imaging technique, the use of an animal model allows scientists and engineers to develop the most safe and appropriate versions of a design before moving to a study involving human patients. Many organisms are useful for studying human biology and diseases at the molecular and genetic level due to shared genetic profiles. These similarities, combined with other factors such as simpler cellular/tissue organization, advances in optical imaging, and genetic engineering allow for observation of relevant biological processes.

2.2.1 *Introduction to model organisms*

While the first animals that are often thought of as model organisms are the traditional "lab rats," there is a much broader spectrum of much smaller organisms available for use in study of biological studies, including insects, yeast, and fish. These organisms still possess remarkable similarity to humans at the genetic and molecular level but provide the ability to analyze physiological processes using systems biology [11], something more difficult in a larger model. For example, the *C. elegans* is a widely used model because their entire body consists of just 302 neurons and about 1000 cells [12], a much more manageable number of cells, connections and functions for global study in comparison to the human body. Every cell in a *C. elegans* can be accounted for, labelled, imaged at a high resolution and in its entirety, and there is still tremendous overlap genetically and molecularly, making the model useful for studying various human diseases with similar mechanisms, such as aging [12]. The *Drosophila melanogaster*, or the fruit fly, is another model organism widely used in biological research [1], [2].

2.2.2 *Drosophila as a human disease model*

Drosophila are an elegant tool for scientists for a number of reasons. The fully mapped 180 Mb genome [13] has provided insight into the similarity of proteins for metabolism and gene expression between the fly and the human genomes, indicating that the fly is an appropriate platform to examine human disease at the cellular level, as many fundamental pathways are conserved [3], [5], [14], [15]. In fact, Reiter et al. showed that 77 % of human genes that were compared to the *Drosophila* genome could be matched to unique *Drosophila* genes for study [5].

It has been demonstrated that 75% of disease genes have a related sequence between Drosophila and humans [2], [4]. The expression of these genes can be manipulated to induce a wide variety of disease-resembling models, including gastrointestinal (13 genes), skeletal development (26 genes), cardiovascular (26 genes) and neurological (74 genes) to name a few categories [5]. *Drosophila* have been used as a model to test novel drugs and investigate the pathways for disorders like cancer, Alzheimer's, diabetes mellitus, Parkinson's, and Huntington's disease [1], [2], [4]. *Drosophila* are attractive compared with the traditional mammalian model organisms for molecular and cellular assays because of the rapid life cycle, ease of population generation, and the transparency of the embryo and larval organism stages [4]. Each developmental stage of the *Drosophila* is ideal for a different form of biological investigation. The embryo is often used for developmental study, examining the processes of cell differentiation or organ formation, often in different disease models. The larval *Drosophila* is often used to examine physiological processes and some behavioral responses such as changes in foraging behavior. The pupa can be used to model development, and the adult fly is useful for modelling more complex organ physiology and complex behavior patterns such as sleep, courtship, memory, aggression, and navigation [2]. Drug response can also be examined in the adult fly [6], [7].

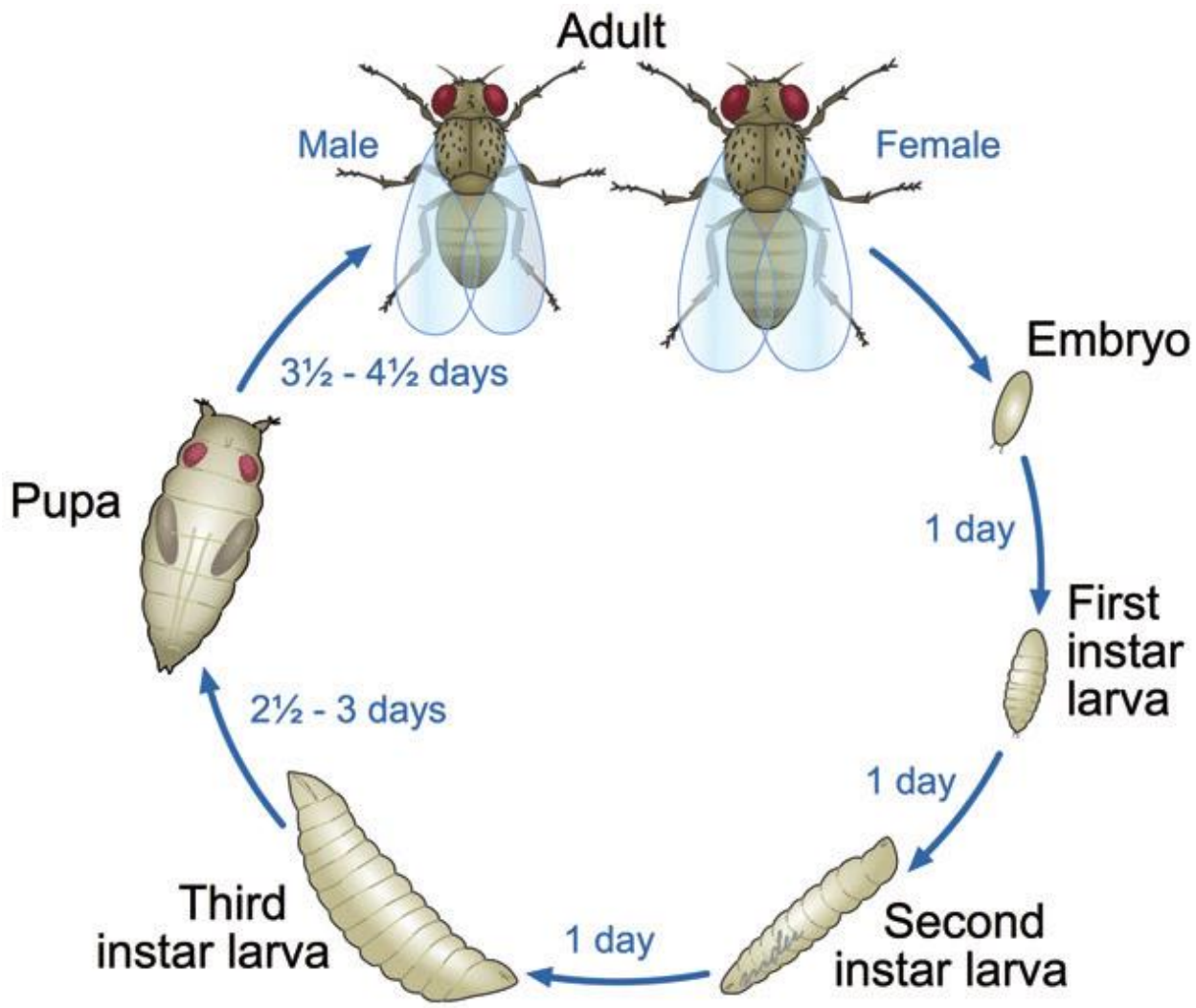

Figure 2.1 Diagram of the Drosophila melanogaster lifecycle [16].

2.2.2.1 Genetic engineering of Drosophila

Researchers can generate mutant strains and design genetic models for their disease of interest through the extremely efficient homologous recombination GAL4-UAS system [1], [8], [10]. This system allows for protein expression in a time- or tissue-dependent manner and was first developed to overcome the limitations of using heat-shock proteins as gene activation tools or

tissue-specific promoters with specific transcriptional regulatory sequences that match the gene of interest [3], [10], [17]. In this method, a gene encoding the GAL4 transcriptional activator from yeast is introduced into the *Drosophila* genome such that it is expressed only in cells or tissues of a certain type, such as neuronal, cardiac, or muscular tissues. A second gene is then introduced that contains a region where GAL4 can bind and induce transcription. This second gene is the desired molecule to be upregulated. This gene will only be induced in the cell type of interest, due to the tissue-specific GAL4 genetic expression [10]. In this fashion, it is possible to upregulate a molecule of interest for modeling disease in a very specific tissue in the *Drosophila*. This expression system is bipartite, in that the GAL4 and the inducible molecule, tagged with an upstream activating sequence (UAS) are located within different flies. This means the molecule of interest is silent until the flies are bred together, creating progeny with the desired traits [8], [10]. Stable stocks of specific *Drosophila* strains can then be genetically engineered and maintained for laboratory research, specific to an exact mechanism or tissue those researchers are interested in examining.

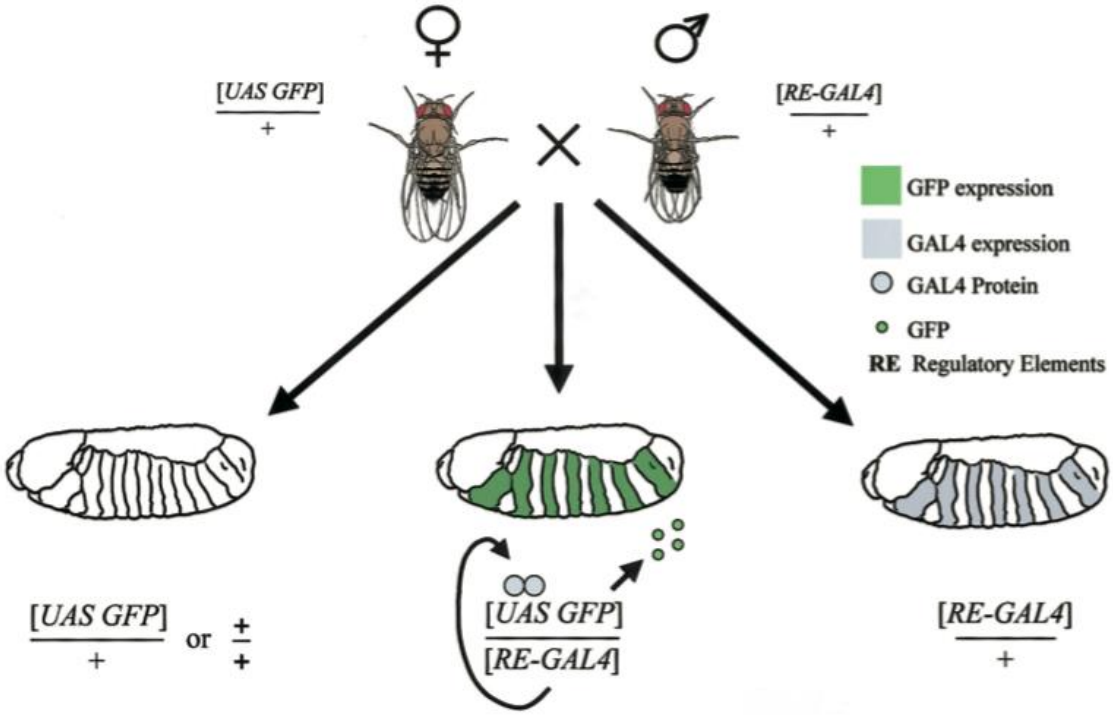

Figure 2.2 The bipartite UAS/GAL4 system in *Drosophila*. When females carrying a UAS responder (UAS-GFP) are mated to males carrying a GAL4 driver progeny containing both elements of the system are produced. The presence of GAL4 in an alternating segmental pattern in the depicted embryos then drives expression of the UAS responder gene in a corresponding pattern [8].

2.2.2.2 Disease models using Drosophila

Given the genetic overlap, and the ability to induce genes of interest in specific parts of the fly model, it is no surprise that they have provided a great deal of insight into disease physiology in humans, for a wide variety of diseases. For example, the molecular physiology of Alzheimer's disease has been thoroughly investigated in the fly. Orthologous proteins exist in the fly for several proteins of interest in the progression of this disease state, such as *B amyloid protein precursor*, or *Presenilin*. The *Appl* gene (amyloid protein precursor orthologue in the fly) mutant

shows a behavioural deficit. Researchers found that when introducing the human gene to the mutant fly, the behaviour was rescued, showing that not only do the genes serve a very similar function, but that they can do so in both a vertebrate or invertebrate [9], [18].

Parkinson's Disease has been modelled in *Drosophila* as well. Flies do not have an identical analogue of the gene responsible for this disease in humans, *SNCA*, which encodes the neuronal protein alpha-synuclein in the presynaptic terminals [19]. Instead, the human gene is inserted to the fly genome, and misexpression of the mutant is able to cause neurodegeneration in the fly eye [20]. Additionally, the ubiquitin pathway can be disrupted by mutating the fly homologue of human *PARK2* (called *park* in the fly), which causes degeneration of muscles and models the Parkinson's phenotype. The cells in the fly also become hypersensitive to free radicals, making the neurons more sensitive to toxins and causing degeneration prematurely [21]. Using the fly for a model in this case makes it faster to discover molecules that can rescue these phenotypes, allowing for a better understanding of these molecular relationships and potentially drug solutions to some of the phenotypes expressed in this disease state [4].

Aging is another human condition that has been investigated in the fly as a model. Here, flies are advantageous not just for their genetic malleability, but also because their short lifespan allows an accelerated timeline for the study of this process. While mice and nematodes are also used to study the molecular physiology of aging, the fly demonstrates many age-related declines in function quite quickly, with mammalian homologues to the genes being tested [13]. The average fly lifespan is 50-80 days, and the senescence phenotypes manifest within 2-8 weeks depending on the phenotypes being examined [22]. Additionally, it can be assumed that the adult flies are

post mitotic based on this short lifespan, and any senescence observed should be attributed to homeostatic decreases, not cellular replication issues [23]. A number of genes have been identified that can increase the lifespan in the *Drosophila* when expression is changed, including *superoxide dismutase*, and *methuselah*, which are code for a free-radical scavenger and a G-protein-coupled receptor respectfully [24], [25]. It has also been shown that aging involves a decrease in resistance to heat shock and oxidative stress, related to a down-regulation of genes involved in chaperone activities at the molecular level or genes that act as detoxification agents or act to repair damage from free radicals [26]. Similarly, the *Drosophila* responds to aging and oxidative stress by upregulating the same heat-shock and antioxidant proteins and innate immune response genes as well as increasing purine biosynthesis, further linking these two physiological processes and suggesting a relationship [27]. Senescence related to aging has been widely examined, including decline in exploratory activity [28], [29], impaired olfactory learning and memory [30], decreased reproduction [31]–[33], and decreases in cardiac function [22], [34], [35]. Functional senescence is less examined than survival as an endpoint in model organism study, but can be more useful to researchers when trying to identify decline in specific organ systems or processes that will fail with age, and represent changes to quality of life as opposed to length of life in certain disease states [22]. The TOR (Target of Rapamycin) signalling pathway, a regulator of lifespan and health in nearly all eukaryotic species, was first identified in yeast [36] but the relationship between this pathway and growth and aging in organisms was first shown in the *Drosophila* [37]–[39]. This pathway responds to growth factors, nutrients, and physiological stress, and in response regulates mRNA translation, transcription, metabolism, and many cell activities, effecting the long-term organism health and lifespan. The fly model has

made discovery and further understanding of this critical signalling pathway in mammals like humans possible.

2.2.3 *Drosophila anatomy relevant to neurological study*

When conducting neurological study of the *Drosophila* 3rd instar larva, it is important to understand the basic larval central nervous system anatomy. Virtualflybrain.org provides open access reconstruction software to facilitate location of specific structures throughout the adult and larval brains, with over 20,000 images made available from researchers [40]. The two primary structures are the bilateral brain lobes and the ventral nerve cord, both of which are shown in **Figure 2.3**. Each of these structures can be further subdivided into nerve tracts or lobes based on the position. Some lobes to note are labelled below. Not pictured are the imaginal discs, epithelial sacs of tissue located just above the brain lobes. These discs are very evident during dissection of the *Drosophila* brain.

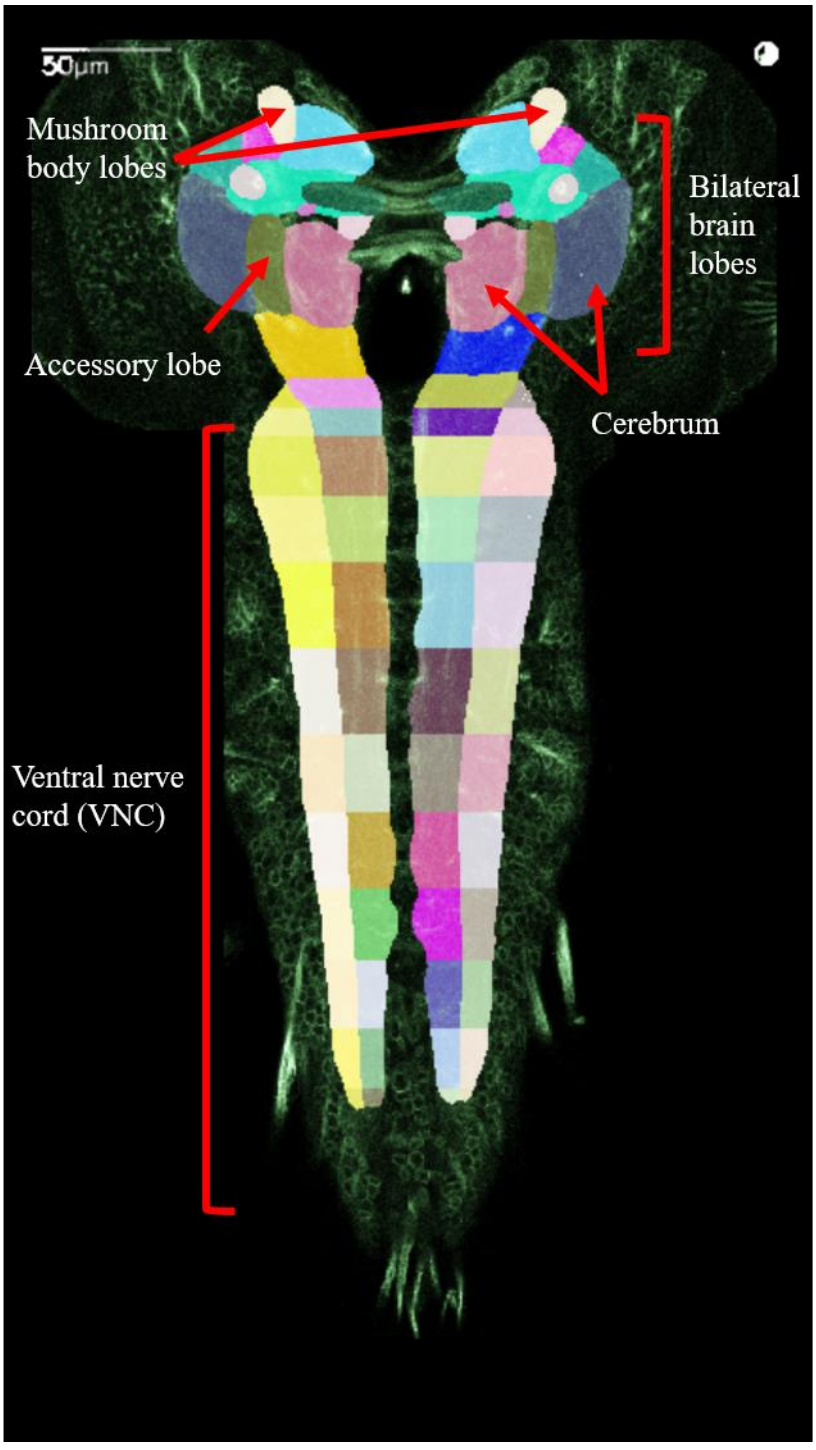

Figure 2.3 Anatomy of the *Drosophila* 3rd instar larva central nervous system. Image adapted from virtualflybrain.org [40].

The CNS is positioned in the anterior 1/3 of the larval body, towards the mouth region. The entire CNS is loosely attached to the *Drosophila* body wall and is suspended in the hemolymph filled body cavity of the animal with the other organs. This means the CNS moves longitudinally when the hemolymph moves, which creates a need for proper immobilization of the organism in order to conduct any neurological imaging. This is elaborated upon in later sections of this chapter.

2.3 Microfabricated devices for optimizing *Drosophila* study

While *Drosophila* are clearly a strong model organism for many human disease states at the molecular and genetic level, their small size also impedes the ease of manipulation and management of experimental cohorts. Embryos can be difficult to manage because they are approximately 1 mm, with thousands of 5 μm diameter cells [41], [42]. Larvae, while larger and easier to manipulate, are extremely motile, and their motion introduces complications during imaging. Adult flies must remain confined within isolated chambers during experiments or can escape during studies, and as a result, are used primarily for behavioural study and less for examining molecular physiology within cells. Over time, biological scientists have partnered with engineers to develop a solution to working with large sample sizes of these organisms and optimizing data collection. This solution is the introduction of microfluidic devices to small organism research.

Microfluidic devices are tools created with the goal of optimizing a scientific procedure through automation and parallelization. Automating a procedure can lead to highly repeatable

experimental conditions, which can facilitate reproducibility. Scaling and parallelizing will allow for experiments to be performed on hundreds of organisms simultaneously, therefore providing high throughput. Microfluidic devices can also reduce reagent volumes, simplifying user operation, reduce fabrication costs, or speed up reaction time. Each microfluidic device is designed to target a specific procedure, and a common fabrication technique is the use of soft lithography to create a mold of microfluidic channels that can be used to cast polydimethylsiloxane (PDMS) in the form of these channels. Inlet and outlet ports can be integrated and the cast PDMS is removed and bonded to a flat surface, sealing the hollow channels from the environment. Devices like this allow greater control over experiments and can be used in a wide variety of research fields. In small organism research, microfluidic devices have been created to improve storage and observation of growing populations, transfection and injection of individual organisms, and even to perform developmental assays [40-53]. Most microfluidic devices have been designed for use with the *Drosophila* embryo, some for use with the larvae, and only a few for use with the adult fly. This is because as a genetic or molecular model, the transparent and unmoving embryo is easily manipulated and observed during development. Similarly, the larva is transparent and can be used for study of organ function in certain disease models. The adult fly is not transparent and is often used as a behavioural phenotype model instead of a molecular physiology model.

2.3.1 *Embryos*

Two of the most common types of microfluidic devices for use with *Drosophila* embryos facilitate injection or orientation, and in some cases, a combination of both. Orientation devices

are useful for enhancing the automation, throughput and repeatability of an assay, as manual orientation of each embryo can be time consuming. Injection devices are similarly advantageous, especially because manual injection of these small organisms takes highly trained operators and the site of injection can vary between individual specimens. Combining both orientation and injection into a single microfluidic device design can vastly increase the number or organisms to be tested and can simplify the process of testing, while minimizing procedural variability caused by manual human manipulation of the embryos.

One application of microfluidic devices for injection of *Drosophila* embryos is investigating the function of genes through RNA interference (RNAi). This process requires the injection of small pieces of double-stranded RNA to the embryo within the first hour of development, and then observing the continued development of the embryo for phenotypic changes [43]–[45]. These changes to the organism represent changes in expression of the gene that was silenced by the dsRNA injected. However, with sample sizes of 100-200 embryos per gene screen, manual injection of each embryo with a micropipette is not efficient. Instead, several groups have developed piezoelectric microinjectors for this application [44]–[47]. Delubac et al. designed a device that specifically combines an integrated microinjector with a microfluidic system for positioning and alignment of embryos [46]. The principle behind this device is that the microinjector will precisely come into contact with the embryo at the exact same place with each injection when properly aligned, and that the force and pressure applied to the embryo by the microinjector tip can be finely controlled. The microfluidic device is fully automated and can retrieve, align and orient many embryos simultaneously. This allows for high-throughput injection of the embryos before subsequent ejection. Proper alignment and orientation of the

embryo is important, as many developing organs like the heart, GI tract or brain will be away from the central axes, and assays could have different results based on the position of these organs during manipulation of the embryo (i.e. microinjection to the dorsal vs. ventral side of the embryo may result in injection of the RNAi into the wrong organ). The microfluidic device uses sheath flow to ensure that successive embryos enter the chamber one at a time, and a top flow that causes the embryo to be aligned with the microinjector horizontally, with a 95 % efficacy [46]. Injection occurs following detection of the embryo in the microinjector channel. A diagram of the sheath flow mechanism for separating consecutive embryos is shown in **Figure 2.4** [46]. A top flow is applied to the embryo during immobilization in this microinjector region of the device, as without top flow the embryo will tilt 50 % of the time during injection; the top flow prevents tilting for 95 % of the embryos. This is described further in **Figure 2.5**. Using this device, only 52 % of injected embryos progressed to the larval stage, but this was comparable to the results seen using manual injection methods [48]. The system operates at a rate of 3-4 s per injection. The group demonstrated a high throughput of 231 embryos injected in 14 minutes [46]. Some limitations of this system include ensuring appropriate age of the embryo, as older embryos may have already formed the cellular blastoderm and this can interfere with the injection [46]. Additionally, using a CCD camera to automate the injection process will require technical maintenance and repair and must still be monitored during the conduction of injections.

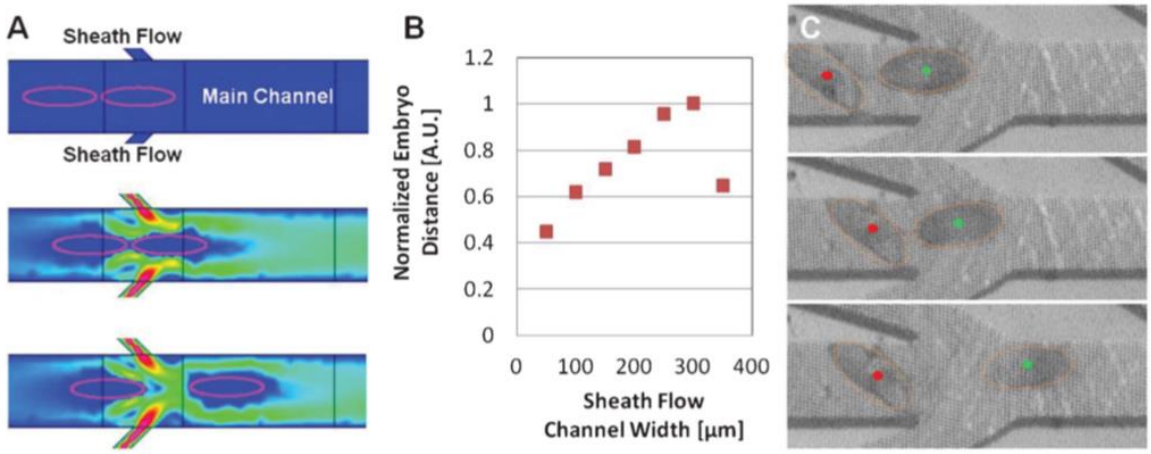

Figure 2.4 Simulation and experimental verification of separation of embryos in close proximity to each other by sheath flows. (a) CFD simulation of injection of sheath flows into the main channel and resulting embryo separation (time steps between images: 70 ms). (b) Simulation results demonstrating the effect of channel width on normalized separation distance between embryos. (c) Experimental verification of the separation effect. Sheath flows rapidly accelerate the leading embryo away from the following embryo (time steps between images: 300 ms) [46].

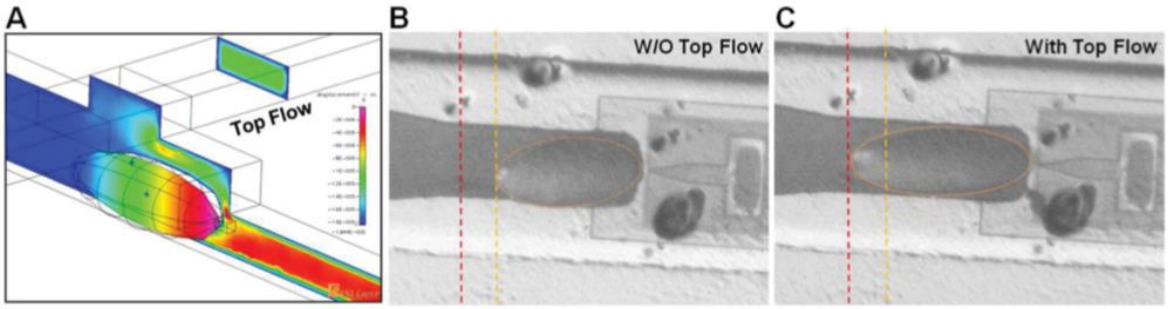

Figure 2.5 Simulation and experimental verification of embryo position stabilization through applied top flow. (a) CFD simulation indicates that when the embryo is in contact with the injector, a vertical flow component, introduced through top flow channels, ensures that the embryo remains gently pressed flat against the floor of the channels instead of making an abrupt tilting motion which might cause extended damage to the embryo membrane through the injector. (b) Without top flow more than 50 % of the embryos undergo some tilting motion. (c) With applied top flow, more than 95 % of the embryos remain in a stable, horizontal position [46].

Other high-throughput microfluidic devices have been designed for assays with *Drosophila* embryos, specifically ways of appropriately orienting embryos with minimal manual manipulation. The effect of changing temperature via laminar flow on biochemical processes in the embryo has been previously investigated and characterized by another group [49], [50], using a microfluidic two-inlet "Y" junction channel, that assessed the effects in a single embryo at a time. Increasing throughput of an assay like this improves the rate at which experiments can be conducted by researchers. Dagani et al. created a device for examining thermal perturbation of embryo development by passing microfluidic currents of different temperatures past embryos fixed within the microchannel by oil-adhesion pads [51]. The embryos were fixed and immobilized on the oil pads when an alcohol surfactant is removed, allowing an increase in adhesion forces. When the assay was complete, the alcohol surfactant was reintroduced, which decreased the adhesive force and allowed the flow through the channel to push the embryos out of the device [51]. A diagram of the self-assembly immobilizing mechanism is depicted in **Figure 2.6**. This device ensured the embryos were deposited in the same place with each use, that the adhesion of the embryo to the surface was strong, and that the orientation was consistent, and allowed for researchers to examine hundreds of embryos in a much shorter time than would be possible manually. The researchers were able to show that thermal perturbation of the embryo can disrupt the formation of primary epithelial cells, and is a promising tool for further investigations of environmental disruption [51]. A strength of this device is the reversibility of the immobilization mechanism, but appropriate changing of alcohol surfactant composition of the fluid in the microchannels is essential for maintaining adhesion of the embryos to the oil pads.

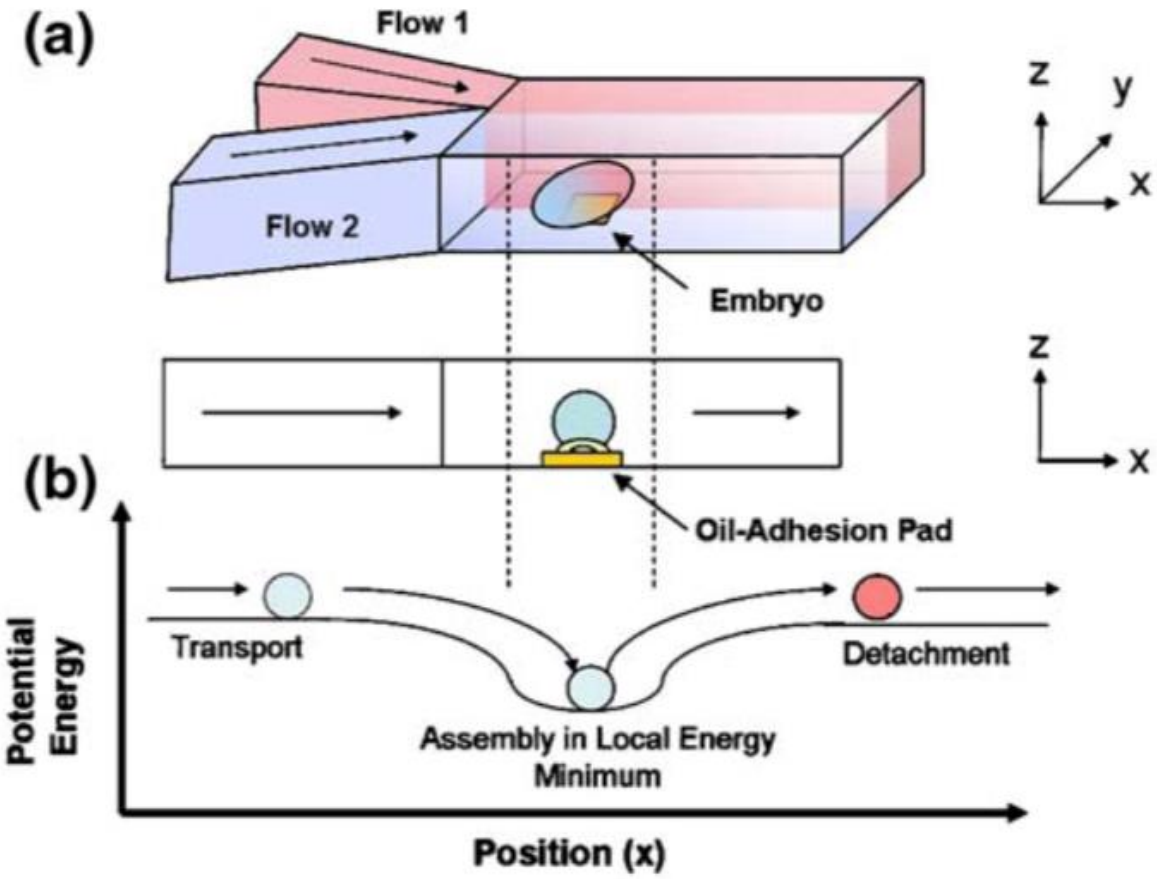

Figure 2.6 Self assembly of embryos on "energy wells" within the microchannel. (a) Embryo assembled to pad with binary (for example, hot and cold) flows surrounding it. (b) Principle of self assembly of embryo in "energy well." Oil-adhesion pads are modeled as energy wells for immobilizing an embryo in the microchannel. Embryo is pulled into pad via capillary force from the oil adhesive. Embryo is immobilized until sufficient force overcomes the adhesion and detachment occurs [51].

While alignment and orientation are important for automated biological assays, there is also a requirement for imaging of the embryos at a rate that matches the rest of the automation. If the imaging throughput is too slow, no amount of improvement in rate of positioning, injecting, or exposing embryos to stimuli will increase the throughput of the entire procedure. Advances have

been made to increase imaging throughput of *Drosophila* embryos. A microfluidic device has been designed that allows for automated parallel imaging of embryos [52]. Loading is accomplished by first suspending the embryos in a liquid buffer, PBS, and then the suspension is pumped through the microfluidic device. Several hundred small traps (500 μm x 150 μm) are positioned vertically across a long, serpentine channel, and as embryos move past the traps, a cross-flow array creates a driving force that orients and immobilizes the embryos within the traps, seen in **Figure 2.7**. More than 700 prepared embryos are then uniformly positioned for high-throughput imaging, using any number of embryo imaging preparations, including immunostaining [52]. The device is versatile because embryos are prepared external to the trap, allowing for multiple biological assays to be conducted. It is also an improved design because the chip can be placed in a traditional microscope and does not require any special fixtures. One limitation to be considered is that the loading buffer must be replaced with a more transparent medium before imaging. The imaging medium should also contain glycerol for fixed embryos, as this device is not compatible with living specimens. Additionally, this device is not reusable.

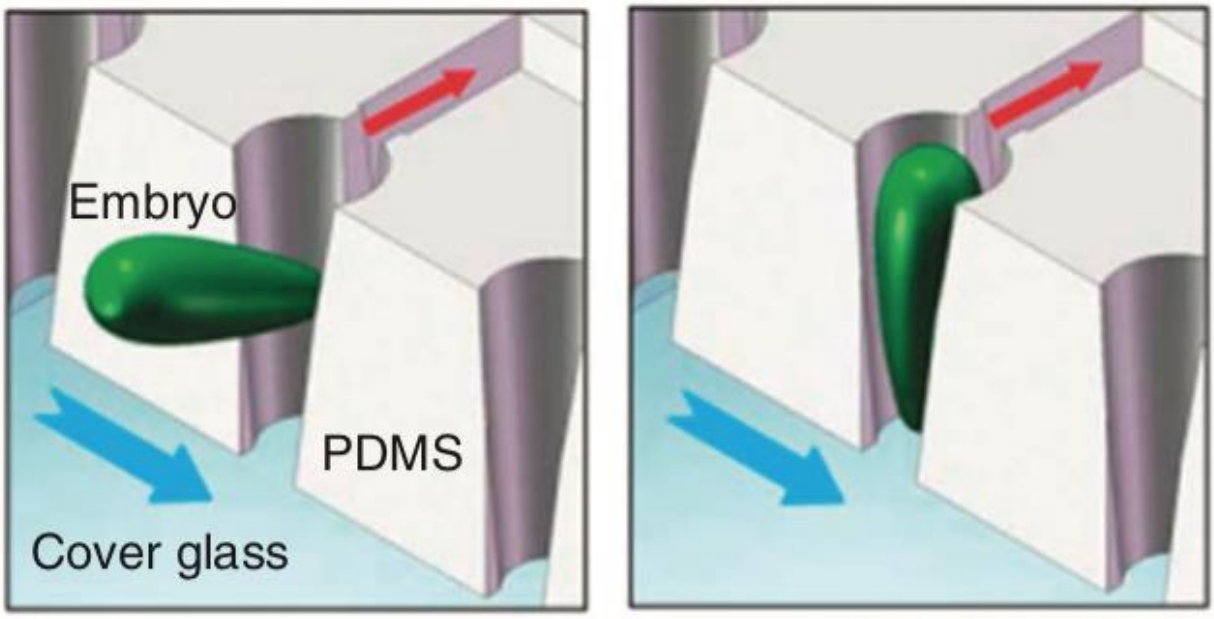

Figure 2.7 Schematic of the end-on orienting principle for imaging oblong fruit fly embryos along the dorsal-ventral axis. As the embryo travels along the serpentine channel (blue vector arrow) the cross-flow (red vector arrow) from the trap catches the embryo and orients it along with the narrow portion of the central axis towards the cover glass [52].

2.3.2 *Larvae*

A variety of devices have been fabricated for the purposes of larval assays. There are two main types of larval assay, behavioural assays where researchers investigate movement, and imaging assays, where organs are identified and visualized within an organism. This could mean investigating the heart or the central nervous system in response to some external stimuli. The larva is a very mobile organism, however, and it must be immobilized. Contraction of segmentally connected skeletal muscles causes motion of the hemolymph filled body cavity of the larva, and even if the outer body is immobilized, the organs inside can move longitudinally in response to these contractions [53]. Conventionally, larvae are anaesthetized, or glued to a

substrate, as this allows for live imaging, but anaesthesia alters the physiological responses and gluing only immobilizes the outer body, still allowing for inner organ motion. Mondal et al. created a microfluidic device that can immobilize early developmental stages of *C. elegans* or *Drosophila* 1st instar larvae using only mechanical pressure [54]. The microfluidic chip consists of two spaces separated by a deformable membrane. When an animal is in the lower channel, as seen in **Figure 2.8**, the membrane can be deflected down towards the animal, pinning it in place between the glass cover slip and the first PDMS layer. The substrate for deflection is a column of water that fills the upper space as well as the majority of the column, which can be compressed using 14 psi of nitrogen gas [54]. This device held organisms still enough that anterograde and retrograde movement of molecules such as pre-synaptic vesicles within the cells could be imaged over periods of time ranging from milliseconds to hours. Additionally, the complicated fabrication and operation processes have been simplified by manually feeding organisms into the device and by preparing the devices outside of clean room facilities. In fact, spatiotemporal resolution was markedly improved with this immobilization technique. Similar experiments conducted using anaesthesia showed cessation of molecular trafficking, preventing study of these physiological processes. However, while the new device solves the anaesthesia issue, it is limited to 60 min of imaging of a live larva before suffocation occurs.

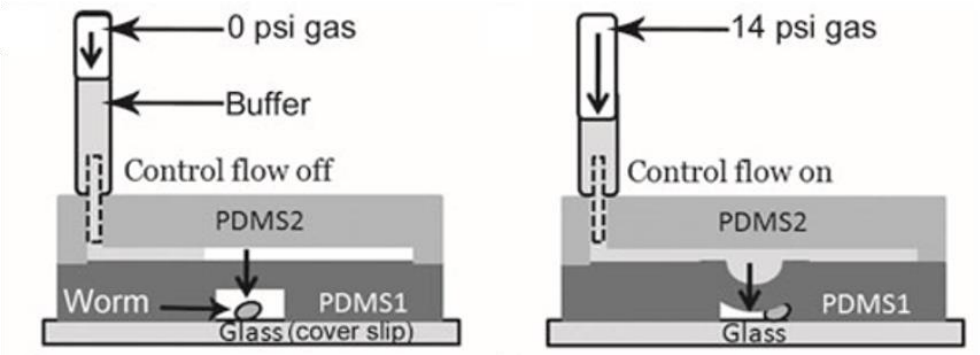

Figure 2.8 Schematic of PDMS membrane device used for *C. elegans* and *Drosophila melanogaster* 1st instar larva immobilization. A deflected PDMS membrane using 14 psi nitrogen gas in the control channel in the PDMS2 layer was used for immobilizing animals present in the flow channel in the PDMS1 layer [54].

Another group demonstrated the ability to image neuronal cell biology in a mechanical immobilization device for the purpose of investigated the sub-cellular responses to axotomy over periods of seconds to upwards of 10 hours [55]. The 3rd instar *Drosophila* larva was immobilized using a combination of mechanical deformation of a PDMS membrane for short term immobilization, or when a longer immobilization period was desired, mechanical deformation and CO_2 diffusion through the PDMS membrane to anesthetize the larva. The microfluidic chamber was imaged from below the cover glass using a fluorescent microscope, which allowed for examination of GFP-tagged molecules in the ventral nerve cord. Researchers found that axotomy causes a fast response of calcium flux in the first seconds after severance, as well as changes in axonal transport of vesicles in the first three hours. Finally, it was possible to observe regeneration of the proximal stump and degeneration of the distal stump after 7 hours [55]. This device overcame the spatiotemporal imaging limitations due to organism motion and allowed for sustained imaging for many hours because of the nutrient and gas exchange components of the

chip. The device does rely on CO2 as anaesthesia however, which can affect the natural physiological response of the larval body. A diagram of the chip can be seen in **Figure 2.9** [55].

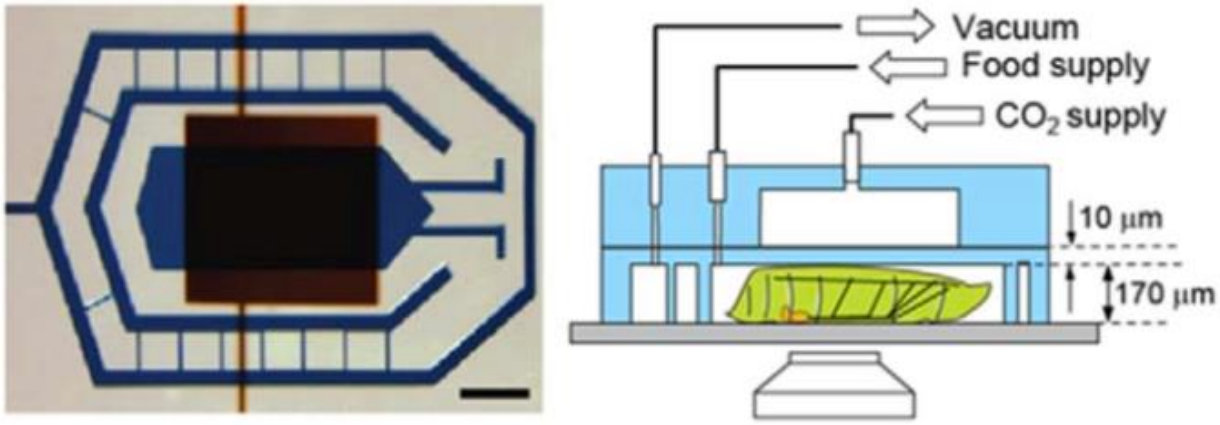

Figure 2.9 The two-layer LI-chip (Long-term Immobilization). The first PDMS layer (labeled with blue colour) has the larva immobilization microchamber and is connected to two microfluidic channels to supply food to the larva head (typically delivered every 30 min). A second PDMS layer (labeled with red colour) is vertically integrated into the first PDMS layer to deliver CO2 through a 10 μm thick PDMS membrane. A microfluidic network surrounding the immobilization chamber is used to create a tight seal between the PDMS and the glass coverslip. Scale bar, 1 mm [55].

Ardeshiri et al. demonstrated a device that immobilized a 3rd instar *Drosophila* larva using suction for the purpose of studying cardiac responses to toxins [56]. The PDMS device consisted of a loading channel, a trapping region equipped with suction channels and chemical infusion channels, and an orientation channel. The larva was inserted via the loading channel and upon reaching the animal trap region, was captured pneumatically by the orientation glass capillary. The orientation capillary was rotated to orient dorsally, and then negative pressure applied via the side suction channels to immobilize the larva in the desired position. The larva was then exposed to different chemical stimuli through the chemical infusion channels, allowing for

changes to the heartbeat of the larva to be observed by a microscope objective above the region of interest, shown in **Figure 2.10**. These cardiac screens in responses to chemicals showed that cardiac activity increases with excess oxygen and arrests with sodium azide, carbon dioxide, or a lack of oxygen, and allowed for examination of recovery after these chemical stimuli were removed, which was independent regardless of concentration of each stimulus [56]. This device can continue to be used for other drug screening assays due to the versatile orienting procedure for imaging. The device did not fully immobilize the internal organs within the hemolymph, however, and while in this assay the researchers were monitoring the heart rate in beats per minute, the device may not be appropriate for higher resolution imaging of organ tissue.

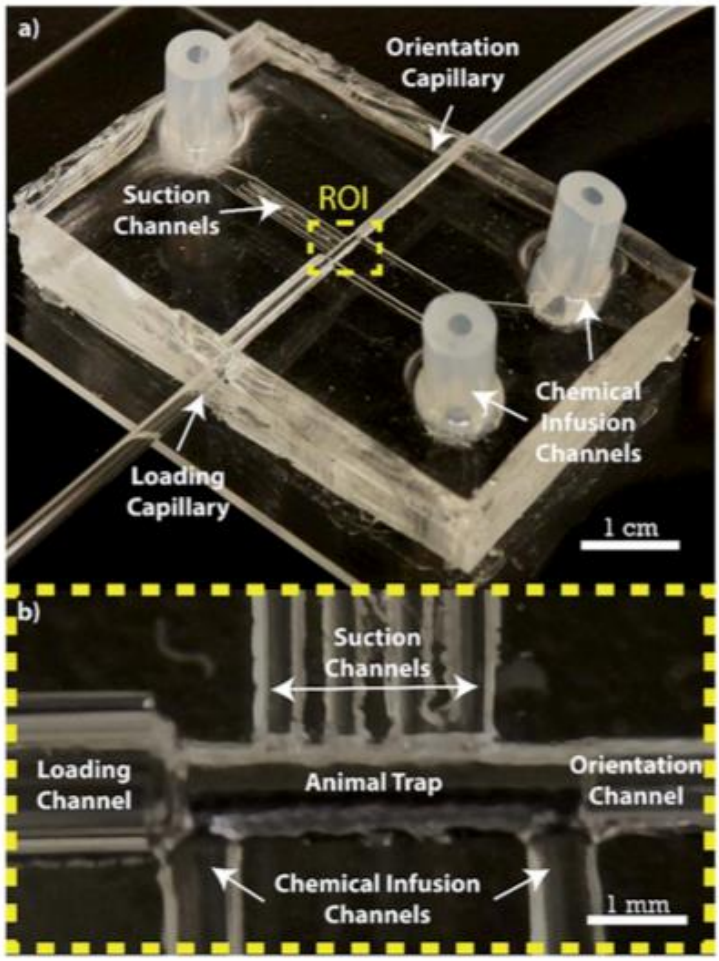

Figure 2.10 (a) Hybrid microfluidic chip used for 3rd instar *Drosophila* larva orientation, immobilization, chemical exposure, and monitoring of cardiac activities. Region of interest (ROI) in (a) is magnified in (b). Loading and orientation glass capillaries were installed in the corresponding guide channels shown in (b) and rotated manually for larva orientation [56].

2.3.2.1 3D Segmental Pinning of Drosophila Larvae

For a neural imaging application, the burrowing motion larvae exhibit even when the outer body surface is immobilized in a microfluidic device still poses a problem [53]. The *Drosophila* cephalopharyngeal skeleton (CPS) located in the anterior body region is responsible for this

burrowing motion, and contractions of the associated segmental muscles along the body wall allow for motion of the internal body organs during complete outer body immobilization, preventing high resolution of the central nervous system to be obtained when imaging due to a spatiotemporal resolution limitation of any high resolution imaging technique [53], [57], [58]. Ghaemi et al. attempted to overcome this obstacle by introducing a 3D segmental pinning design to the immobilization region of a microfluidic device [58]. The working principle was that two 3D gates will compress the larval body at two regions, the primary gate around the thoracic segments and the secondary gate just beyond the mouth and nose region (**Figure 2.11**, (a)-(b)). The central nervous system is then localized between the two gates, and the burrowing motion was minimized, allowing visualization with much less deviation of the region of interest from the field of view (**Figure 2.11** (c)). This device is a vast improvement on some of the previous devices discussed, but there is still some minor movement of the central nervous system during imaging. Additionally, there is a limitation in the depth of images that can be obtained using this device. Conventional fluorescent or confocal imaging has a depth limit, due to the thickness of the device and the surrounding tissue to be penetrated. In order to obtain a better resolution, full 3D rendering of the central nervous system tissue, the images obtained should be acquired more rapidly than via confocal imaging, with a greater capacity for depth of imaging, or the ability to rotate the sample readily and image from the opposite side.

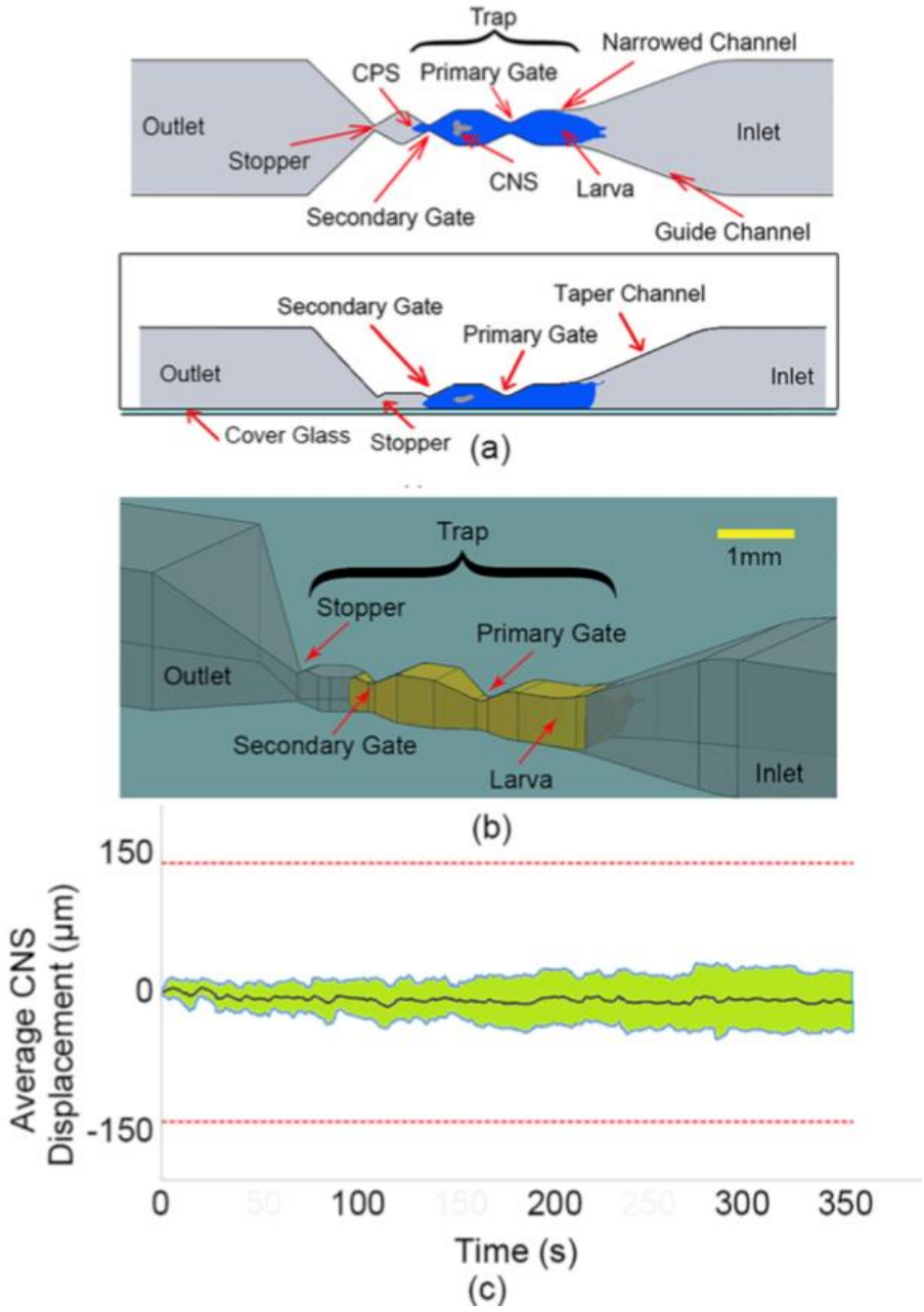

Figure 2.11 (a) and (b) Schematic design of the 3D segmental pinning chip – top view (top image) and side view (bottom). (c) The CM movement of the larva's CNS for 10 different larvae over time, inside the 3D segmental pinning chip. The black line shows the average CNS movement of 10 larvae, while the two blue lines indicate the standard deviation for each average data point [57].

2.3.3 *Limitations to existing immobilization devices*

These devices fall short of meeting the goals of interpreting the activity of the whole brain as mentioned at the beginning of this chapter. To develop an understanding of the interconnectedness of the brain regions during responses to stimuli, a device must hold a larva immobile to such an extent that the motion occurring during imaging is negligible and does not cause motion artifacts. The device must also not cause immobilization in a way that alters the natural physiological responses, by anaesthetizing or performing any form of surgery on the larva. Finally, the temporal resolution of the imaging system must be high enough that the time between sequential images allows for interpretation of the signals being sent between neurons. The devices discussed above all meet some of these design criteria, but none can provide the high spatial and temporal resolution while unaltering the brain physiology of the larva.

2.4 Neuronal Imaging

Given the interest in visualizing the nervous system of model organisms like the *Drosophila melanogaster*, researchers require methods of identifying the neurons within these structures inside of a specimen. A variety of imaging techniques exist for visualizing both full neuronal cells as well as individual proteins or nucleic acids within these cells. Many require introduction of novel molecules to the organism tissues, but as mentioned previously, genetic encoding of indicators is also possible, as described further below.

2.4.1 *Methods of Neuronal Imaging in Model Organisms*

Identifying cells or molecules of interest can be done exogenously or endogenously. Exogenous labels are molecules originating outside of the regions of interest that are introduced by researchers as markers. These exogenous labels are often tags attached to short proteins or RNA molecules that will pair with specific molecules of interest within cells. Many stains and tags are used to identify regions of the cell, such as the nucleus or cell membrane. Immunostaining uses antibodies to proteins of interest to label the localization of these proteins within cells of a model organism or excised tissue or organ. Radiolabelling is also possible, using atomic isotopes to generate labels that will be recognizable compared to non-radioisotopic atoms of the same species. Dye injection to regions of interest in an organism will identify sharp borders between cells or organ regions. For higher resolution, tissues or organs can be excised and often better contrast can be obtained. The main limitation of exogenous labelling is that tissue must often be fixed, meaning live imaging is not possible using these methods. There are some cases where an exogenous labelling method in living organisms, such as injecting a dye to the blood stream or having a patient swallow a contrast agent for the purposes of imaging activity in the vasculature or gastrointestinal system respectively, but these are limited by low resolution. Large organ structures are visible, but no activity at the cellular or molecular level can be visualized.

In contrast, endogenous labelling involves manipulation of the genetic material, for example inserting transgenes, in order to produce genetically encoded molecules that can be visualized using microscopy techniques. These endogenous labels originate within the organism itself, and are expressed in response to transcriptional or translational regulation, as a result of genetic

engineering. This is very useful because markers that are expressed intrinsically within an organism can be visualized in a living organism, unlike many exogenous labelling techniques. Additionally, these molecules are often more than just labelled proteins, but can show differential expression under different physiological conditions, genetically encoded biosensors that allow researchers to directly observe the qualitative and quantitative activity in live cells and even live organisms [59]. The introduction of genetically encoded biosensors is limited by the understanding of the genetic sequences of an organism. In organisms with fully sequenced genomes, researchers must first determine whether a gene in the animal that shares a similar sequence to a disease gene in humans can be used to model that disease state in the animal. Following the identification of the gene of interest for study, researchers must also determine the most appropriate biosensor to be introduced to the model. For example, a GFP could be useful for labelling ubiquitously, but a Förster resonance energy transfer (FRET) sensor could be used to show activity. Additionally, the location of insertion of the transgenes introduced must be precise. A gene inserted into the middle of existing coding material could disrupt normal function and cause a lethal phenotype. Misinsertion to a non-coding, non-transcribed region may mean the gene is never expressed and the insertion produces no results. Methods such as the GAL4-UAS bipartite system discussed above are useful for ensuring appropriate tissue-specific expression, providing the appropriate parent strains have already been designed and can be used for crossing.

2.4.1.1 Genetically Encoded Fluorescent Molecules

One example of an endogenous encoded biosensor that is seen frequently in neuronal imaging in the *Drosophila* model is a genetically-encoded calcium sensor (GECI) called GCaMP. Associating fluorescent signals with calcium is advantageous in studies where quantifying the activity of cells like neurons or muscles, in which activity is related to the influx of calcium to the intracellular environment, as this type of probe will allow observers to note activity differences between cells of the same population. The GCaMP molecule is a high-affinity Ca^{2+} probe composed of a single GFP molecule[60]. This probe improved the signal-to-noise ratio compared to previously created GFP-based calcium probes, showing much faster binding kinetics and dissociation kinetics that were completely independent from the Ca2+ concentration in the cell [60]. The mechanism is quite simple: the probe consists of a circularly permutated GFP protein, a calmodulin (CaM) region which binds to calcium, and an M13 fragment from the myosin light chain kinase protein. Upon calcium influx, the ions bind to CaM, which in turn binds to M13, causing a conformational change to the GCaMP protein and quenches solvent exposure to the fluorophore, allowing the molecule to fluoresce in response to the incident light [60]. This GCaMP probe has been re-engineered over the years to improve the functionality; researchers examined the mechanism of the molecular structure and search for mutations in the protein sequence that can improve this function based on how the mutations change the crystal structure and activity of the molecule [61]. Tian et al. developed the GCaMP3 GECI probe, which showed increased baseline fluorescence, a greater dynamic range, and higher calcium affinity compared to previous iterations, in addition to being able to show changes in fluorescence in response to single action potentials [62]. This group used the improved sensor to

visualize the neural activity in a variety of model organisms, including worms, flies and mice. The dynamic range of the GCaMP3 probe was increased even further with the introduction of the GCaMP5 series of GECI's [63]. The group increased the signal-to-noise ratio by 2- to 3- fold for each of 12 new GCaMP5 sensors created, with some GCaMP5 variants showing the ability to detect twice as many visual stimulus-responsive cells than the GCaMP3 was able to [63]. From this set of 12 probes, there are unique improvements on GCaMP3 allowing researchers to choose which GCaMP5 variant is the ideal expression tool for observing calcium changes in the specific application. These variants are shown in **Figure 2.12**.

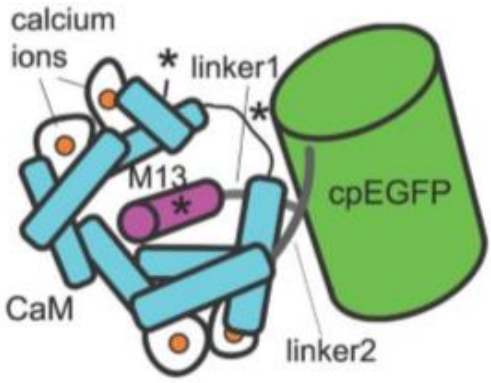

	M13pep	Linker1		cpEGFP	Linker2		CaM	
GCaMP3	A	L	E		T	R	D	R
	52	59	60		302	303	380	392
GCaMP5A	-	-	-		-	-	Y	-
GCaMP5B	-	H	P		-	-	-	-
GCaMP5C	-	Q	P		-	-	-	-
GCaMP5D	-	-	-		L	P	-	-
GCaMP5E	-	H	P		L	P	-	-
GCaMP5F	-	Q	P		L	P	-	-
GCaMP5G	-	-	-		L	P	Y	-
GCaMP5H	-	Q	P		L	P	Y	-
GCaMP5I	-	H	P		L	P	Y	-
GCaMP5J	-	H	P		-	-	Y	-
GCaMP5K	-	-	-		-	-	Y	G
GCaMP5L	V	-	-		L	P	-	-

Figure 2.12 Design of GCaMP5s, with a schematic of the GCaMP3 structure with sites of engineering shown. Adapted from Akerboom et al. [63]. Letters represent amino acid substitutions.

For many applications, especially those investigating temporal processes like development, live imaging is preferable, and as such, the neuronal imaging technique must be able to accommodate the needs of an intact, living organism without interfering with viability. Some of the complications associated with live imaging is the inherent dynamics of cells and their contents, as well as inhomogeneous optical properties. Any imaging process has measurable temporal

restraints – an image can only be acquired as fast as is mechanically possible. Some microscopes have slight temporal delays as the objective focus moves from plane to plane when acquiring a z-stack of images. Capturing a video may be limited to a maximum frame rate. If molecules or cells are moving during imaging, motion artifacts can arise, and often small changes may be missed. If tissues are not optically transparent, internal processes may not be visible without disrupting the organism by removing pigment from the tissue or extracting an embryo from the chorion, which will affect survival of the organism. It is necessary to consider whether organisms can be sacrificed or must still be alive for the imaging application. Selection of model organisms with transparent exteriors, such as the *Drosophila* 3rd instar larva, or the *C. elegans*, makes them more readily useable.

2.4.2 *Fluorescence Imaging Techniques*

When examining live physiological responses, the common optical tool is fluorescence imaging. As described above, it allows researchers to view activity within tissues and cells in a minimally invasive way, although the thickness of the tissue of interest dictates whether live organisms can be used. A number of different microscopes have been developed, each with different strengths and weaknesses regarding fluorescence imaging. It is critical for any research project that the appropriate imaging tool be selected to optimize results for fluorescence studies.

2.4.2.1 Fluorescence Microscopy

The fundamental strength in fluorescence microscopy is that using this technique illuminates the region of interest only. Through the use of fluorescent probes for labelling or intrinsic

fluorescent gene products, the specific molecules, cells, or tissues of interest can be visualized against a dark background, making it more clear what is of relevance to the observer compared to widefield microscopy [64]. The theory behind this concept is based on the principle of excitable electrons. Fluorophores, often synthetic molecules that take advantage of conjugated double bonds, must absorb enough energy from a photon to allow electrons within the fluorophore to transition to a higher electronic excited state. Higher energy photons than this minimum required energy can also cause rotation or vibration changes [64]. Upon absorbing this energy, the fluorophore must eventually return to its original ground energy state through the expulsion of a photon with a lower energy than the excitatory photon possessed. This is because vibration and internal conversion of the molecule have removed some excess energy, called the Stokes shift [64]. Examples of these energy differences, seen as wavelength shifts between the excitation and emission spectra, are shown below in **Figure 2.13**. Cyan fluorescent protein (CFP) has an absorbance wavelength distribution centered around 425 - 450 nm, indicating these wavelengths of light are absorbed and used to increase the electronic excited state. Following the loss of some energy and ejection of photons from the molecule, it is shown that the emission wavelength distribution of CFP is centred around 475-500 nm, a considerable shift in the visual light spectrum [64]. Researchers select the fluorescent protein given the known excitation and emission spectra, and if studying multiple unique components of a tissue, can select multiple fluorescent proteins as labels and image them simultaneously. There is minimal overlap in the fluorescence emission wavelength of DsRed and GFP proteins, as seen in **Figure 2.13**, which indicates minimal cross-talk and that the two unique components could be visualized as two different fluorescent colours using the same microscope.

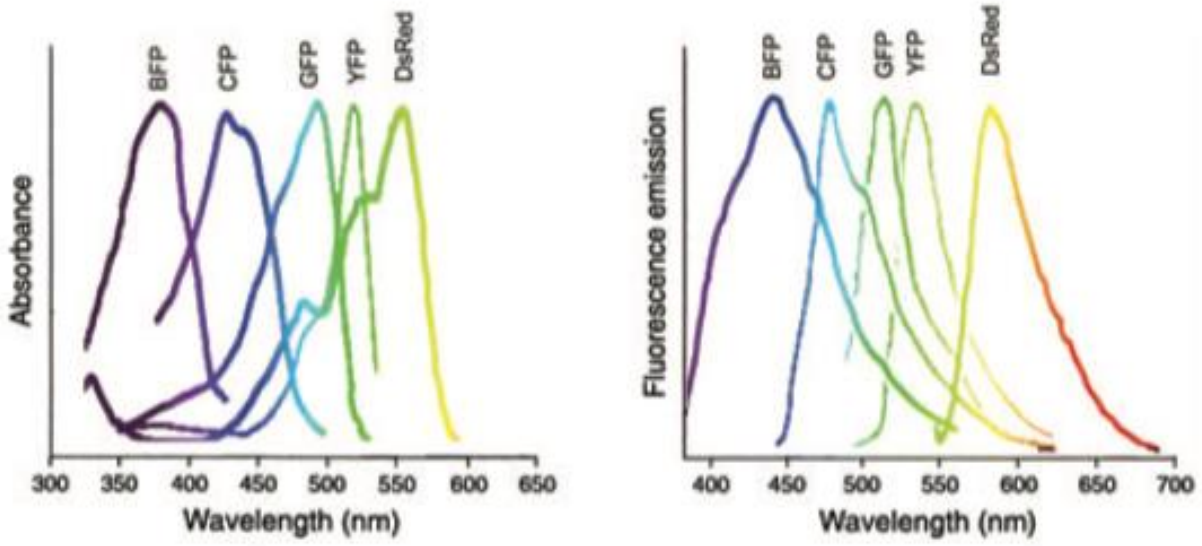

Figure 2.13 The mutated spectral variants of fluorescent protein from the *Aequorea* species of jelly fish and *Discosoma* species of reef coral have substantial overlap in both excitation and emission spectra. Recent attempts to generate more red-shifted fluorescent proteins have raised the possibility that eventually cross-talk will not be the major problem for fluorescent proteins either. Data from the Contech website. [64].

The traditional fluorescent microscope is of a wider field of view, allowing broad examination of samples at a lower resolution. However, this lower resolution can also cause background noise issues, reducing the signal-to-noise ratio and making discrimination between individual fluorophores difficult.

2.4.2.2 Confocal Laser Scanning Microscopy

A method for overcoming confounding background noise in imaging started to be developed in the 1960s. Patented by Marvin Minsky in 1961, confocal microscopy was used to eliminate the majority of the signals occurring out of the focal plane by restricting the illumination and minimizing the light able to reach the objective with a pinhole [65]. The sample is then scanned

within the same plane of interest by moving the pinhole, and additional planes are scanned by moving the sample itself. An image is compiled via this raster scanning and can be visualized with much higher contrast and higher resolution compared to traditional epifluorescent microscopy. It was quickly discovered that this imaging technique was suitable for thicker, biological samples, as the ability to image only the focal plane at a time was convenient for applications like cells, molecules and tissues [66], [67]. Laser scanning of these various cells by confocal imaging was compared to conventional epifluorescent imaging and demonstrated how the confocal microscope makes it much simpler for researchers to examine cellular processes occurring [67]. An example of the improvement in resolution is shown in **Figure 2.14**. The top panel shows a sea urchin egg using conventional fluorescence imaging, and the bottom panel shows the same sea urchin egg imaged using confocal microscopy. The fibres within the egg during mitosis can be distinguished from the other fibres readily by confocal microscopy, but are not clearly visible in the conventional image [67].

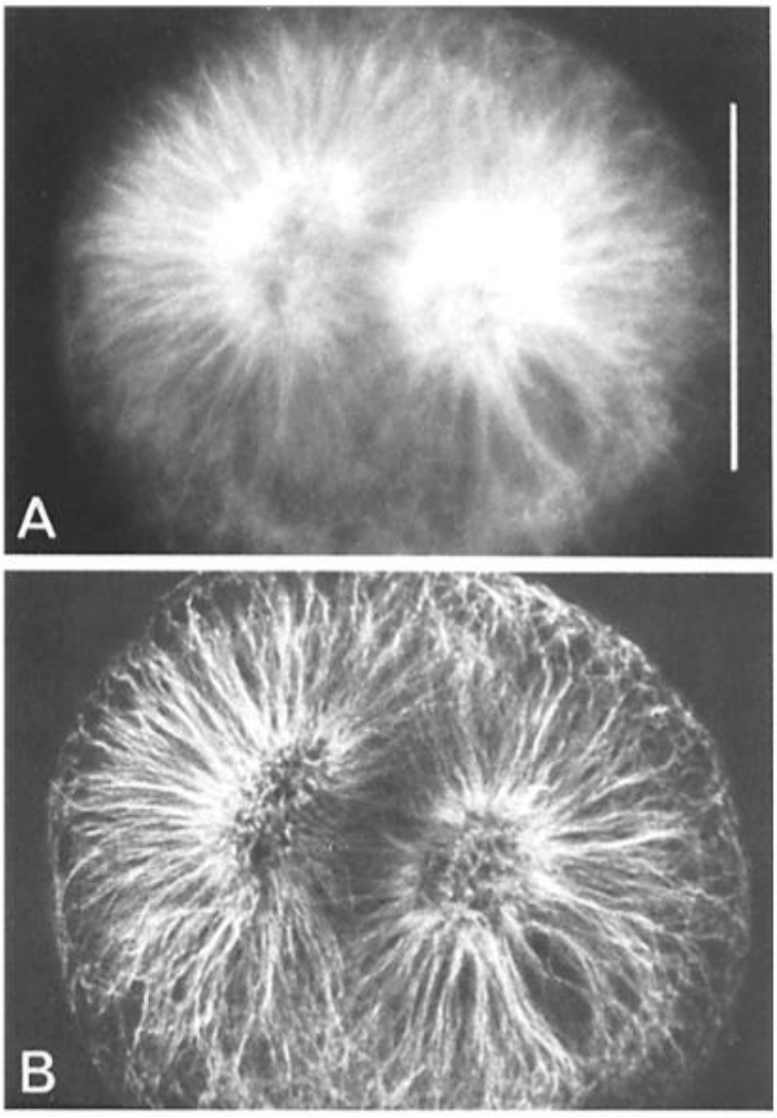

Figure 2.14 Fertilized egg of a sea urchin (*Psammechinus*) stained with antitubulin. (A) Conventional image for comparison with (B) confocal. Note the improved detail in the confocal image at the periphery and in the mitotic centres. Scale bar, 50 µm. [67].

Confocal fluorescence microscopy still has some limitations. Increasing the spatial resolution and signal-to-noise ratio results in a decrease in temporal resolution, and in longer studies, can affect the viability of the sample. Exposure of living cells to light can cause phototoxicity in the creation of free radicals during the fluorophore response, which ultimately damages the organism

at the cellular level [68]. Over long imaging times, photobleaching can also occur, as functional fluorophore density decreases, which reduces the signal-to-noise ratio. These four factors, sample health, signal-to-noise ratio, spatial resolution and temporal resolution, must be considered and a balance found to optimize imaging in a study. This trade-off between the variables is depicted in **Figure 2.15** [68]. Depending on the need of the study, any of these four variables could be optimized, but will require a decrease in the other variable categories. To improve imaging of living tissues and organisms, a solution that requires less time to obtain images is favorable.

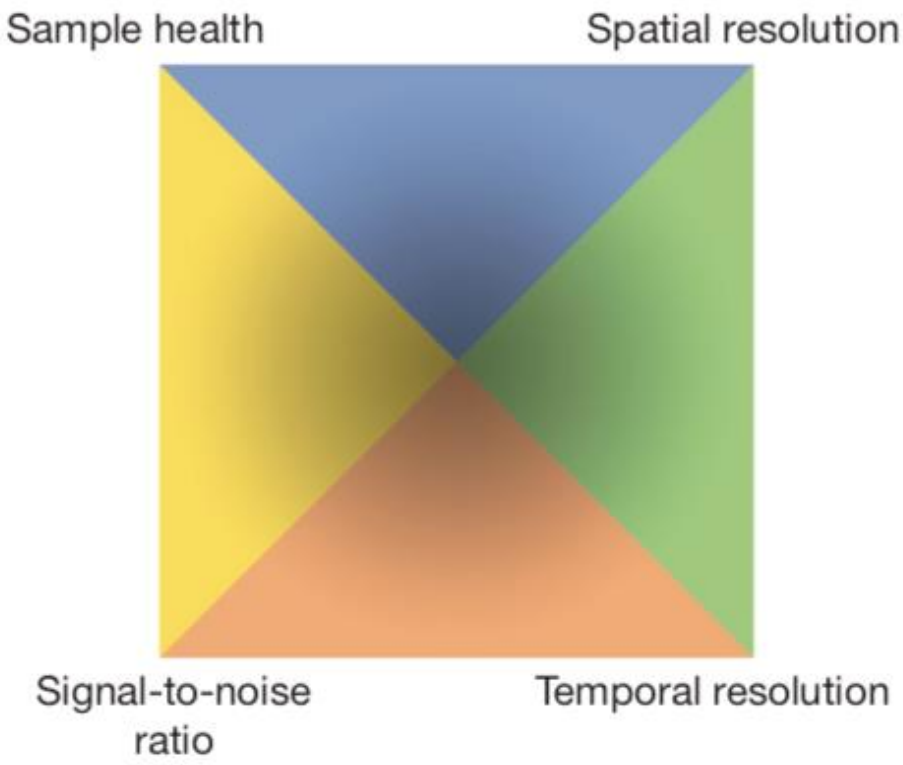

Figure 2.15 The four main considerations for live imaging. This is also known as the "pyramid of frustration", as no single parameter can be optimized without compromising the others. [68].

2.4.2.3 Light Sheet Fluorescence Microscopy (LSFM)

To combat the limitations of confocal microscopy for imaging live tissues and organisms, a novel technique called selective plane illumination microscopy (SPIM) was developed [69]. This technique is better known today as light-sheet fluorescence microscopy (LSFM). This method moves away from previous technologies by illuminating the sample perpendicularly to the axis of detection. The illumination light is focused using a cylindrical lens so it forms a "sheet" of light that will only illuminate the focal plane of the specimen at any given time, shown in blue in **Figure 2.16** [69]. In this manner, the other regions of the sample not currently being imaged will not experience photobleaching or phototoxicity, extending the imaging lifetime of the fluorophores. In fact, the total number of fluorophore excitations required to completely image a 3D sample is reduced significantly compared to the number of excitations seen using confocal microscopy [69]. One of the added benefits of the sheet illumination approach is that structures at greater depths of up to 500 µm can be imaged clearly, unlike when using confocal microscopy. Additionally, since the axial resolution of the image is related to the width of the light sheet, an improvement in axial resolution from 20 µm to 6 µm can be seen when moving to this imaging apparatus [69]. The sample is mounted within the chamber perpendicular to both the objective and illumination planes, usually vertically suspended, as can be seen in **Figure 2.16**. This allows for another unique component of the LSFM, multi-angle imaging. The sample can rotate about the suspension shaft axis, allowing the same regions of interest to be imaged from multiple angles and reconstructed with post-processing software techniques after acquisition. The image acquisition is also very rapid compared to conventional confocal microscopy, with 3D structures being captured in just seconds, with each sheet being illuminated

for periods as brief as 30 ms [69], [70]. To characterize operation of this novel imaging technique, this research group visualized muscles in a transgenic Medaka line, using GFP in the muscle tissue, as well as investigated embryogenesis of the *Drosophila melanogaster* in vivo.

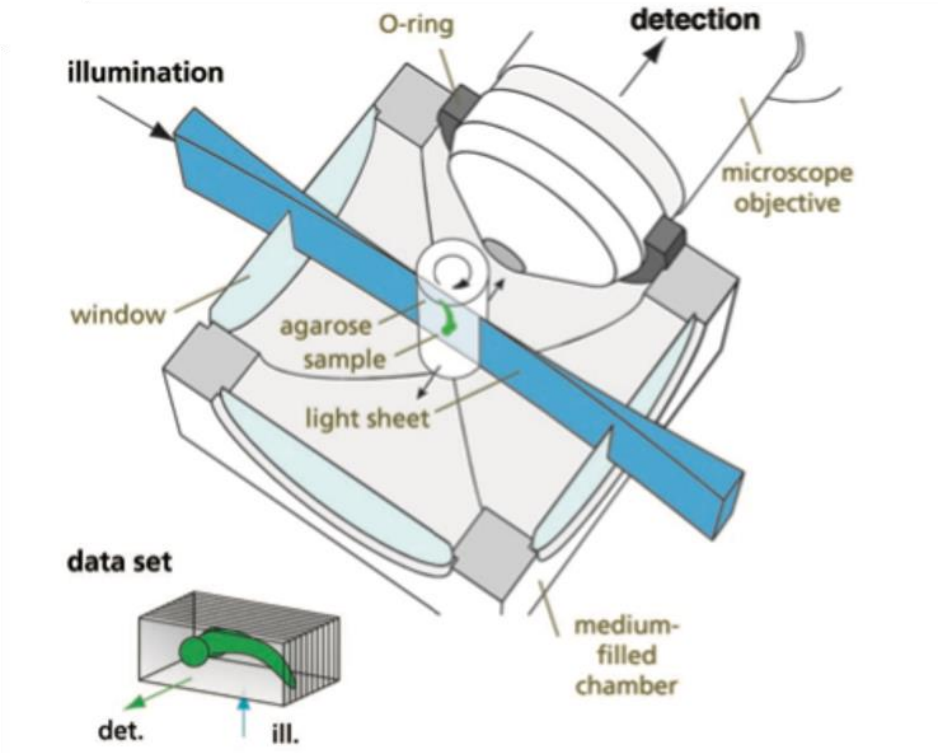

Figure 2.16 Schematic of the sample chamber. The sample is embedded in a cylinder of agarose gel. The solidified agarose is extruded from a syringe (not shown) that is held in a mechanical translation and rotation stage. The agarose cylinder is immersed in an aqueous medium that fills the chamber. The excitation light enters the chamber through a thin glass window. The microscope objective lens, which collects the fluorescence light, dips into the medium with its optical axis orthogonal to the plane of the excitation light. The objective lens is sealed with an O-ring and can be moved axially to focus on the plane of fluorescence excited by the light sheet. In a modified setup, for low-magnification lenses not corrected for water immersion, a chamber with four windows and no O-ring can be used. In this case, the objective lens images the sample from outside the chamber. Det., detection; ill., illumination [69].

2.4.2.4 Neuronal Imaging using LSFM

LSFM has already been shown to be an extremely adept technique for whole-brain functional imaging at the resolution of single neurons in another organism, the larval *Danio rerio*, or zebrafish. Using a 1.5 % agarose gel, a 5-day old albino larval zebrafish can be embedded in a 1.5-2.0 mm ID/OD capillary tube. The larval head region is extruded from the capillary into the imaging chamber of the light-sheet microscope, which is filled with water from the fish colony facilities, shown in **Figure 2.17**(a). This group was able to take high resolution images of a volume of 800 x 600 x 200 μm^3 once every 1.3 s [70]. The volumetric area was broken up into steps of 5 μm which could be imaged every 30 ms, with an exposure time of 5 ms per image, depicted in **Figure 2.17**(b). The thickness of the light-sheet was 4.25 ± 0.80 μm, which allowed for a lateral spatial resolution high enough to ensure individual cells could be distinguished from each other [70]. Using this imaging strategy, it was possible to identify regions of cells in the larval zebrafish brain that activated following similar patterns, and the researchers were able to draw associations between different groups of cells in the hindbrain with correlated activity patterns. This information can then be used to help interpret the functional role these cells may play in the larval zebrafish, such as involvement in locomotion due to the involvement of concurrent spinal cord activation, and anatomical overlap with neurons that are associated with swimming [70], [71]. There are some limitations to this technique, such as the laser sheet scanning past the larval retina. The activity in the brain could be related to laser excitation of the retina once each time a volume is scanned. This technique is also extremely rapid at 1.3 s per volume scan rate, but a greater scanning speed could facilitate more accurate temporal resolution

of spike timing within individual neurons [70]. The zebrafish larva in this setup is held in place using agar gel, and this is effective for a vertebrate organism in this case. However, a *Drosophila* larva shows contraction of muscles in this setup, and as a result the hemolymph moves the internal organ tissues around within the larval body. Thus, an alternative immobilization mechanism needs developing, as mentioned above, to facilitate adequate immobilization of this model organism to execute a research study similar to what Ahrens et al. have accomplished.

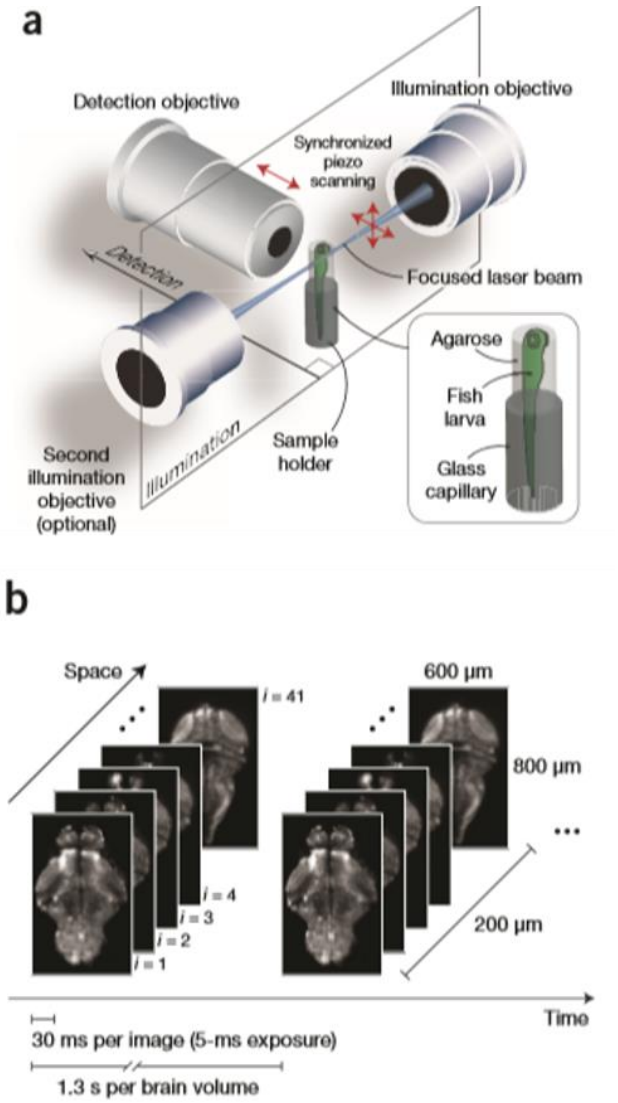

Figure 2.17 Whole-brain, neuron-level light-sheet imaging in larval zebrafish *in vivo*. (a) Fast volumetric imaging of the larval zebrafish brain with light-sheet microscopy. The living zebrafish is embedded in 1.5 % agarose gel and positioned in front of the water-dipping detection lens. The light sheet is generated by fast vertical scanning of a focused laser beam, and it illuminates a 4 µm-thick volume section of the fish. Fluorescence is recorded orthogonally to the light sheet with a fast scientific complementary metal-oxide semiconductor (sCMOS) camera. Fast volumetric imaging is performed by step-wise axial movement of the detection objective in synchrony with displacement of the light sheet while the specimen is kept stationary. Optionally, a second light sheet is used to illuminate the specimen simultaneously from the opposite side. (b) High-resolution images are recorded in steps of 5 µm every 30 ms, with an exposure time of 5 ms per image. A volume of 800 x 600 x 200 μm^3, containing the entire brain, is recorded once every 1.3 s. [70].

LSFM has also been shown in the chick embryo, investigating the different chronological phases of development. This group introduced non-diffracting light beams to the existing digitally scanning fluorescence light-sheet microscope to improve the penetration depth of the light into the larger sample, also improving the depth of field. The incident laser light sheet passes through an acousto-optical tuneable filter. The modulated light sheet is spatially filtered and then relayed into a galvo-scanner. The light sheet is then passed into the illumination objective and collected by the detection objective [72]. The results emphasize that a larger range of focus can be obtained for images of more developed, larger embryos, improving results for researchers investigating development [72]. The traditional Gaussian beam focus is thin, it only maintains this thin region over a length of about 10 μm, and the Bessel beam can maintain the thin region for over 100 μm. The Bessel beam illumination allowed a 0.2 mm thick sample to be imaged completely, shown reconstructed in **Figure 2.18**, while normal Gaussian beams prevent clear imaging of curved surfaces like a late stage chick embryo due to scattering. Penetration depth was equal with both Gaussian beams and Bessel beams, but the Bessel beam was more suited to curved surfaces [72].

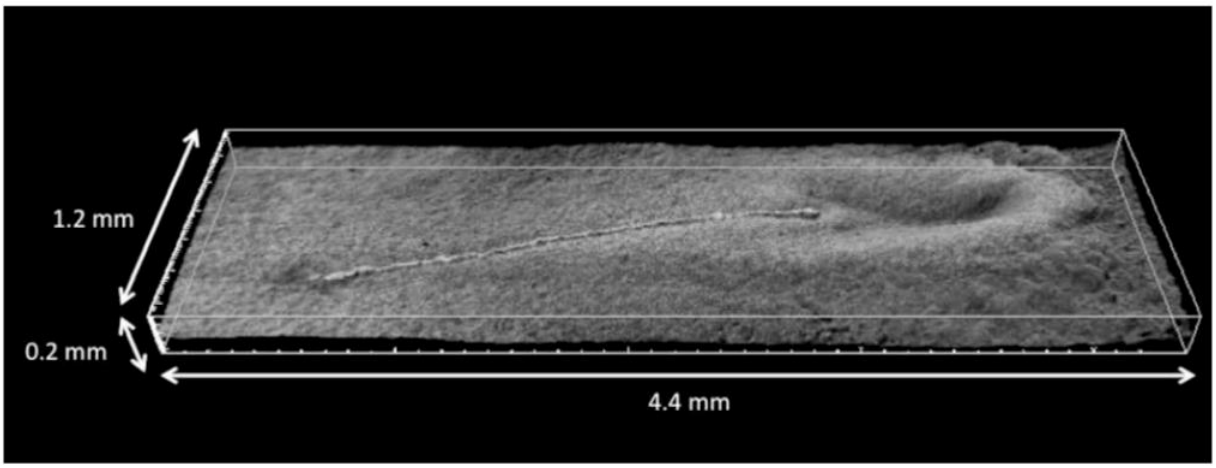

Figure 2.18 Three-dimensional reconstruction of the surface of a post-streak embryo, showing the primitive streak and the head fold with cellular resolution over a depth of 0.2 mm imaged with the Bessel beam illumination and synchronous line-readout detection [72].

Lemon et al. presented a technique to measure the whole-central nervous system in a larval *Drosophila* after the CNS had been isolated and embedded in agar [73]. The *Drosophila* CNS, when extracted from the body and sensory input to the brain region, still produces patterns of activity that can be related to behaviour, such as locomotor patterns [74]. This group used the genetically encoded calcium indicator GcaMP6s to image fluorescence changes of the neurons with a modified LSFM microscopy technique called hs-SiMView microscopy, using either one- or two-photon excitation. Mapping of the activity of the entire central nervous system was possible and allowed for complex activity patterns that corresponded to the fictive motor behaviours could be investigated [73]. The group was able to investigate the relationship between higher-order brain centres coordinate the activity of the motor centres throughout the larval body, as well as investigate the timing relationships between these centres.

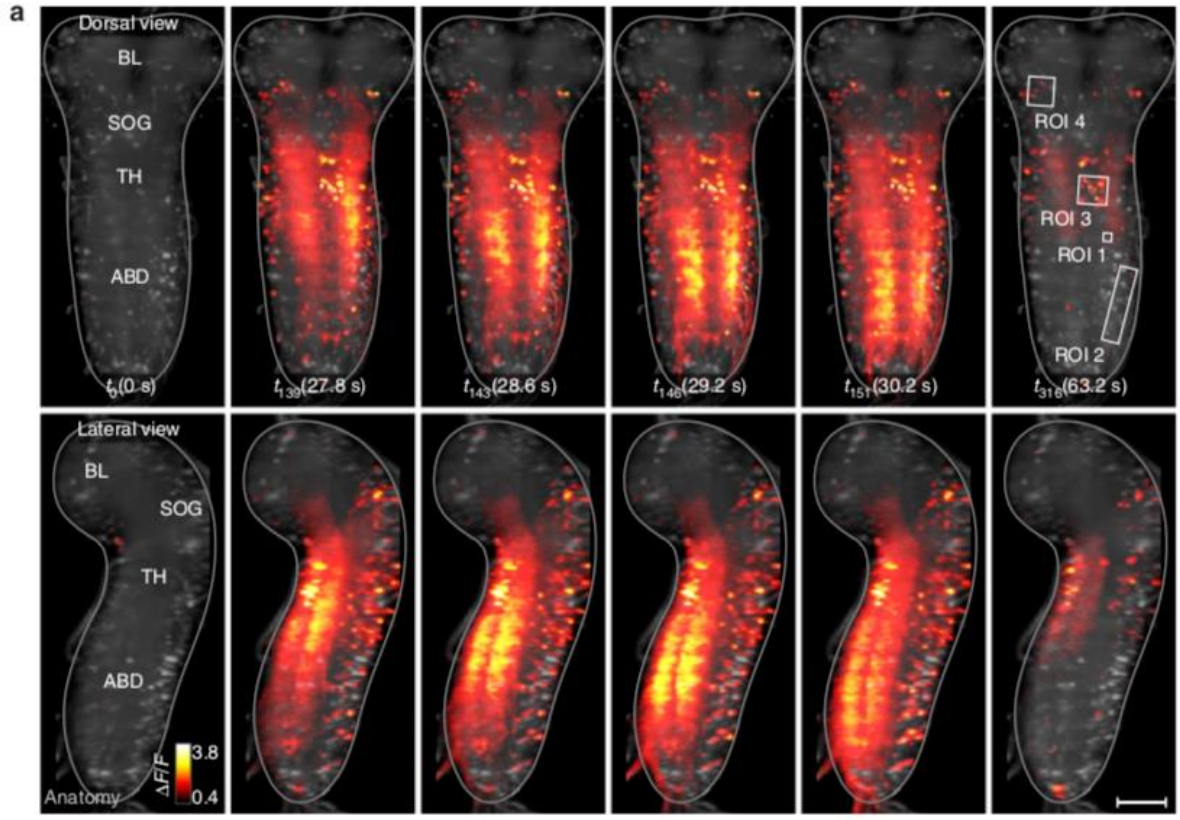

Figure 2.19 Whole-CNS functional imaging of the isolated Drosophila larval nervous system. Whole-CNS functional imaging at 5 Hz of a Drosophila third instar larval CNS expressing 57C10-GAL4,UAS-GcaMP6s, using hs-SiMView light-sheet microscopy. Imaging was performed with one-photon excitation at 488 nm, maintaining a constant imaging speed of 370 frames per second (491 MB per second) for a period of 1 hr. Image panels show maximum-intensity projections of deltaF/F (colour look-up-table) and CNS anatomy (grey, gamma-corrected GcaMP6s baseline fluorescence) from dorsal (top) and lateral (bottom) views, for six time points during a backward locomotor sequence. Outline indicates CNS boundary. ROI 1 shows an example of rapid changes in deltaF/F across two locomotor waves. ROIs 2-4 show examples of slow changes in deltaF/F across a bout of locomotor waves. Images are median filtered. ABD, abdomen; BL, brain lobes; SOG, suboesophageal ganglion; TH, thorax. Scale bars, 50 µm [73].

The one-photon excitation was maintained at a constant 370 fps speed for a period of one hour, allowing a much higher temporal resolution, tenths of seconds instead of tens of seconds seen in the state-of-the-art LSFM [73]. The one-photon excitation offered faster imaging acquisition and

allowed for longer experiments, but two-photon excitation provided better signal-to-background levels, allowing for better resolution of the molecular components and cellular bodies. However, the larval brain must be dissected in this approach, and while the technological developments of the microscope are incredible, a need to obtain a truer physiological model of the *Drosophila* CNS will be important in better understanding the way these brain regions interact with each other.

Other groups have also made modifications to the light-sheet microscope in an effort to improve the spatiotemporal resolution. Lattice light-sheet microscopy uses ultrathin light sheets derived from two-dimensional optical lattices, which are then scanned across a series of z-slices similar to how the conventional light-sheet microscope operates [75]. The ideal 2D lattice can propagate indefinitely in the y direction without changing the cross-sectional profile in x and z [75]. A fast switching spatial light modulator (SLM) is introduced to the light plane. This SLM has a pattern written onto it that creates the amplitude of the lattice light sheet, so that when the incident light passes through the SLM and is filtered by the excitation objective it produces a point spread function that matches the spacing of the lattice pattern [75]. This thinner sheet improves the axial resolution compared to the Bessel and Gaussian beams from previous studies. To characterize the efficacy of this technique at improving the spatiotemporal resolution, the group imaged a wide variety of biological processes, including cell division and migration, as well as microtubule growth. The results show that this manipulation of the sheet of light to reduce the thickness of the beam does increase the resolution of the images, and allows for the tracking of the movement of single molecules and molecular structures in real time. The imaging system

used in this study had a maximum rate of 1000 planes per second, but this is still too slow to study some biological systems, especially the rapid movement of molecules within cells.

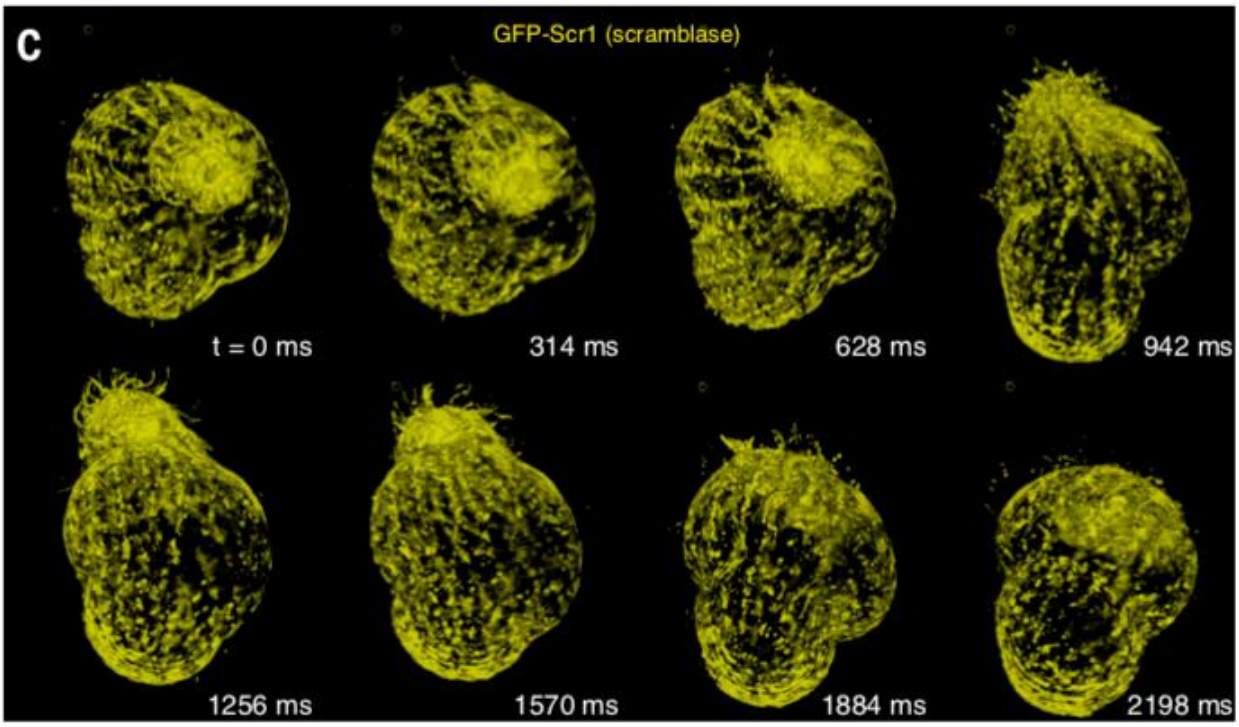

Figure 2.20 Volume renderings at eight consecutive time points of a single specimen of the protozoan *T. thermophila* taken from a 4D data set spanning 1250 time points. Imaging at 3 ms per frame in a single plane reveals the motions of individual cilia [75].

Fadero et al. introduced another modification to LSFM, called lateral interference tilted excitation (LITE), which involves using a tilted light sheet to illuminate the focal plane of the detection objective while avoiding the limitations of orthogonal excitation on spatial resolution [76]. The LITE method involved directing a collimated, coherent beam of excitation light through a photomask and cylindrical lens to form a non-symmetrical wedge of light which converged to the minimal thickness light-sheet at the focal plane of the objective lens [76]. The

photomask was patterned to make the focusing beam patterned and lengthen the light sheet [76]. Essentially, they were able to increase the spatial resolution while imaging fixed organisms compared to conventional LSFM. In the conventional light-microscope, the numerical aperture (NA) of objective lenses must be low (less than 1.1) to accommodate for the distance of the sample from the objective to allow for the orthogonal incident and detected light paths [76]. This means that higher resolution oil-immersion objectives cannot be used with LSFM, causing a resolution limitation that isn't encountered in confocal imaging. LITE takes the advantages of high resolution in confocal microscopy and rapid image acquisition time of LSFM and combines them into a novel tilted light sheet approach that allows for the use of a 1.49 NA oil-immersion objective, improving spatial resolution [76]. However, certain advantages of the LSFM are still lost with this development, including the ability to image a sample from multiple views. Novel sample chambers also had to be engineered for this study, which require flat, optically clear and homogenous sides that will accommodate light entering the chamber at the interface between the coverslip at the bottom of the chamber and the side wall. This requires an additional fabrication step that LSFM and confocal microscopy do not.

2.4.3 *Drosophila Live Neuronal Imaging*

As mentioned previously, there have been advances in imaging live neurological responses in the *Drosophila melanogaster* in the last several years with the creation of the 3D segmental pinning chip [57], [58]. This standardized immobilization technique made it possible to examine the CNS activity of the *Drosophila* in response to chemical and acoustic stimuli, unaltered by anaesthesia or dissection and at high resolution with minimal motion artifacts. Larvae were loaded into the

3D segmental pinning chip pneumatically and the entire chip and a small microscope were placed in a sound-proof box equipped with a speaker installed in the roof of the box. This microfluidic chip pinches the larva at two pinning gates which allow for minimal motion of the CNS over a period of 5 minutes. The results of this motion can be seen in **Figure 2.11**. The same group also investigated the CNS response to sodium azide, a known neurotoxin for *Drosophila*, using a modified version of the 3D segmental pinning chip that involves a bend in the channel to immobilize the larva more effectively, reducing motion artifacts in images further [77]. Ten individual neurons in the ventral nerve cord (VNC) of one larva are pictured in **Figure 2.21** below, showing a response to the chemical stimulus 5 seconds after exposure. Exposure of the larva to the chemical was possible through the integration of an auxiliary channel that connected to the mouth/nose region of the organism [77]. While these devices are easy to use and compatible with a variety of microscopes, they are not currently able to be used in a LSFM application, restricting the temporal resolution of any imaging conducted. The immobilization mechanism does improve the ability to study neurological responses in *Drosophila* 3rd instar larva greatly.

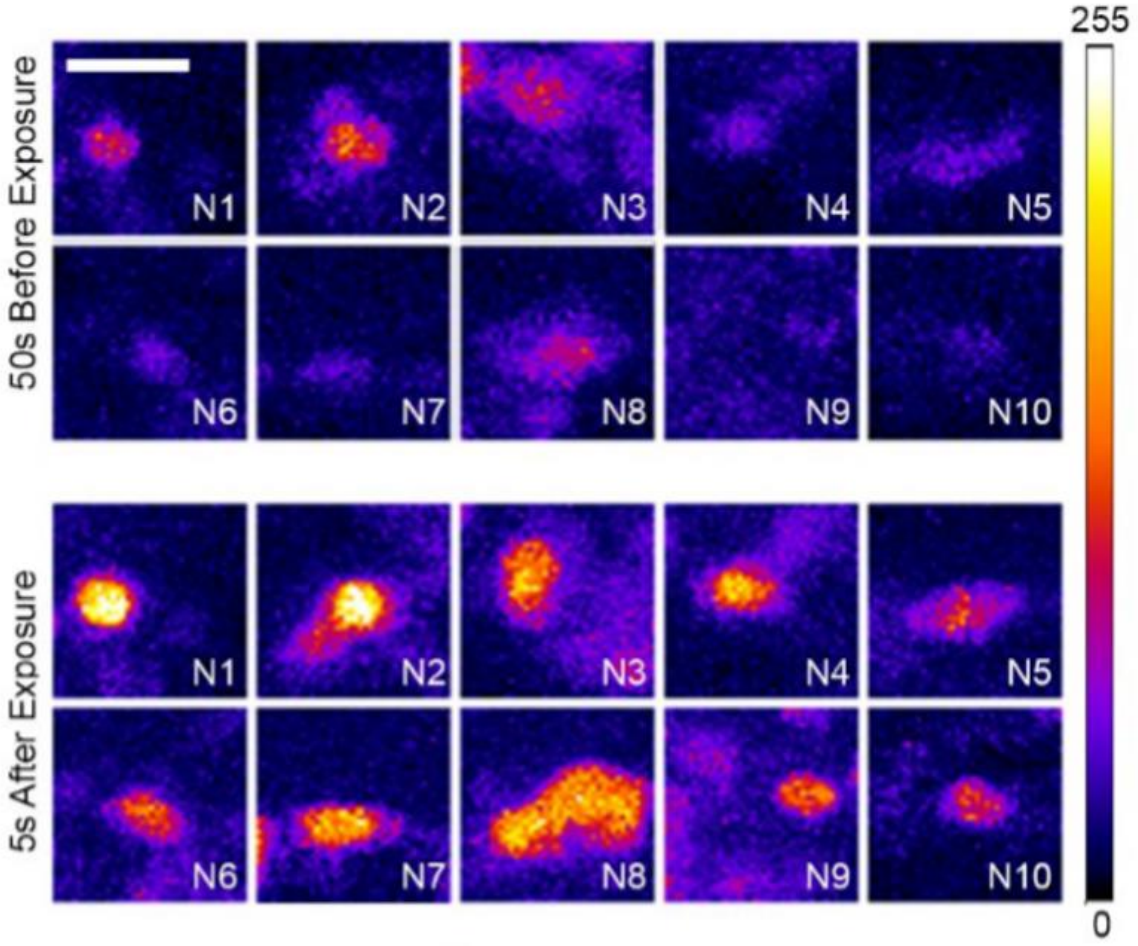

Figure 2.21 Neuronal activities of *Drosophila* larva during chemotaxis response. The panels show the calcium activity of the single neurons from one larva in response to the sodium azide 50 s before and 5 s after exposure. Scale bar 5 µm [77].

2.4.3.1 LSFM for live Drosophila Neuronal Imaging

Unfortunately, while a confocal microscope can provide extremely high spatial resolution, in a living specimen, it is of interest to track activity between neurons in response to stimuli, and therefore, a higher temporal resolution is desirable. An increase in temporal resolution while not giving up high spatial resolution can be obtained by modifying a light-sheet fluorescence

microscope. In brief, the light-sheet microscope has great potential to achieve the spatiotemporal needs for obtaining high-resolution images of live neuronal activity in *Drosophila melanogaster* larvae, but at this time the *Drosophila* CNS has only been examined in a LSFM when dissected out of the larval body. The immobilization chip by Ghaemi et al. has significant potential to hold a live larva still enough to achieve high spatial resolution, but must be adapted in order to be compatible with the mounting apparatus in the LSFM [77]. In addition to manipulating the device mounting technique, the shape of the device should also be changed to accommodate orthogonal incident and emission light.

2.4.4 *Goals of Research*

This thesis aims to modify existing microfluidic immobilization tools to be compatible with a light-sheet microscope, allowing an increase in spatiotemporal resolution of the central nervous system of a *Drosophila* larvae, increasing the potential to image stimuli-response neuronal behaviours in the central nervous system in real time, and increasing the versatility of this model organism for biological researchers of neurological disease. The primary goal of this research is to create a fabrication process for a high-quality, reproducible, reusable immobilization device for *Drosophila melanogaster* 3rd instar larvae to perform light sheet microscopy on a live animal. The device should immobilize the CNS of the larva so that it remains within the field of view of the microscope over periods of ten minutes or longer. The desired resolution is <5 µm while at an appropriate magnification to view the entire larval brain simultaneously. Additionally, the device should be simple to work with, ensuring it is accessible to all groups interested in using it for improving their research.

2.5 Summary

The *Drosophila melanogaster* is an ideal model organism for neurological study because of its short life cycle, transparent larval life stage, ease of genetic manipulation, and the similarity of the *Drosophila* genome to the human genome. Databases such as Homophila exist that allow for the comparison of human disease genes to analogs in the fly, which allow researchers to create models of disease states in the fly using the bipartite genetic engineering GAL4-UAS system. Working with the *Drosophila* larva, however, poses a few issues, the greatest of which is their perpetual burrowing motion. This motion makes it difficult to image the central nervous system of the larva, as the organ moves around in the hemolymph filled body cavity in response to the longitudinal wave-like motion. Recently, engineers have started using microfluidic devices to ease the process of working with small model organisms like the *Drosophila* and *C. elegans*, and more specifically, a 3D segmental pinning chip has been developed that immobilizes a 3rd instar *Drosophila* larva while allowing imaging of the central nervous system within a fluorescent or confocal microscope. This segmental pinning design was adapted in this research project and incorporated into a novel shape of device for use in a LSFM to achieve high spatiotemporal resolution of the CNS during prolonged imaging. The next chapter will introduce the conceptual design of the novel device and the experimental setup for characterizing the efficacy of the device for this application.

3 Conceptual Design and Experimental Setup

3.1 Introduction

With the growing use of *Drosophila melanogaster* as a model for human neurodegenerative diseases, it is becoming increasingly clear that a technique to optically examine the activity of the central nervous system of these organisms at high resolution is an important step to continuing to increase our knowledge about the mechanisms of such diseases. As previously discussed, live imaging techniques have shown improvements in spatial resolution through the use of immobilization devices [54]–[56]. The microfluidic immobilization techniques introduced by Ghaemi et al. have vastly improved the ability to capture unaltered physiological responses using fluorescence, but to begin to examine the activity of the entire brain region in response to external stimuli, further progress is required [58]. Whole brain activity can be visualized by light sheet microscopy that has fast acquisition times, small photobleaching effect and the ability to scan over a thick layer of tissue. However, current formats of immobilization are not suited for incorporation into a light sheet microscope. This chapter will discuss the conceptual design and layout of such a device that can immobilize a live 3rd instar *Drosophila* larva while maintaining a physiological state unaltered by anaesthesia and allowing for three dimensional reconstructions of the central nervous system activity to be imaged rapidly over time.

3.2 Design Criteria

Since the 3D segmental pinning design developed by Ghaemi et al. is effective for immobilization of the body of the larva, it will be integrated into this design [58]. Its external features are incompatible with LSFM and need to be modified which will form the main elements of the design criteria. The criteria include enabling the microfluidic device to be suspended into the main chamber of the light sheet microscope as well as ensuring that the outer surface of the device is smooth and does not distort the incident or the emitted light so that imaging can be performed. The device must also hold the larva immobile without the backpressure applied in the original 3D segmental pinning device [58]. This is because the light-sheet microscopy sample chamber is completely enclosed and attachment of tubing to regulate pressure during imaging is not possible.

3.2.1 *Device Design*

The design for the microfluidic immobilization device created for this light-sheet neuronal imaging application is shown in the schematic in **Figure 3.1**. There are three main design components – the immobilization channel, the mechanical stopper, and the mounting attachment. The inlet port allows for entry of the larva. The tapered channel aligns the larva for insertion to the immobilization region. Pressure is applied via the inlet channel to insert the larva into the immobilization region. A mechanical stopper is introduced following complete insertion to prevent the larva from evacuating the immobilization region during image capture. The outlet port is used to apply pressure to eject the larva following imaging.

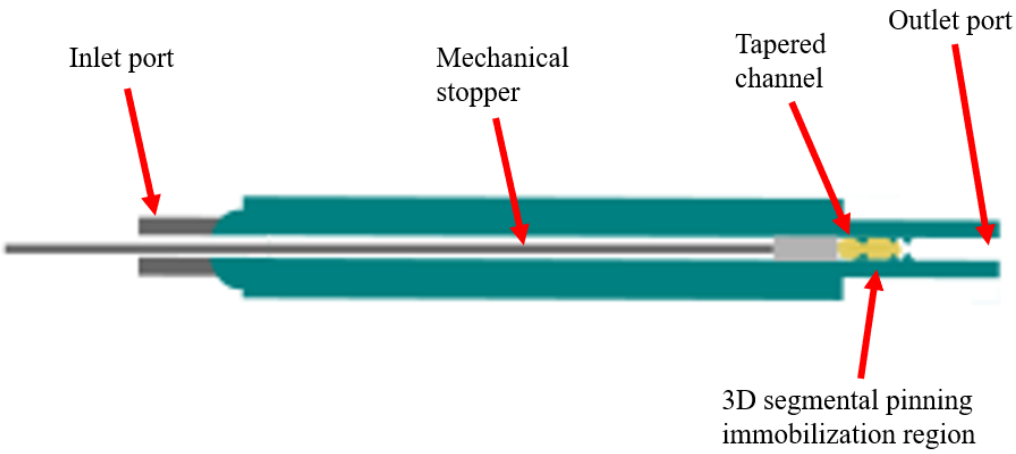

Figure 3.1 Device design schematic. Important regions are labelled in the Figure. The microfluidic device is ~4.0 cm in length, and at the narrowed region surrounding the immobilization region, 4.0 mm x 4.0 mm in cross sectional area. Mounting attachment is not pictured in this schematic.

3.2.2 *Immobilization Region*

3.2.2.1 3D Segmental Pinning Region

One of the key components of the device design is the 3D segmental pinning immobilization region. This region, or trap, of the microfluidic device must be able to pinch the *Drosophila* larvae in such a way that the burrowing motion generated by the musculature of the outer body is minimized, preventing the periodic motion of the organs within hemolymph in the body cavity. A two-point pinning strategy was employed previously to effectively immobilize the outer body of the larva and minimize the internal motion of the organs [58]. The primary (1^{st}) and secondary (2^{nd}) gates are spaced to align with the thoracic body segments of the larva directly dorsally and ventrally to the CNS respectively, ensuring the CNS will be positioned between the two gates. This is to minimize longitudinal body motion and the motion artifacts that result from the

longitudinal motion due to shifting of organs in the hemolymph. The 1st gate (200 µm x 450 µm) and 2nd gate (100 µm x 425 µm) allow the larva body to pass through, but the stopper (100 µm x 100 µm) is too small to allow larval exit from the immobilization region. A drawing of the immobilization region is shown in **Figure 3.2**. The magnitude of these values was selected based on the dimensions of the average larval body. The narrowed channel in the region of the immobilization trap was 770 µm x 700 µm in cross sectional area. Additionally, it was important that the immobilization is relatively rapid and user friendly. The immobilization trap was ideal because a larva will naturally orient itself headfirst at the opening to the trap ~30 s after loading, easing the procedure for the user. One modification to the design that was incorporated was the way that the immobilization is sustained. The previous design used a low pressure of 0.2 bar during imaging to maintain the larval immobilization. However, it was not feasible to incorporate a pressure inlet into the light-sheet microscopy chamber due to its geometry. Therefore, a physical tool to maintain the immobilization was incorporated to ensure the larva remained within the pinning region for longer periods of time required for this imaging application. Finally, it was important that prolonged immobilization in the trap would not injure the larva or decrease the viability of the organism.

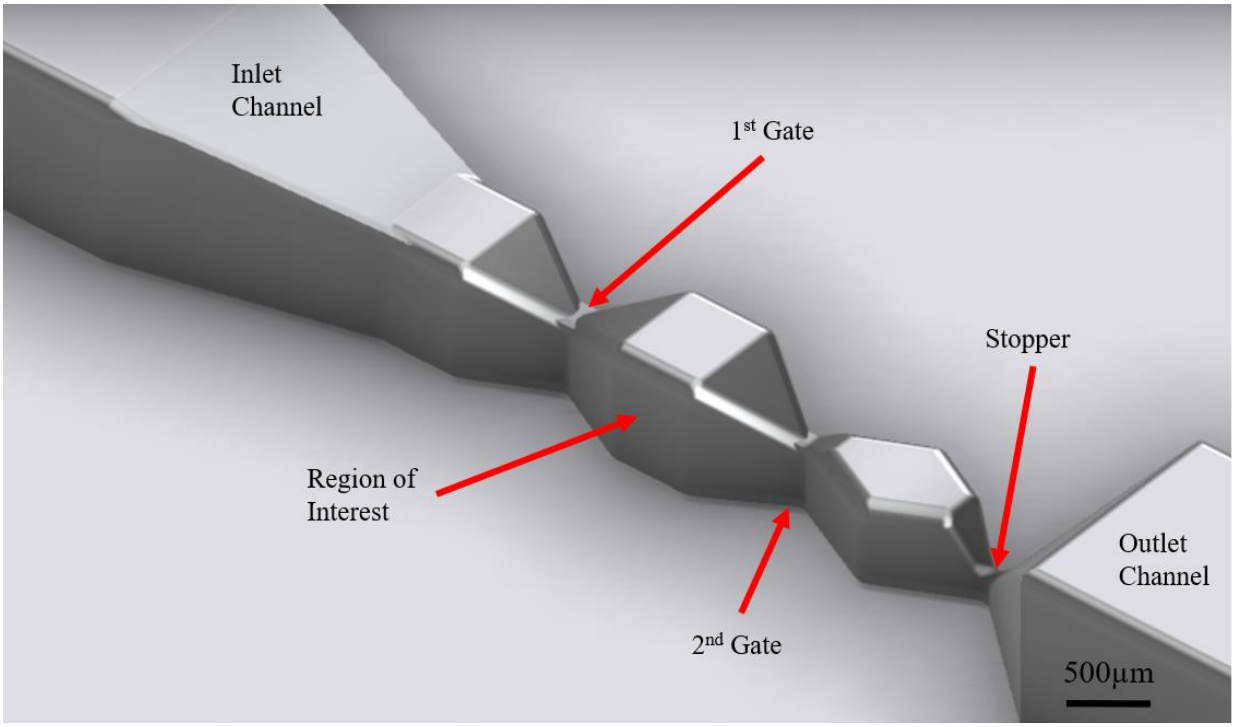

Figure 3.2 Drawing of the immobilization region of the 3D segmental pinning device. Design was adapted from Ghaemi et al., [58].

3.2.2.2 Mechanical Barrier

The light sheet microscope setup does not allow any external pressure connections to be included during operation and therefore the required backpressure cannot be applied during imaging to keep the larva completely immobilized as previously done [58]. To substitute for the backpressure and maintain larval position in the 3D segmental pinning region, a 1.0 mm diameter mechanical stopper was inserted to the inlet channel and placed directly behind the dorsal region of the larval body. This mechanical stopper used is supplied with the light-sheet microscope capillary tubes and is used as a plunger for drawing agar up into a capillary tube for standard imaging. The white, thick 1.0 mm region is a small plastic cylinder, which is attached to

a longer, 6 cm metal shaft that allows for manipulation of the plastic plunger within the narrow tube. This effectively prevents the larva from leaving the immobilization region and escaping from the device by crawling out of the inlet channel. The inlet channel was able to accommodate the mechanical stopper, but the narrowed channel in the immobilization region, which was 770 µm x 700 µm in cross sectional area, ensured the stopper did not enter this region and injure the larva. This mechanism extends the duration of imaging possible using this device. A photo of the mechanical stopper fully inserted to an unloaded microfluidic device is shown in **Figure 3.3** below. The channel has been false-coloured to increase contrast for visualizing the pinning gate features.

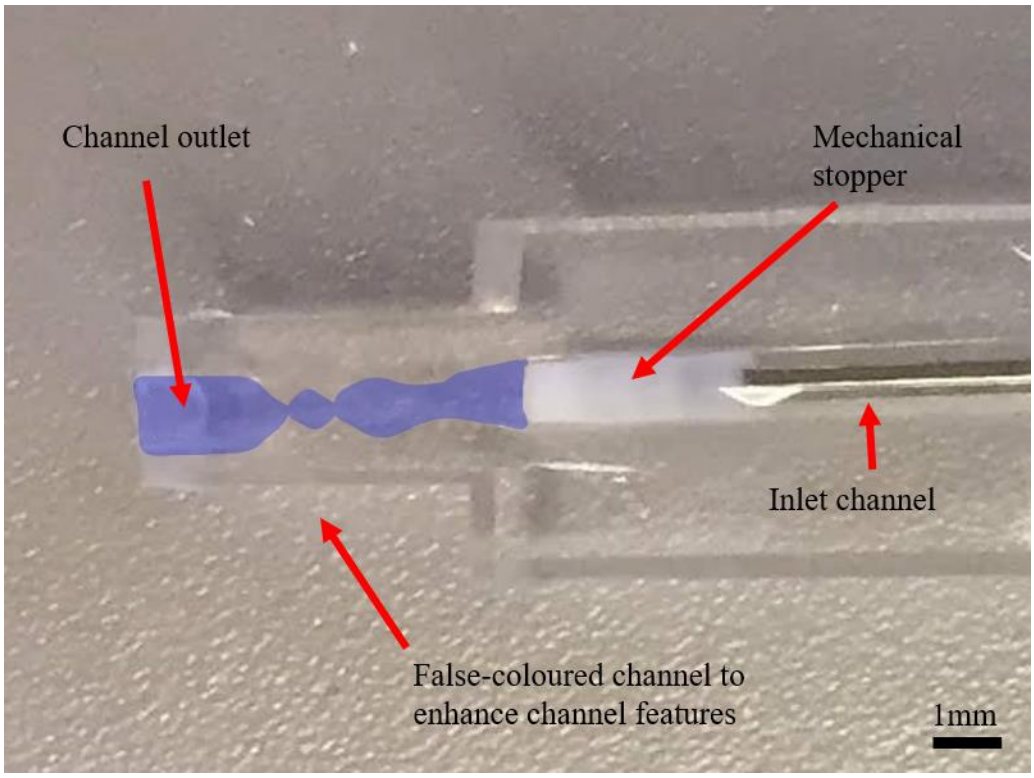

Figure 3.3 Image of the mechanical stopper inserted to an unloaded microfluidic device.

3.2.3 *Drosophila Loading System*

The design of the immobilization chip requires that the larva enter and exit the device through the inlet channel. The outlet channel is used as an outlet for fluid during loading, and the syringe is inserted to the outlet channel to apply pressure to the larva to evacuate the channel, which will be discussed in the unloading section of this chapter. This also means that automated multi-throughput screening is not possible. The inlet channel must be wide enough to allow free crawling motion of the larva to assist in movement of the larva to the opening of the immobilization trap but must be narrow enough to fit within the narrow constraints of the outer walls of the device. Additionally, the channel must be able to tolerate a pneumatic loading pressure of 0.8 bar [58], and be able to form a tight seal with a luer-lock connector for applying this pressure uniformly. In order to accommodate all the design constraints a suitable channel size of 1 mm x 2 mm with a wall thickness of at least 1.5 mm was determined. The minimum wall thickness ensured that the surface area of the bonded interface is large enough to tolerate the loading pressure.

3.2.4 *Device-mounting apparatus design*

The primary design criteria for the mounting apparatus is that it should be compatible with the existing sample mounting equipment for the light-sheet microscope. There should not be any additional tools required for use, and any operator should be able to assemble the components readily. A 1 mL syringe is set into the microscope, and the additional mounting apparatus, a machined piece of acrylic, is attached to this syringe from within the imaging cavity, shown in

Figure 3.4(a). The acrylic attachment was designed in SolidWorks CAD Software and machined, shown in **Figure 3.4**(b). The attachment point of the mount to the microscope suspension mechanism must be a tightly fitted joint that will not require extra stabilization and is readily reversible for switching between specimens for imaging, as shown in **Figure 3.4**(c). Due to space constrictions within this microscope, the imaging chamber should be removed from the internal cavity of the microscope during device attachment, and then replaced gently. The chamber is shown inserted to the microscope in **Figure 3.4**(d)-(e). This imaging chamber was not present in **Figure 3.4**(a). The imaging chamber itself is a small cube, approximately 1.5 cm x 1.5 cm x 1.5 cm. The design included threading for thumbscrews to be placed to fix the device into the attachment at the base and was fitted onto the end of the 1 mL syringe with only slight pressure and no need for additional fixation or adhesion. This point of attachment is also easily reversed, simplifying the mounting procedure for the user of the device. The syringe should be cut at the 0.35 mL mark – this ensures the syringe is long enough that the acrylic connector can be attached to the syringe when pre-mounted inside the microscope, and short enough that the microfluidic device of length 4.0 cm that will be attached to the connector is can be moved lower to be in line with the objective, as shown in **Figure 3.4**(a). It is also important to monitor the position of the attachment fixation screws to ensure they are not able to damage the imaging chamber or other microscope components.

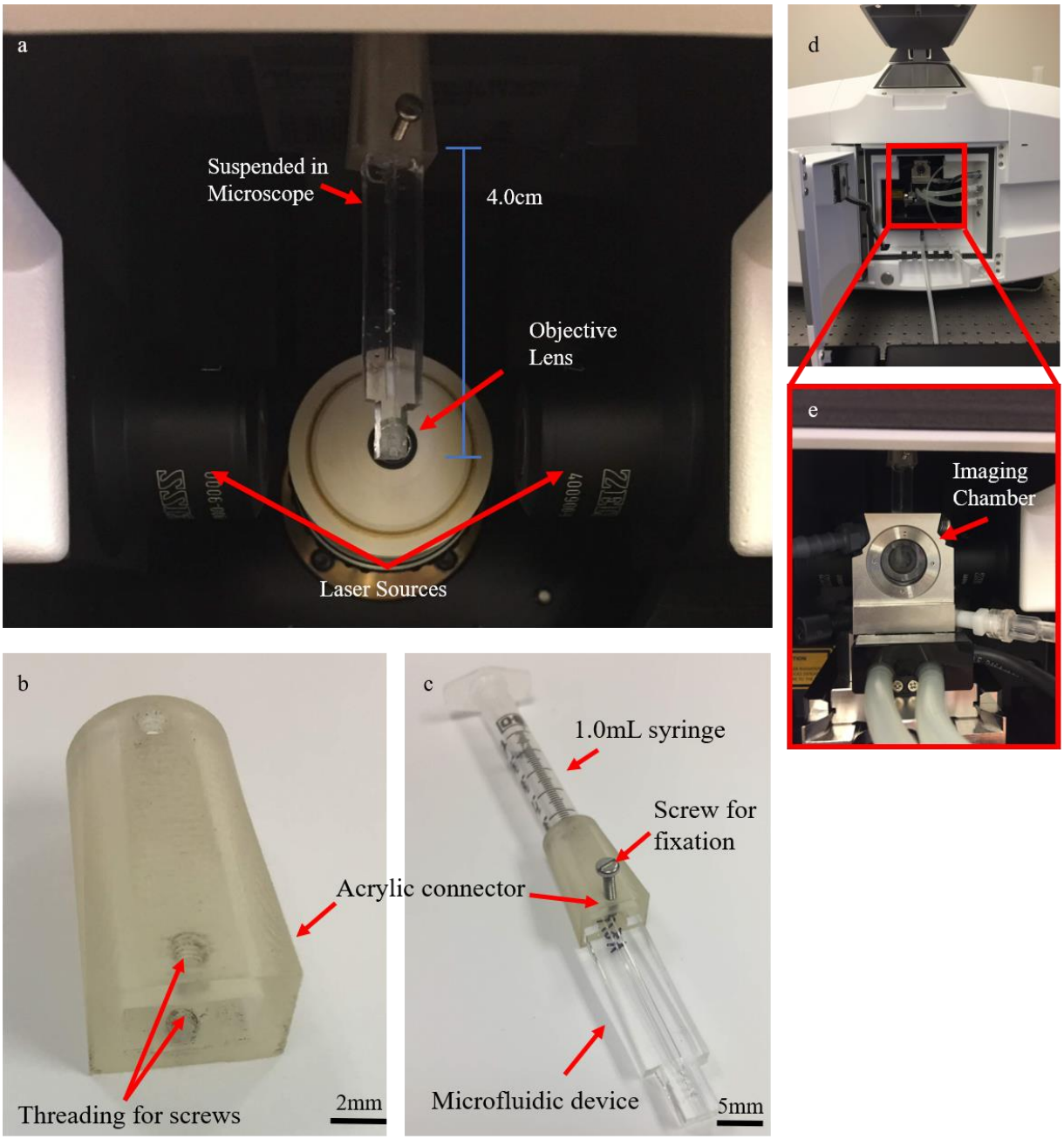

Figure 3.4 Design of apparatus for mounting the device in the light-sheet microscope. (a) The assembled mounting apparatus within the light-sheet microscope. (b) Magnified view of the machined acrylic mounting attachment. (c) Assembly of the attachment to the microfluidic device and 1.0 mL syringe used for mounting. (d) Light-sheet microscope with open compartment doors. (e) Expanded view of the internal imaging chamber illustrating the need for the design criteria.

3.2.5 *Device wall design to facilitate fluorescent microscopy*

Two factors are important for the design of the immobilization region of the device. They include the choice of the material and the wall thickness of the device at that location through which imaging is to be done. Traditional suspension of samples in a light-sheet microscope involves the embedding of the materials in 1 %-2 % agarose gel. Samples are drawn into a capillary tube or small cut-off syringe using a gentle suction force applied with a plunger, or alternatively can be placed in the desired orientation with a pair of forceps. The diameter of capillary selected should be based on the diameter of the specimen; the specimen should take up no less than 1/3 of the diameter of the capillary and no more than 2/3. This technique was used to obtain control images of *Drosophila* larvae central nervous systems, but a live specimen embedded in the agar is not restrained and can burrow, generating motion artifacts in the image, the problem this project was designed to rectify.

The appropriate material should possess similar refractive properties as agarose gel. The use of a polydimethylsiloxane (PDMS) microfluidic device instead of agarose gel is an ideal substitution for holding the sample because the refractive index of these materials is similar, and more importantly, very close to that of water, the medium used to fill the imaging chamber. Similar refractive index (n) values for the different mediums the light must pass through is ideal to prevent refraction across medium interfaces, and can be illustrated with Snell's law [78]:

$$n_1 sin\theta_1 = n_2 sin\theta_2$$

[Equation 3.1]

where n_1 is the refractive index of medium 1, $n_2$is the refractive index of medium 2, $sin\theta_1$ is the angle of the incident light from the normal plane in medium 1, and $sin\theta_2$ is the angle of the light from the normal after it passes across the medium interface into the second medium. Matching the refractive indices of two mediums as closely as possible (such as water and PDMS) will minimize the refraction of the light as it passes through the medium interface.

The thickness of PDMS surrounding the immobilized larva is also relevant. A limitation in imaging of large samples is the thickness of tissue to be passed through by the incident light. While the use of a light sheet microscope improves the illumination of the fluorophores and allows for imaging of thicker tissue samples than conventional confocal microscopy, the *Drosophila* larva is quite large, ~1 mm in diameter, and imaging of the central nervous system will require passing the incident light through several hundred micrometers of tissue in addition to any PDMS surrounding the sample. Given a fixed light wavelength and numerical aperture of the objective, the focal length of the objective is fixed at a certain distance from the surface of the objective lens. The PDMS layer must be thin enough to not prevent the sample region of interest from reaching the spatial position of the focus of the microscope, but must be thick enough to be able to tolerate the loading pressure of the microscope. It was found that 1 mm thick PDMS walls were ideal for imaging and were able to tolerate the loading pressure well. Thinner layers would rupture at the narrowest regions of the channel, and thicker would prevent the microscope from focussing on the region of interest due to spatial constraints. For light-sheet microscopy, the device itself moves laterally inside the microscope when shifting between different planes in a z-stack image. For multi-side imaging, the device must be able to rotate

freely within the imaging chamber without interfering with the chamber walls or the internal structures of the microscope. These factors led to a proposed maximum device width or thickness of less than 0.5 cm, and a net length of the device of 4-5 cm to prevent interference with the imaging chamber.

3.3 Workflow for using the microfluidic device

The microfluidic immobilization device workflow for light-sheet imaging of *Drosophila* consists of 5 main operating steps: loading, immobilization, mounting, imaging, and unloading. First, the 3rd instar larva was selected from a fly vial to be imaged and loaded into the device (Step 1, **Figure 3.5**). Once the larva was in the immobilization region and secured, the device was mounted onto the microscope (Step 2, **Figure 3.5**). Neuronal imaging of the larva was then conducted (Step 3, **Figure 3.5**). Following completion of neuronal imaging, using a sCMOS camera, (Step 4, **Figure 3.5**), the device is unmounted from the microscope and the larva unloaded (Step 5, **Figure 3.5**). The following section explains the experimental setup and procedures for each of these steps.

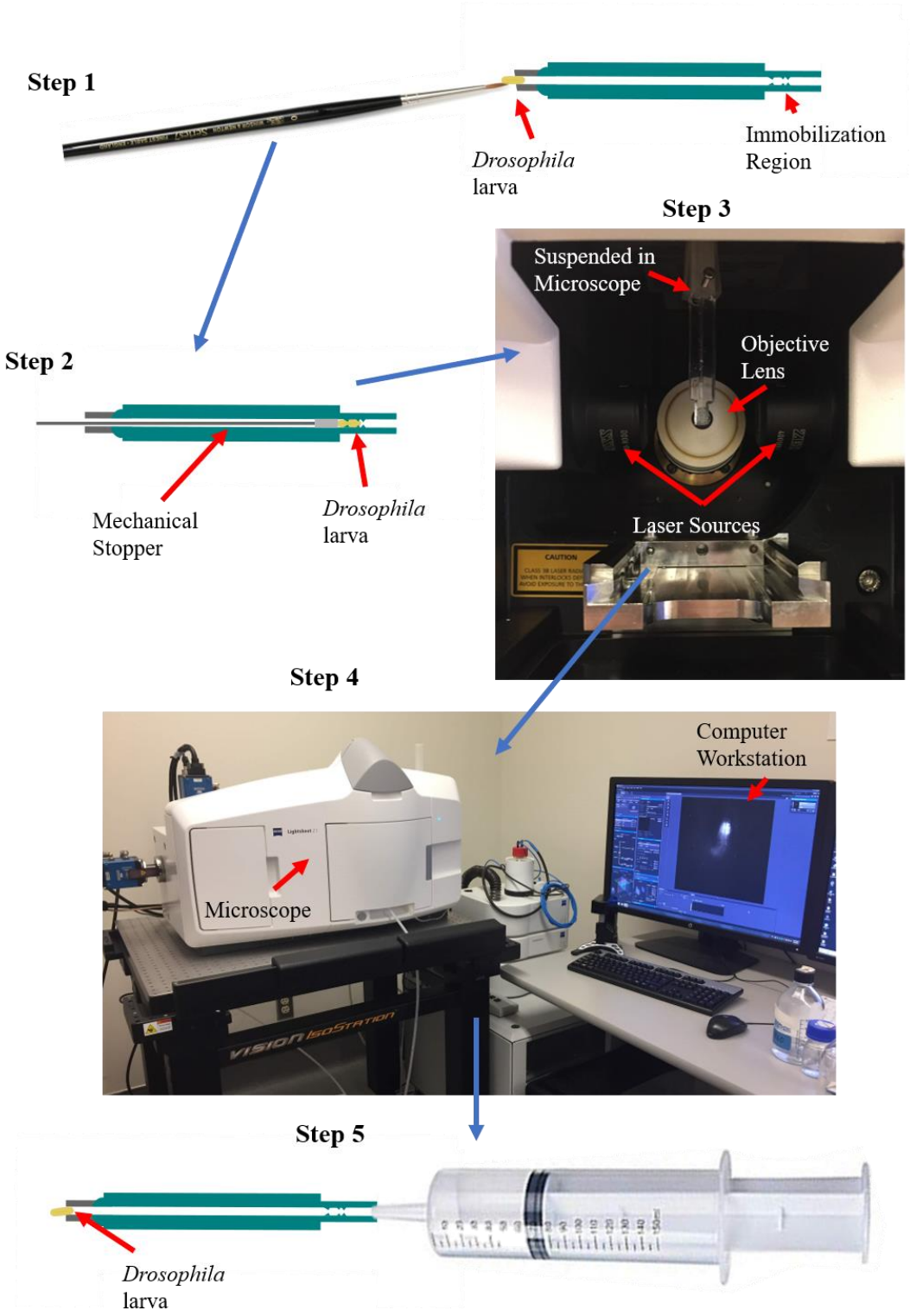
Step 1
Drosophila larva
Immobilization Region
Step 2
Mechanical Stopper
Drosophila larva
Step 3
Suspended in Microscope
Objective Lens
Laser Sources
Step 4
Computer Workstation
Microscope
Step 5
Drosophila larva

Figure 3.5 Overall conceptual design of the neuronal imaging process using the light sheet microscope. (Step 1) Loading, (Step 2) Immobilization, (Step 3) Mounting, (Step 4) Neuronal imaging and (Step 5) Unloading. Blue arrows indicate sequence of steps.

3.3.1 *Drosophila Loading Procedure*

The loading procedure for preparing a larva for imaging consisted of 5 steps. First, a microfluidic device was selected, and a fluidic interconnect attached to a 20 mL syringe was inserted to the inlet port. DI water was washed through the device to prepare it for larval insertion (Step 1, **Figure 3.6**). Next, a 3rd instar larva was removed from the vial with a moistened fine paintbrush and rinsed in DI water to remove any remaining food particles from the larval body (Step 2, **Figure 3.6**). The larva is then inserted to the inlet port gently using the paintbrush, with the head of the larva directed toward the immobilization region of the channel (Step 3, **Figure 3.6**). The fluidic interconnect was reinserted to the inlet port and gentle pressure was applied with the syringe to move the larva toward the immobilization region. When the larva head was at the entrance of the primary pinning gate, a pressure of 0.86 ± 0.17 bar was applied to fully move the larva to the appropriate position in the immobilization channel (Step 4, **Figure 3.6**). A 1.5 mm diameter mechanical stopper was then threaded into the device through the inlet channel to rest gently against the tail of the larva and prevent the escape and subsequent evacuation of the device of the animal (Step 5, **Figure 3.6**). For more precise pressure control, a peristaltic pump or syringe pump can be used, but manual control of the pressure using the syringe was found to be adequate for ensuring proper loading of the larvae.

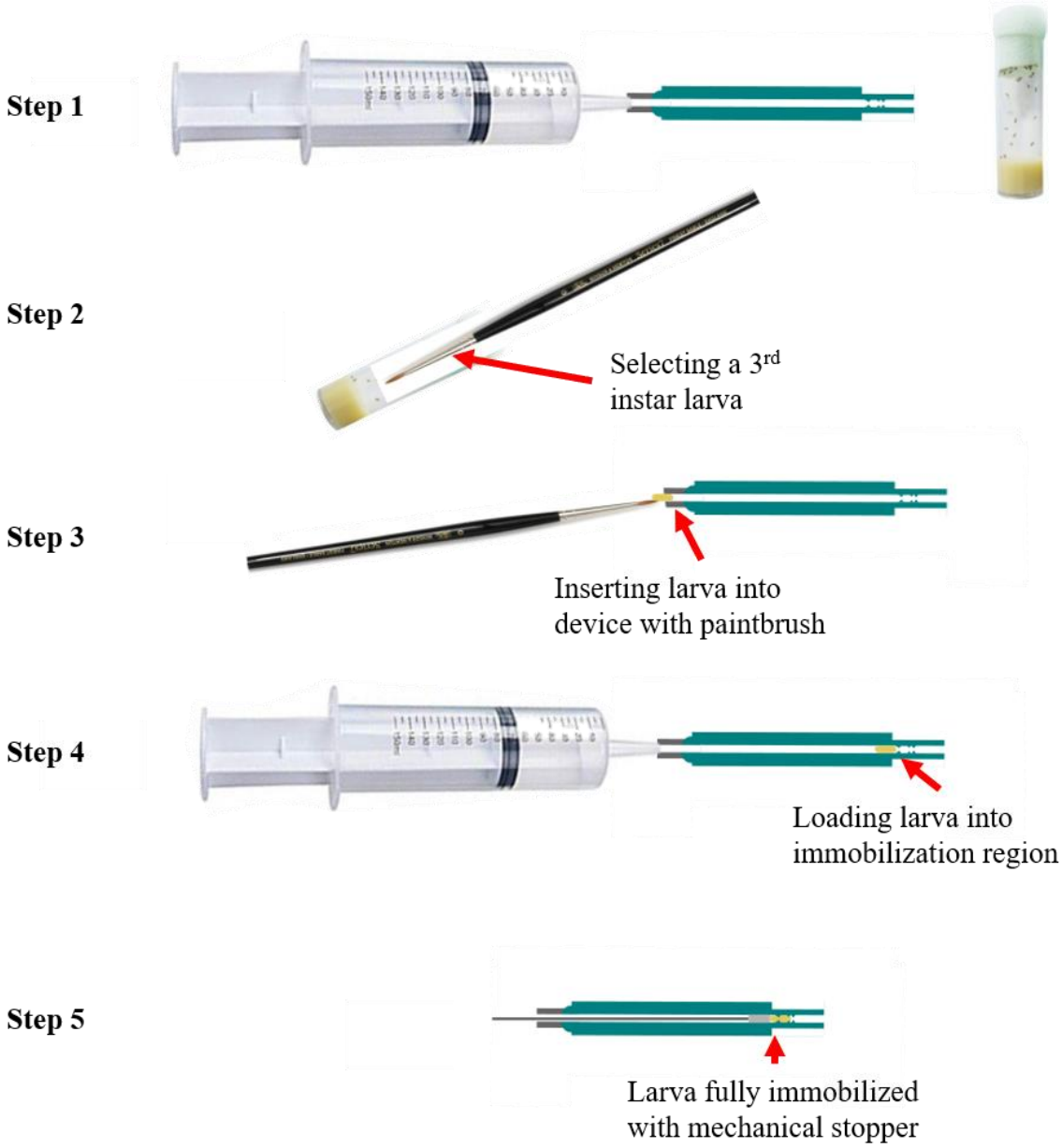

Figure 3.6 Loading procedure for imaging *Drosophila* larvae. (Step 1) Device was rinsed with DI water to prepare for loading. (Step 2) A 3rd instar larva was selected from the vial with a small paintbrush. (Step 3) The larva was inserted to the inlet channel with the paintbrush. (Step 4) The larva was pushed into the immobilization region of the channel using the DI water syringe. (Step 5) A mechanical stopper was inserted to the device to prevent the larva from escaping the immobilization region during imaging.

3.3.2 *Drosophila Unloading*

Ejection was conducted with the same fluidic interconnect and syringe containing DI water as in the device loading section, but insertion of the connector occurs at the opposite end of the device. The syringe and interconnect were inserted at the outlet port were used to apply gentle pressure to the channel (Step 1, **Figure 3.7**) until the larva moved backwards out of the immobilization region into the inlet channel. The pressure was applied until the larva moves completely out of the device (Step 2, **Figure 3.7**). The larva can then be returned to a vial of food or disposed of appropriately. A schematic representation of the unloading process is shown in **Figure 3.7**.

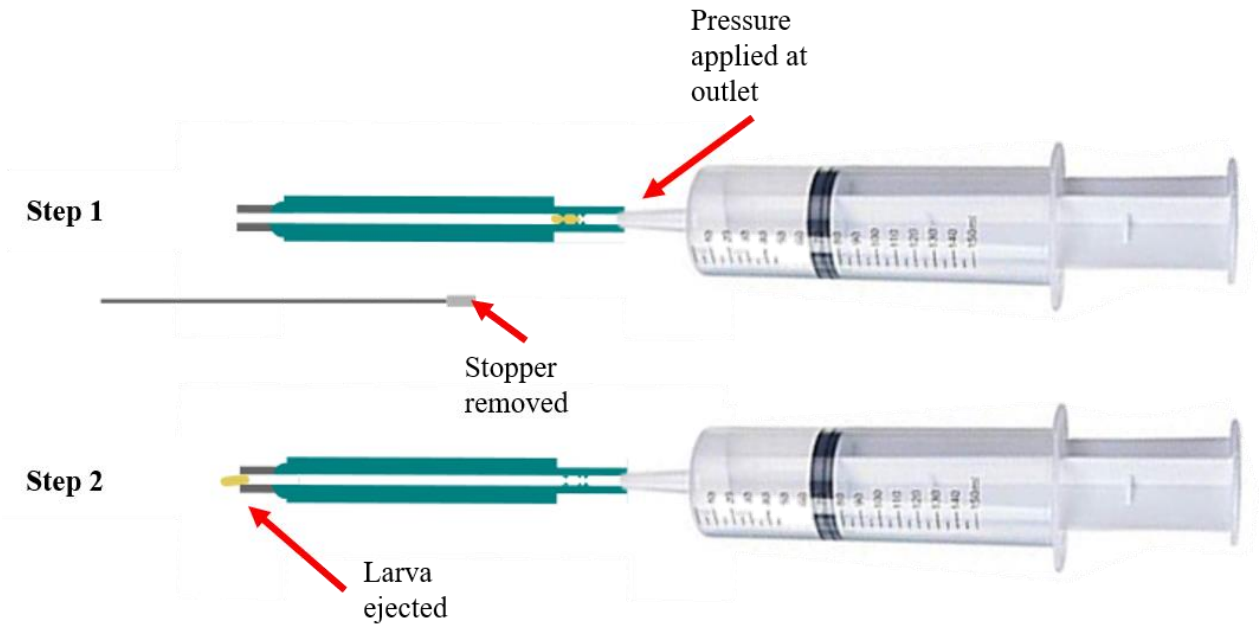

Figure 3.7 Unloading procedure for device. (Step 1) DI water in a syringe is used to apply pressure to the outlet port after removing the mechanical stopper. (Step 2) The larva is ejected via the inlet port and can be placed in a separate vial for observing recovery or returned to original vial.

3.4 Experimental Methods

3.4.1 *Animal Preparation*

The strain of *Drosophila melanogaster* used for this study were of the genotype w, Cha-Gal4/CyO; UAS-GCaMP5/TM3, Sb. The GCaMP5 GECI expression pattern was driven by the transgene *Cha-Gal4*, the promoter of the gene choline acetyltransferase (Cha) which induced the expression of the Gal4 transcription factor, and the *UAS-GCaMP5* transgene which included the binding site for this Gal4 transcription factor, such that the larva expressed the GCaMP5 calcium sensor in all genes expressing the choline acetyltransferase gene [10], [63], [79]. This was phenotypically expressed as calcium indicators being present in all cholinergic neurons. Third instar larvae were identified prior to imaging and brought to Mount Sinai Hospital where the light-sheet microscope was located. Loading of animals into the devices occurred at this laboratory location immediately prior to imaging.

3.4.2 *Excision of Larval Brain for Control Imaging*

The larva, in DI water under a dissecting microscope, was pinched using fine dissecting forceps at the mouth region and approximately 1/3 of the body length away from the mouth, and gentle pressure was applied until the body separated into two pieces. The rear portion of the larva was set aside, and the brain lobes and ventral nerve cord identified within the remaining tissue. Fatty tissue, skin, and other organs were gently scraped away from the brain tissue until just the lobes and ventral nerve cord remained. Warm, uncured agarose gel was then poured over the brain and

the tissue and agar were gently drawn up into a 1mm diameter capillary tube and allowed to cure. This preparation represents the current neuronal imaging technique used for *Drosophila* GECI imaging with high temporal resolution. The hemolymph filled body has been removed and the agar surrounding the tissue minimized, but while high resolution is possible, this preparation does not represent a true physiological response, as the brain is no longer within the larval body.

3.4.3 *Pressure Testing of Devices*

To investigate the tolerated pressure in the microfluidic devices, the outlet port of the device was sealed, and the device was attached to a three-way fitting. A syringe filled with water was attached opposite, and a 1.5 bar pressure transducer was placed at the third position. Pressure was manually applied to the device via the syringe gradually, at a rate of ~0.1 bar/s, while recording quantitative data using the OMEGA pressure transducer software. The layout of this testing setup is shown in **Figure 3.8** below.

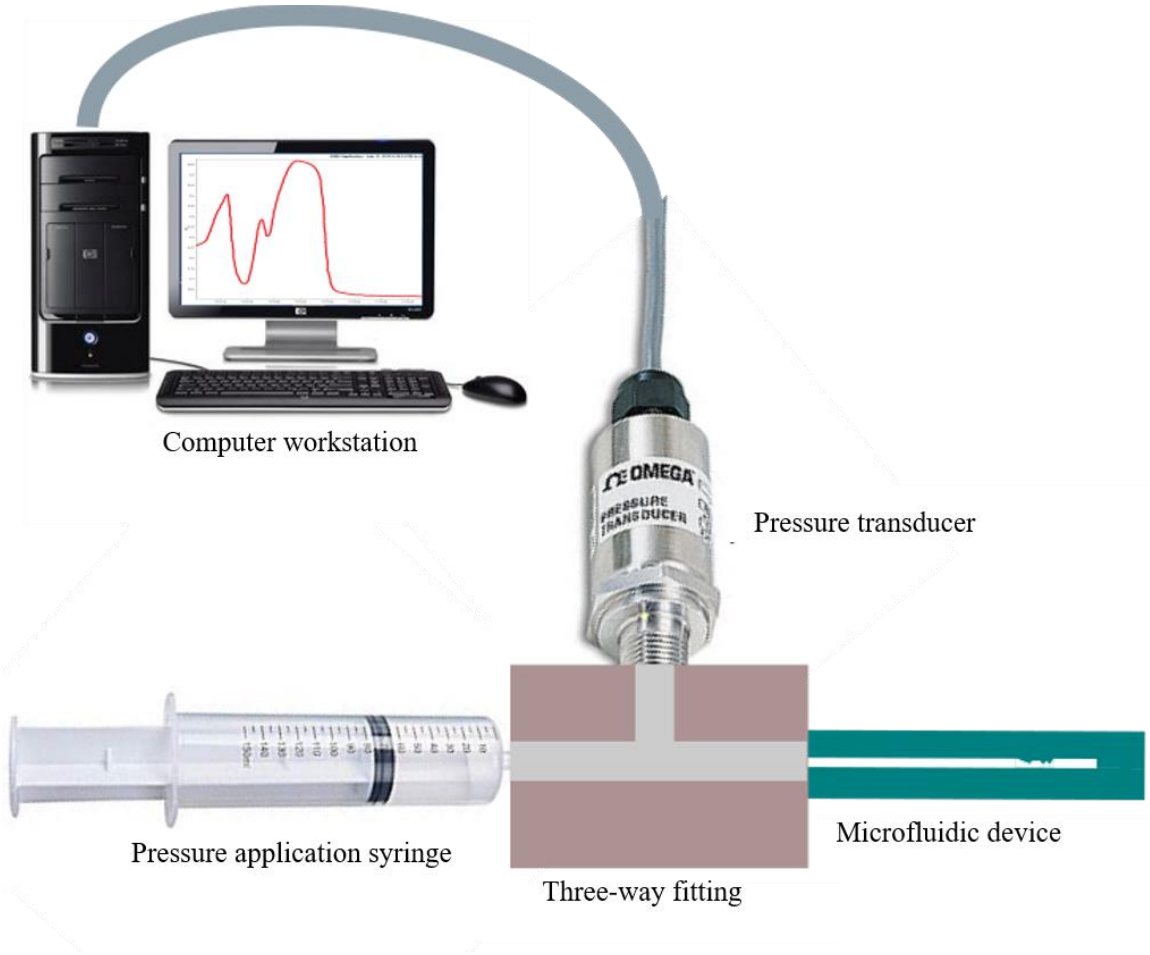

Figure 3.8 Experimental setup for measuring pressure tolerance of the microfluidic device.

3.4.4 *Neuronal Imaging*

The experimental methods for neuronal imaging included 5 primary steps. First, the mounting apparatus was assembled and attachment to the microfluidic device was tested (**Figure 3.9**, Step 1). The mounting apparatus was then inserted through the top door of the microscope and aligned. The microfluidic device remained attached to the connector, which was inserted through the side door of the microscope, and the connector was reattached to the syringe of the mounting

apparatus (**Figure 3.9**, Step 2). The media chamber was then inserted to the microscope and aligned with the lenses, and the microfluidic device suspended within the chamber (**Figure 3.9**, Step 3). The media chamber was then filled with DI water and the doors of the microscope are closed (**Figure 3.9**, Step 4). Neuronal imaging was now conducted using the positioning controls and the computer workstation (**Figure 3.9**, Step 5). The incident light sources were two 30 mW, 488 nm lasers, set to the lowest intensity possible for each individual trial. This was in the range of 1-3 % for the agar-embedded excised brains, dead larvae, and the larvae within the microfluidic devices. The lasers are mounted on opposite sides of the imaging chamber (**Figure 3.9**, Step 2 identifies the laser sources) and only one source was illuminated at a time. The image is acquired (by a sCMOS camera) at each z-slice twice, once from the left laser illumination and once from the right, before the sample moves 1-2 μm to align the next slice with the light-sheet path. The process was repeated until the entire volumetric stack was acquired. Reconstruction of the left and right illuminated z-stacks is conducted using the ZEN lite software, creating a DualSide Fusion image stack.

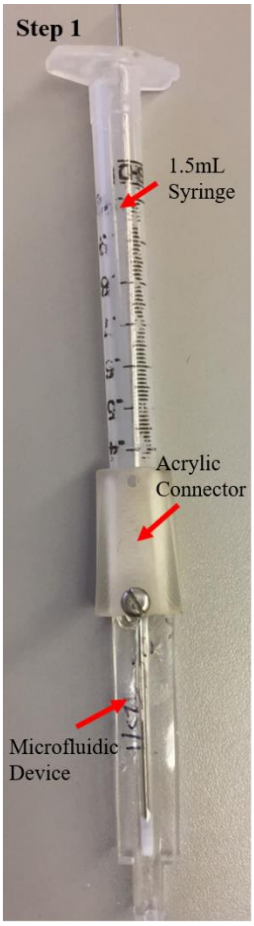
Step 1
1.5mL Syringe
Acrylic Connector
Microfluidic Device

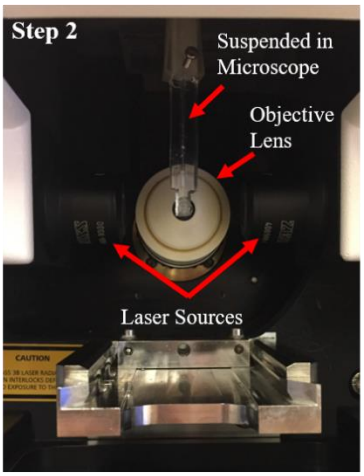
Step 2
Suspended in Microscope
Objective Lens
Laser Sources

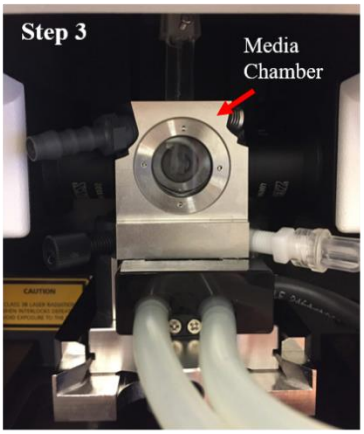
Step 3
Media Chamber

Step 4

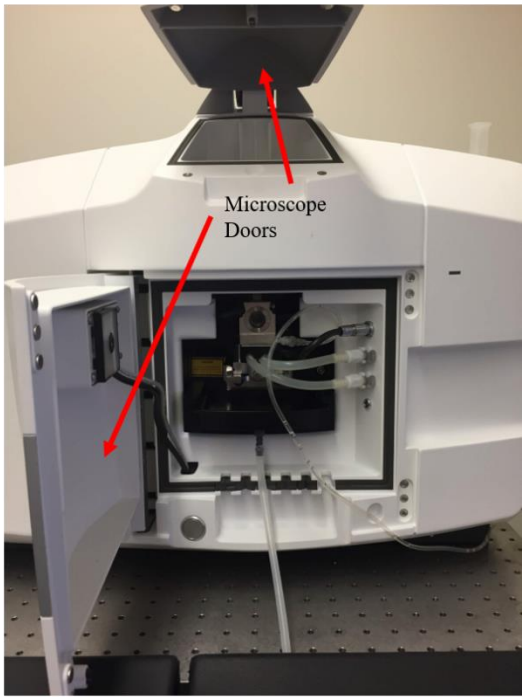
Microscope Doors

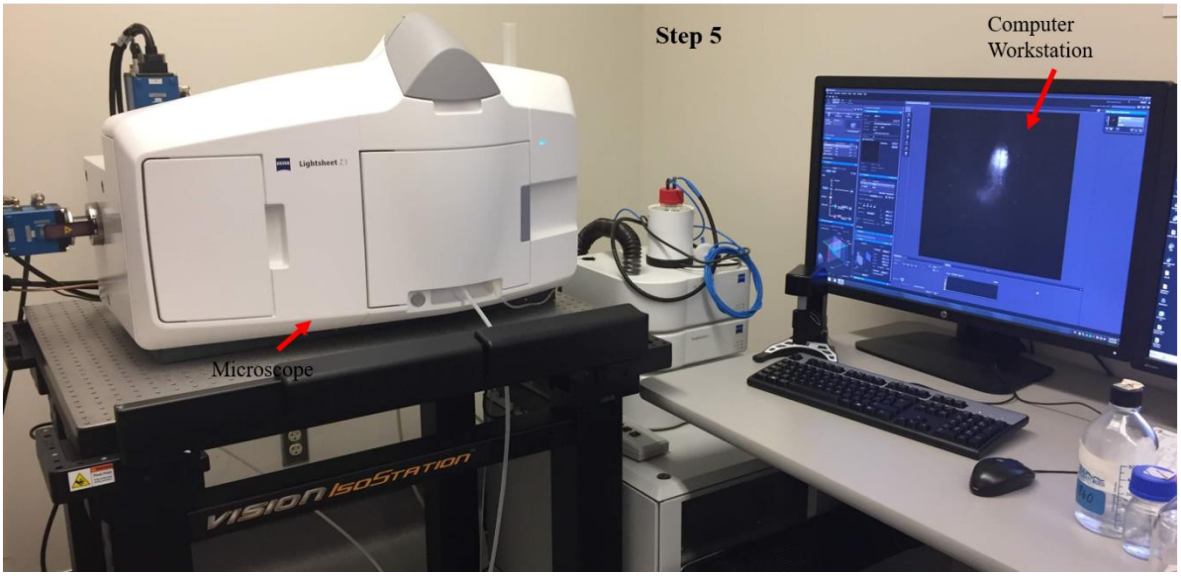
Step 5
Computer Workstation
Microscope
VISION IsoStation

Figure 3.9 Neuronal imaging procedure. (Step 1) The microfluidic device was attached to the mounting apparatus, (Step 2) and the device is mounted in the light sheet microscope. (Step 3) The media chamber is inserted to the microscope (Step 4) and the chamber is filled with water and the doors of the microscope are closed. (Step 5) The microscope is prepared for imaging and proper orientation and focusing can be conducted using the workstation for image acquisition.

3.5 Summary

This chapter introduced the proposed microfluidic device design and operation parameters, as well as the advantages of using this device as an alternative to other methods of live neuronal imaging in *Drosophila* larvae. This device will maintain the strong immobilization ability demonstrated by other devices, while allowing for image acquisition to occur more rapidly and prevent premature photobleaching or phototoxicity. The unique design will also allow for imaging to occur from multiple sides of the larva. The next chapter will discuss the fabrication of the microfluidic device.

4 Device Fabrication

4.1 Introduction

The design criteria for this device and the conceptual design were discussed previously. This chapter discusses the evolution of the fabrication process in order to achieve the design criteria. The initial iteration (Iteration I) used existing, well-characterized microfluidic fabrication techniques in order to produce the device geometry and meet the design criteria. Iteration I was unable to tolerate the pneumatic pressure required to load a 3rd instar *Drosophila* larva to the immobilization region, making this iteration inappropriate for the application. The fabrication process was modified in Iteration II which used a novel sacrificial template in order to produce the intended 3D shape required inside the microfluidic device. The sacrificial material used was not able to be completely extracted from the PDMS cast around the material, and as a result the device did not provide the optical clarity required to allow for high resolution images to be obtained by the microscope. The next version (Iteration III) used a different type of bonding, called adhesion-assisted plasma bonding, to form the required device and meet all needs of this project.

4.2 Fabrication

Developing the fabrication process flow for this uniquely shaped microfluidic device required adaptation of existing fabrication techniques currently used. First, as the desired device is an elongated rectangular prism or cylindrical shape, the traditional bonding of a PDMS cast channel

structure to a flat surface like a microscope slide may not appropriately meet the needs of the application. Second, to create an outer surface of the device with a uniform curvature, the PDMS needed to be cured with molds shaping all sides of the device, not just a single face for the channel.

4.2.1 *Iteration I*

A soft lithography fabrication approach was used to create the device. This process consisted of six steps. First, a mold containing the desired 3D features of the inside surface of the microfluidic device was generated via 3D extrusion printing (Objet24, Stratasys). The 3D mold, in addition to the microchannel features, included an outer lip around the perimeter of the mold to allow casting of polydimethylsiloxane (PDMS), and two grooves inset on either side of the channel feature to allow for the placement of two vertical glass slides (25 mm x 75 mm). These glass slides are used to create a smooth outer side wall of the casted microfluidic device and ensure that these walls will be optically clear, and the images obtained through them was free of aberrations and distortions. Next, PDMS was poured into the mold around the vertical glass slides (**Figure 4.1**(a)). Upon curing (**Figure 4.1**(b)), the glass slides were gently removed and the PDMS cast was extracted from the mold. The PDMS channel and a second, long rectangle of PDMS were placed in an oxygen plasma cleaner and treated for 90 seconds on high at a pressure of 250 torr (**Figure 4.1**(c)). The treated surfaces were aligned and adhered (**Figure 4.1**(d)), then placed on a hot plate at 90 °C for 60 minutes, following which the ends of the device were then trimmed away with a no.11 scalpel blade to open the inlet and outlet ports, into which the larva is

loaded and pneumatic pressure is applied. The device was then ready to be used for light sheet imaging of the *Drosophila* larva (**Figure 4.1**(e)).

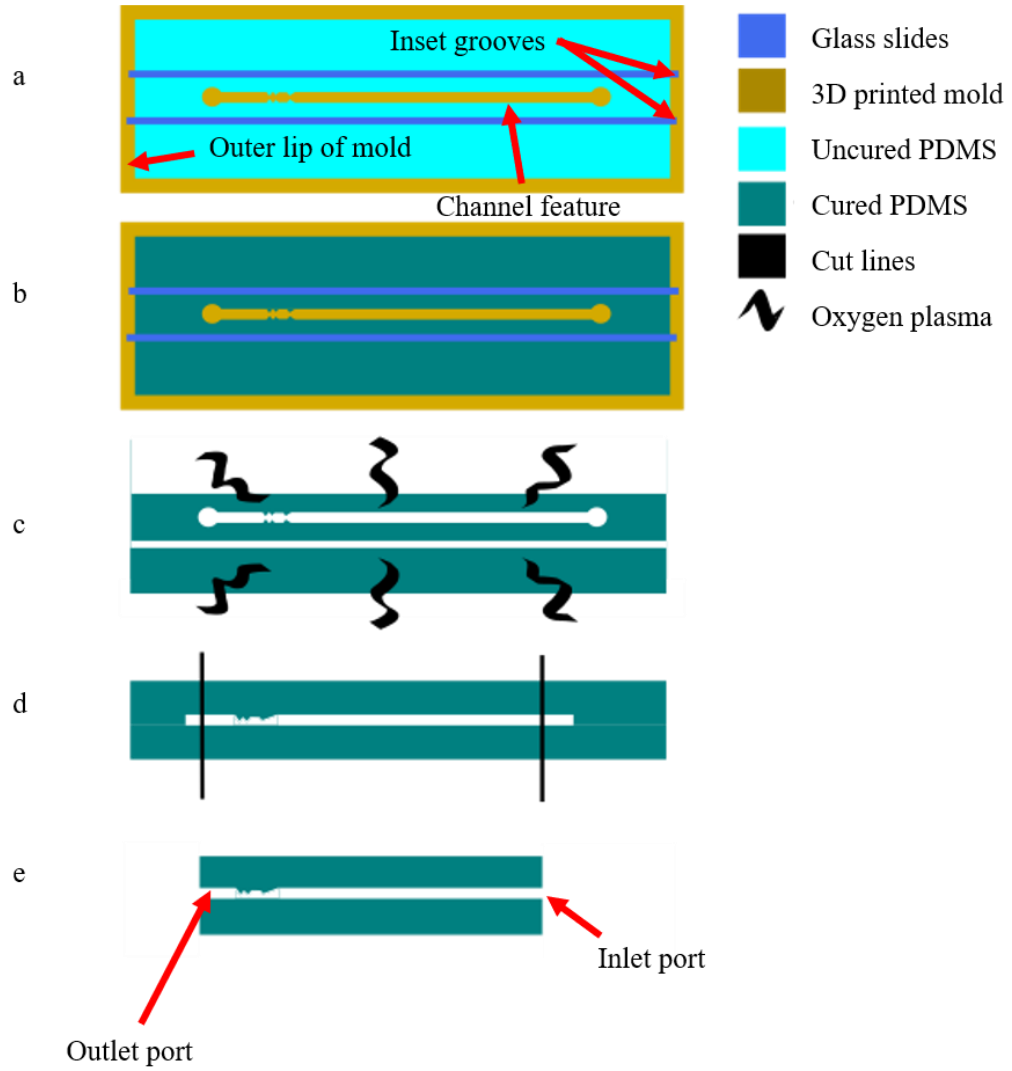

Figure 4.1(a) 3D printed mold and alignment of glass plates within mold during casting of PDMS (b) After PDMS has cured, glass slides are gently removed from the mold (c) PDMS channel and a flat piece of PDMS from the mold are removed and surfaces to be adhered are treated in an oxygen plasma cleaner (d) PDMS pieces are aligned and adhered, and compressed with a weight on the hot plate for 1 hour for stronger adhesion (e) trimming of excess PDMS from ends of device to open up the channel inlet and outlet ports, where fluidic interconnects can be inserted for pneumatic loading.

While the design of this device iteration was sound, two unexpected sources of error were encountered. The primary of which was the problems with the surface treatment of the PDMS using the oxygen plasma. As previously characterized by this research group, the device must be able to withstand a continuous loading pressure of 0.8 bar [58], but the bonding was not able to tolerate this pressure consistently, instead rupturing along the interface or displaying existing leaks along the interface. It was suspected that this low pressure-tolerance at the interface is related to the decreased surface area being bonded in these devices compared to other microfluidic devices in literature. More discussion related to this bonding problem can be found in Chapter 5: Device Characterization and Results. The second, less significant error came about from the PDMS-glass contact during the casting process. Due to the surface tension of the PDMS, a concave interface was formed when the PDMS was casted into the mold between the glass slides. This resulted in a non-flat top surface which was not ideal for imaging purposes. It prevented proper positioning of the device in the microscope during imaging, as the device could not be moved close enough to the objective to align the focal plane with the larva CNS position if the concave side was facing the objective. This was not appropriately rectified by removing the excess PDMS from the edges, nor using different types of glass slide, or by alternative PDMS dispensing techniques.

4.2.2 *Iteration II*

In order to address the limitations of the previous fabrication method, a new approach was conceived where bonding of the device was eliminated. Several groups have used sacrificial materials such as carbohydrate sugar matrices to create vascular networks in cell-hydrogel

mixtures [80], [81]. In these applications, the sacrificial material is broken down by the cells themselves and its dissolution leads to formation of a hollow channel. Alternatively, metals have also been used as sacrificial materials to create unique three-dimensional designs, using solvents to dissolve the metal and evacuate the channel space [82]. Operating on the principle of using a sacrificial template instead of bonding two pieces of PDMS together, a new fabrication approach was designed. A sacrificial template was created in the shape of the 3D microfluidic channel. PDMS was then cast around this sacrificial template and the sacrificial template was dissolved following curing of the PDMS.

The selection of an appropriate material for the sacrificial template was important. Various materials were tested to determine the most suitable one to serve as this material. The ideal substrate, as described in Chapter 3, must accommodate the design criteria of the microfluidic device. This means the substrate should be readily manipulated and cast into the shape of the channel using a sacrificial template PDMS mold of the channel shape. The substrate should also be structurally stable such that it can be removed from the sacrificial template PDMS mold and be moved around during the fabrication process without breaking. The substrate should retain, with high resolution, the fine details of the pinning region of the channel following removal from the sacrificial template PDMS mold. Additionally, the solvents used to remove the template must be biologically inert so as not to harm the *Drosophila* larva when being imaged. Finally, after the sacrificial material is removed from the sacrificial template PDMS mold, the remaining microfluidic device should retain the optical clarity required to obtain high resolution images of the fluorophores in the *Drosophila* central nervous system.

The first material tested was carbohydrate glass adopted from the procedure from Miller et al. [80]. The glucose/sucrose mixture was an ideal material because it was not toxic to organisms and was transparent, but casting of the sugar into the sacrificial template PDMS mold was difficult. The hydrophilic sugar did not wet the hydrophobic PDMS mold properly which made the complete filling of the mold difficult to achieve. To correct this issue, the PDMS surface was treated with oxygen plasma to increase hydrophilicity, which assisted in the filling of the hollow PDMS mold (**Figure 4.2**(a,b)). Despite appropriate filling with the plasma treatment, however, the hygroscopic character of the sugar substrate made it quite soft at room temperature, and if not used immediately, it subsequently lost the intricate 3D features embedded in it over time.

Next, a different sugar, pullulan, was used. This material shared the beneficial attributes of the glucose/sucrose mixture, such as low toxicity and solubility in water, but was more readily dispensed into the desired channel shape. However, upon evaporation of the water in the sugar mixture, the volume of the pullulan shape changed significantly, resulting in a thin film instead completely filling the hollow channel mold. This issue remained following treatment of the PDMS mold with oxygen plasma as well (**Figure 4.2**(c,d)). These thin films were not able to be removed from the PDMS molds.

Finally, paraffin wax was investigated as potential sacrificial material. This material was readily cast into the channel shape because of the shared hydrophobicity of paraffin and PDMS. However, the solid wax could not be extracted without damaging the shape of the pinning region of the channel (**Figure 4.2**(e). This was due to the small 100 µm x 100 µm feature of the stopper gate, where the thin wax connection was not strong enough to maintain the structure without

breaking. Breakage also occurred at the primary and secondary gates in some cases. To overcome this limitation, a fine copper wire (5 cm x 100 µm diameter) was introduced to strengthen the wax in the narrowest regions of the channel. 80 µL of wax filled the channel completely and was easily extracted from the PDMS mold (**Figure 4.2**(f)). The wax was stiff enough that with minimal risk of breakage it could be readily manipulated with fine forceps and moved to the next stage of fabrication.

The fabrication process flow consisted of 9 steps. First, PDMS was cast into the grooved 3D printed mold from the fabrication process for Iteration I (**Figure 4.3** (a)). This PDMS was cured and then removed from the grooved 3D printed mold and placed on a hot plate at 110 ºC, forming the sacrificial template PDMS mold (**Figure 4.3**(b)). The 5 cm length of copper wire is placed inside the sacrificial template PDMS mold (**Figure 4.3**(c)) and 80 µL of pre-warmed paraffin wax was loaded into the PDMS channel using a 20 µL pipette (**Figure 4.3**(d)). The sacrificial template PDMS mold was removed from the hot plate and the wax was cured before being removed from the mold by inverting the mold and pinching in half length-wise (**Figure 4.3**(e)). The sacrificial template was then placed into the bottom half of a cylindrical-device 3D printed mold that has a cylindrical shape and two grooves to hold the template above the base of the cylinder (**Figure 4.3**(f)). The top half of the cylindrical-device 3D printed mold was fixed in place with screws at each corner so that a full hollow 3.5 mm diameter cylinder with the template suspended in the middle was formed (**Figure 4.3**(g)). The top half of the mold consisted of 3 holes which were used to inject the PDMS into the mold using a 16 G needle (2 mm diameter hole in centre of mold) and allow air to escape (1 mm diameter holes at left and right) (**Figure**

4.3(h)). Following curing for 24 hours at room temperature, the mold was opened by removing the screws and the microfluidic device and sacrificial template were removed (**Figure 4.3**(i)).

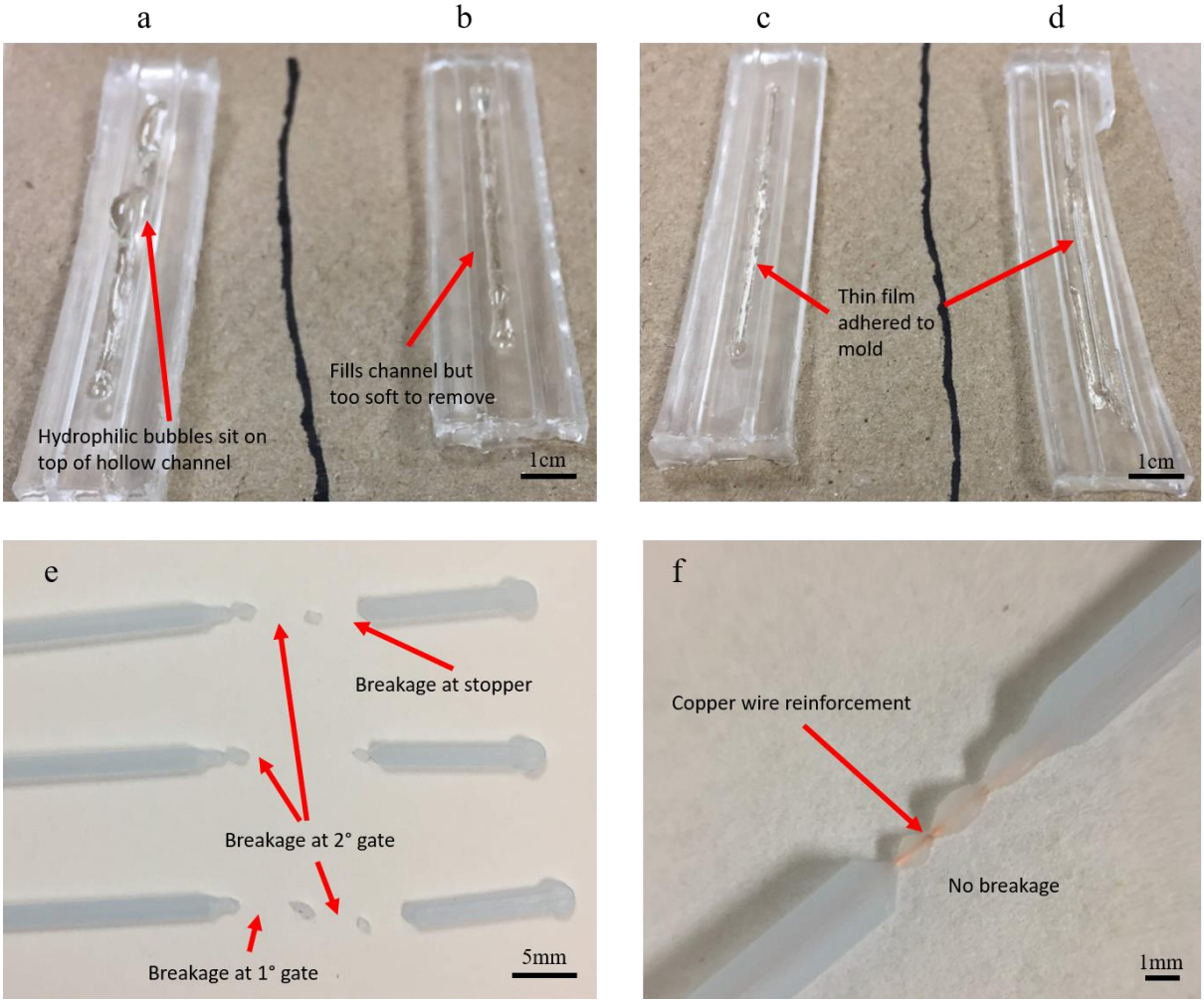

Figure 4.2 Various sacrificial template materials tested to find the most appropriate material for the fabrication application. (a) glucose/sucrose with no plasma treatment to PDMS mold (b) glucose/sucrose with plasma treatment to mold (c) pullulan with no plasma treatment to mold (d) pullulan with plasma treatment to mold (e) wax without reinforcement to prevent breakage (f) wax with copper wire reinforcement.

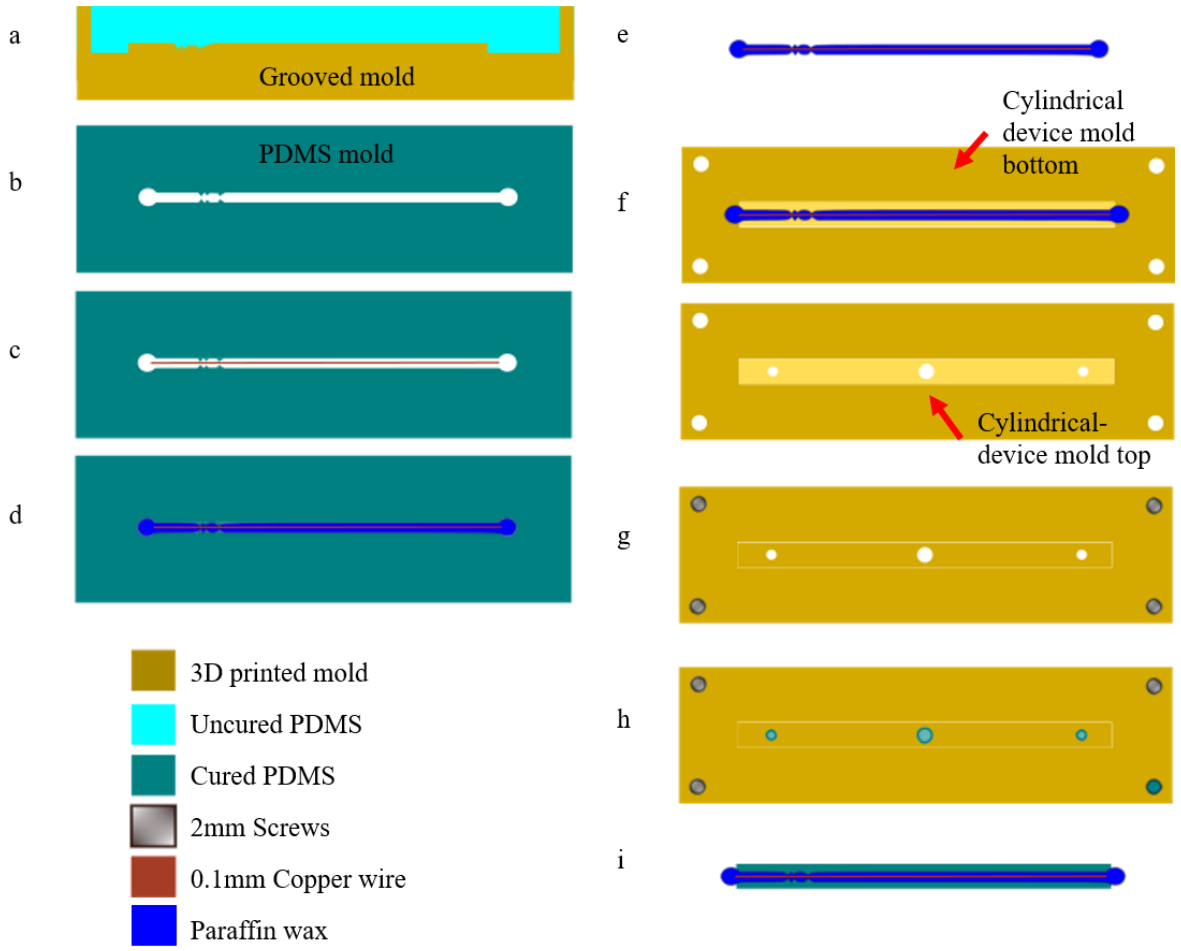

Figure 4.3 (a) Casting of negative channel using 3D printed mold and PDMS (b) Removal of PDMS negative channel, which was then placed on a hot plate at 110 °C (c) 5 cm length of 100 µm diameter copper wire inserted along length of microfluidic channel (d) loading of 80 µL liquid paraffin wax to form sacrificial template (e) after removing PDMS negative channel molds from hot plate, wax solidified to room temperature for 10 minutes and was extracted from cast by inverting mold and pinching in half length-wise (f) 3D printed top and bottom faces for casting cylinder with sacrificial template suspended by mounting in 3D printed bottom face (g) top face fixed to bottom face with 2 mm diameter Phillips-head screws (h) PDMS loaded into device by 16 G needle via centre hole of top mold (i) after completely cured, cylindrical device was extracted for solvation of sacrificial template.

A protocol for wax dissolution was developed from the findings of Lee et al., using a four-step organic solvent substitution process [83]. This protocol is illustrated in **Figure 4.4**. Wax, being

hydrophobic, can diffuse into the PDMS elastomer which has nanoscale pores in it. The dissolution of the wax and subsequent drying at high temperatures led to transport of wax into the PDMS which decreased the transparency of the PDMS significantly. Extraction of the wax using non-polar solvents prevented this issue. Four solvents were selected based on the swelling ratio (S) of PDMS in each solvent [83]. First, the device with the intact sacrificial template is immersed in a 5 mL glass test tube of toluene (S=1.31) and the glass tube is sealed with parafilm. After 6 hours, the toluene is rinsed through the inner, now hollow, channel of the device with an 18 G needle and syringe. The device was then moved to a 5 mL glass test tube of chlorobenzene (S=1.22), the inner channel is rinsed with the chlorobenzene, and the test tube is sealed with parafilm. After 6 hours, the device channel is rinsed with chlorobenzene again, and the device is moved to a 5 mL glass test tube of acetone (S=1.06). The device remains in the acetone for 6 hours, then is moved to an ethanol (S=1.04) test tube for 6 additional hours. Within the first hour in toluene, the device expands readily (swelling ratio of 1.31, [83]) and the wax begins to dissolve into the solvent. Each successive solvent used was slightly more polar than the previous solvent, allowing miscibility of the residual solvent and removal of the more biologically hazardous solvents from the PDMS. Working towards more polar solvents also ensured a slow and uniform de-swelling of the PDMS, given each successive solvent had a smaller PDMS swelling ratio, as the channel could be damaged if this protocol was not in place. Finally, the device was air-dried while suspended to ensure evaporation occurred from all sides simultaneously.

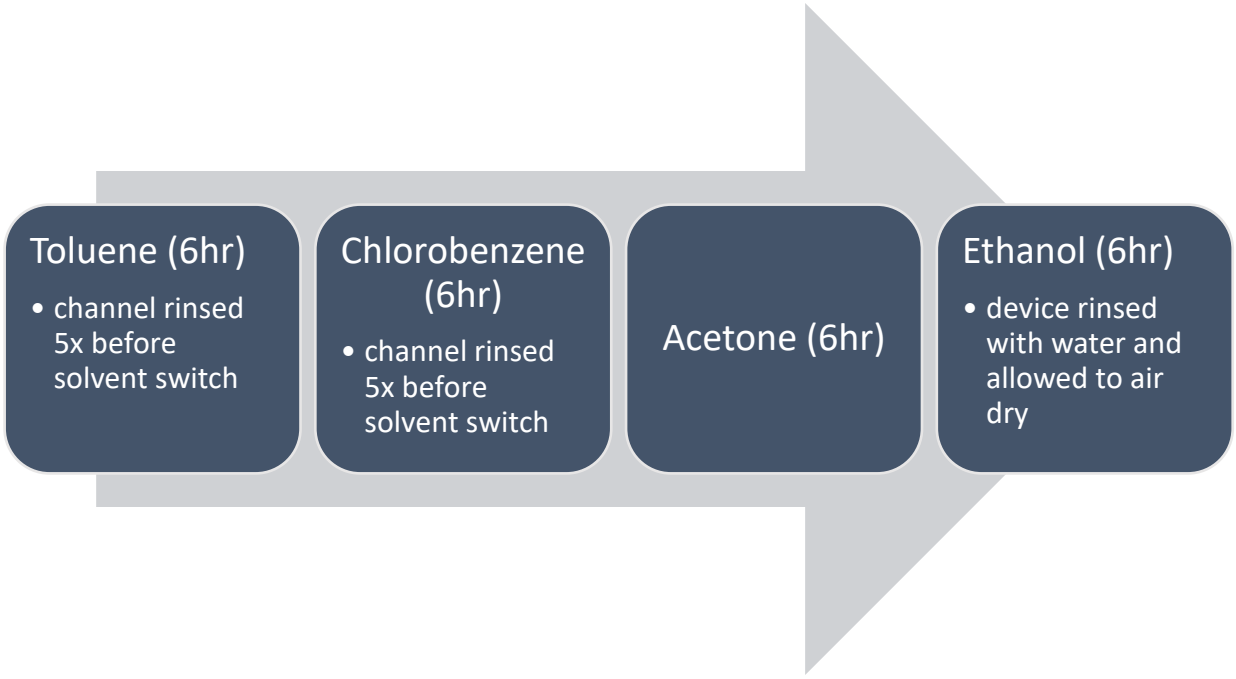

Figure 4.4 Step-by-step solvation process for wax sacrificial template removal from microfluidic device for light-sheet imaging of *Drosophila melanogaster*.

While this fabrication process worked very well and solved several of the limitations in the device described in Iteration I, it was found to be not as optically clear as desired. The decrease in clarity can be attributed to residual paraffin that remain embedded in the PDMS material despite repeated cleaning with fresh solvent. This reduction in clarity blurred some of the fluorescent images. Additionally, autofluorescence of the channel itself around the larva was observed. This autofluorescence is a material property seen in the sacrificial-template device but not in agar or the rectangular devices, indicative of residual wax within the PDMS. Imaging the region of interest in the Iteration II device also required a much higher laser power than agar control images did, likely due to refraction of the incident light upon contact with the wax/PDMS interface of the inner channel wall. This indicates significant loss of signal due to the

material properties of the Iteration II device. Finally, greater laser power shortens the maximum duration of imaging possible due to photobleaching of the fluorophores and phototoxicity to the organism.

In addition to the decreased optical clarity, there were several other limitations to the Iteration II device. The solvent substitution process left the PDMS quite friable due to the removal of the PDMS oligomers that were not completely polymerized, and the device was less tolerant to the insertion of fluidic interconnects. Post processing steps were required to strengthen the inlet and outlet ports of the device and depending on the resolution of the 3D printer used to create the two-part device mold, it was necessary to dip the device in PDMS to smooth the outer surface of the design to ensure the light was able to penetrate the device with minimal refraction. An oven could not be used to shorten the curing time due to the low melting temperature of the sacrificial wax template, lengthening total fabrication time to more than three days, much longer than the previous Iteration I.

4.2.3 *Iteration III*

Since the sacrificial approach did not produce a fabrication process with intended results, a different bonding approach was developed. Since oxygen plasma treatment had proven ineffective for this application in Iteration I, a different approach was taken to prepare the surfaces for bonding in Iteration III, using a handheld corona generator. Additionally, the PDMS was not allowed to fully cure, which enhanced the bonding of the two pieces of PDMS, as in addition to the hydrophilic surface-treatment to improve bonding, the uncured PDMS oligomers

on each piece of PDMS were able to fully cure while in contact with the other piece, allowing for cross-linking of the PDMS pieces to each other. This allowed for the fabrication of devices that were not only optically clear, but also achieved a strong enough bond between the two layers of PDMS that they were able to tolerate the required pneumatic forces for the loading of *Drosophila* larvae.

The fabrication process consisted of six main steps. First, 2 mL of PDMS was poured into a 3D printed mold identical to the grooved mold but without the grooves for the vertical glass slides, instead surrounding the channel with a smooth base. 8 mL of PDMS was cast into a 10 cm diameter plastic petri dish at this same time (**Figure 4.5**(a)). After partially curing for 45 minutes at 60 ºC in an oven, the PDMS was carefully extracted from the molds and the surfaces to be bonded were treated with a handheld corona generator (**Figure 4.5**(b)). The pieces were then adhered and placed on a hot plate for 60 minutes to strengthen the bonding (**Figure 4.5**(c)). Next, the inlet and outlet ports were opened using a no.11 scalpel blade, and the sides of the device were cut down to 2 mm (**Figure 4.5**(d)). A 0.9 mm glass capillary tube was inserted to the inlet channel and a 1 cm piece of silicon tubing (1/16” ID, 3/16” OD) was threaded onto the capillary tube. Uncured PDMS was used to connect the silicon tubing to the PDMS inlet port and cured immediately using a butane torch (**Figure 4.5**(e)). Once cured, the capillary tube was gently removed from the inlet channel and the microfluidic device was trimmed around the region of interest to reduce the thickness of PDMS surrounding the region of interest (**Figure 4.5**(f)).

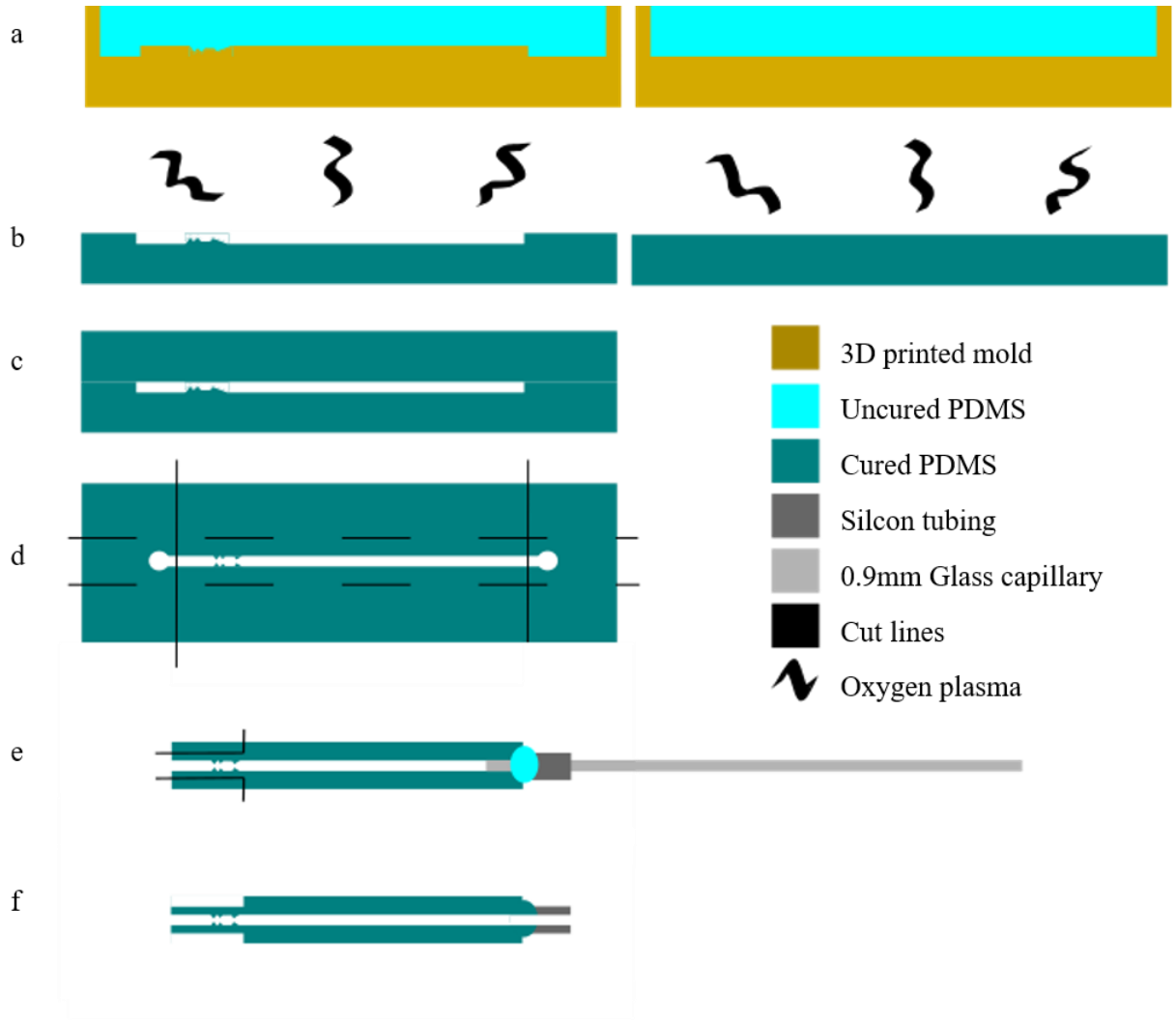

Figure 4.5 Fabrication process flow for partially-cured plasma-bonded PDMS devices. (a) 2 mL of PDMS was poured into an un-grooved 3D printed mold of the microfluidic channel, and 8 mL of PDMS was poured into a 10 cm Petri Dish base (b) the PDMS was allowed to cure for 45 minutes in an oven at 60 °C until almost completely polymerized, then cut out of the molds and the surfaces to be adhered were treated with a handheld corona generator (c) the PDMS was aligned and compressed on a hot plate to ensure strong adhesion for 60 minutes (d) the devices were cut down to a narrow rectangle and the inlet and outlet ports were exposed using a scalpel blade (e) a capillary tube was inserted to the inlet port and a 1 cm length of silicon tubing was threaded and secured to the inlet port using uncured PDMS, which was cured immediately using a butane torch (f) single cuts using uniform pressure were made around the region of interest where the larva will be immobilized, reducing the thickness of PDMS through which the incident laser light enters.

This iteration of the device can be completely fabricated in ~2 hours and showed more promising performance than all previous iterations. Loading of the device was repeatable and the device tolerated the loading pressure over multiple uses. Additionally, it was quite durable and could be re-used many times, as larvae were readily ejected from the channel compared to previous iterations. The device also showed the high optical clarity desired for obtaining clear and focused images of the central nervous system. Characterization data can be found in Chapter 5: Device Characterization and Results.

4.3 Summary

This chapter provides an overview of the fabrication process of three iterations of the *Drosophila* larvae immobilization device for imaging with a light-sheet microscope. New fabrication processes were developed to meet the design requirements, such as smooth optically transparent side walls, 3D structured inner microchannels, and the ability to interface with the connector on the light-sheet microscope. The next chapter will discuss the characterization and testing of the immobilization device in the light-sheet microscope.

5 Device Characterization and Results

5.1 Introduction

This chapter describes the characterization of the microfluidic larval immobilization device and outlines the results obtained conducting light sheet microscopy using the final device Iteration. Several components of the device, including the pressure tolerance and loading of the device, the optical clarity of the device walls, and the immobilization efficacy were characterized. The chapter also presents the z-stack and time series images that can be obtained using this device and describes an initial study of neural response to various ambient temperatures.

5.2 Results

5.2.1 *Characterization*

The novel microfluidic chip designs were tested to ensure they met the functional design criteria, as outlined in the previous Chapter 3: Conceptual Design. A variety of features were investigated, including pressure tolerance, viability of organisms following use of the microfluidic chip, optical transparency of the device used, and the ability of the device to immobilize the organism effectively.

5.2.1.1 Pressure Tolerance of Microfluidic Devices

The microfluidic device to be used for imaging *Drosophila* larva must be able to tolerate the pneumatic pressure required to load the larva at the appropriate position for imaging the central nervous system. To test the pressure tolerance of each device iteration, the outlet and inlet ports were sealed with PDMS. An 18 G needle was inserted to the inlet channel and the needle was sealed in place using uncured PDMS. The PDMS was immediately cured using a butane torch. The pressure testing system depicted in Chapter 3 was used to measure the average pressure tolerated by each device iteration before the devices ruptured. The pressure required to load larva was also measured using the Iteration III design of device and the same pressure testing setup. The pressure causing rupture of the devices must exceed the loading pressure required to position larva in the pinning region by 50 % in order to meet the design criteria. The results of the pressure testing experiments can be seen in **Table 5.I**.

Table 5.I Pressure requirements of microfluidic device and tolerance of pressure for various iterations of device.

	Larvae Loading Pressure	**I Traditional Plasma-bonded**	**II Sacrificial Template**	**III Partial-Cured Plasma-Bonded**
	N=5	N=6	N=5	N=5
Pressure (bar)	0.86 ± 0.17	0.81 ± 0.57	1.41 (max)	1.41 (max)
Pressure (kPa)	86 ± 17	81 ± 57	141	141

Iteration II and Iteration III of the microfluidic device show a much greater tolerance to pressure before bursting, both of which exceed the required pressure of 0.86 ± 0.17 bar for loading a larva into the microfluidic channel. Iteration I failed to meet the loading pressure requirement and device bonding and integrity fails before the loading pressure required is reached. The failure mode for the tested devices that were bonded with traditional plasma-bonding adhesion method showed failure along the bonded interface. In two of them, the pressuring liquid leaked along the existing defects along the interface, and in the other three the interface itself suddenly ruptured during pressurization. Only one replicate ruptured through the bulk of the PDMS and not along the bonded interface, which interestingly tolerated the required pressure for loading. The pressure tolerance of PDMS-PDMS bonding using oxygen-plasma treatment found by Bhattacharya et al. is 58 psi, or approximately 4 bar [84]. This is much higher than what was found in the current study, suggesting that perhaps the decreased surface area impacts the ability to modify the surface hydrophilicity using the vacuum plasma cleaner. The handheld-corona generator in combination with partially-cured PDMS surfaces was more effective because the two pieces of PDMS were able to form chemical bonds from the polymerization in addition to the surface treatment. Additionally, the larger surface area used for bonding before trimming away the excess sides of the device may also contribute to forming a stronger initial bond that can tolerate higher loading pressures.

5.2.1.2 Optical Transparency of Microfluidic Devices

Successful high-resolution imaging of the neural tissue in the larvae is only possible if the devices used possess appropriate optical transparency and clarity. To examine this characteristic,

Iteration II devices were cut in half, so the inner channel was exposed, and placed on a transparent film with text. The Iteration III devices were not bonded to the flat second piece of PDMS, and placed on the same transparent film. A widefield microscope was used to observe the clarity of the lettering through the channels in each iteration, as well as a control channel with no pinning features and a thin layer of agarose gel. These images are shown in **Figure 5.1**.

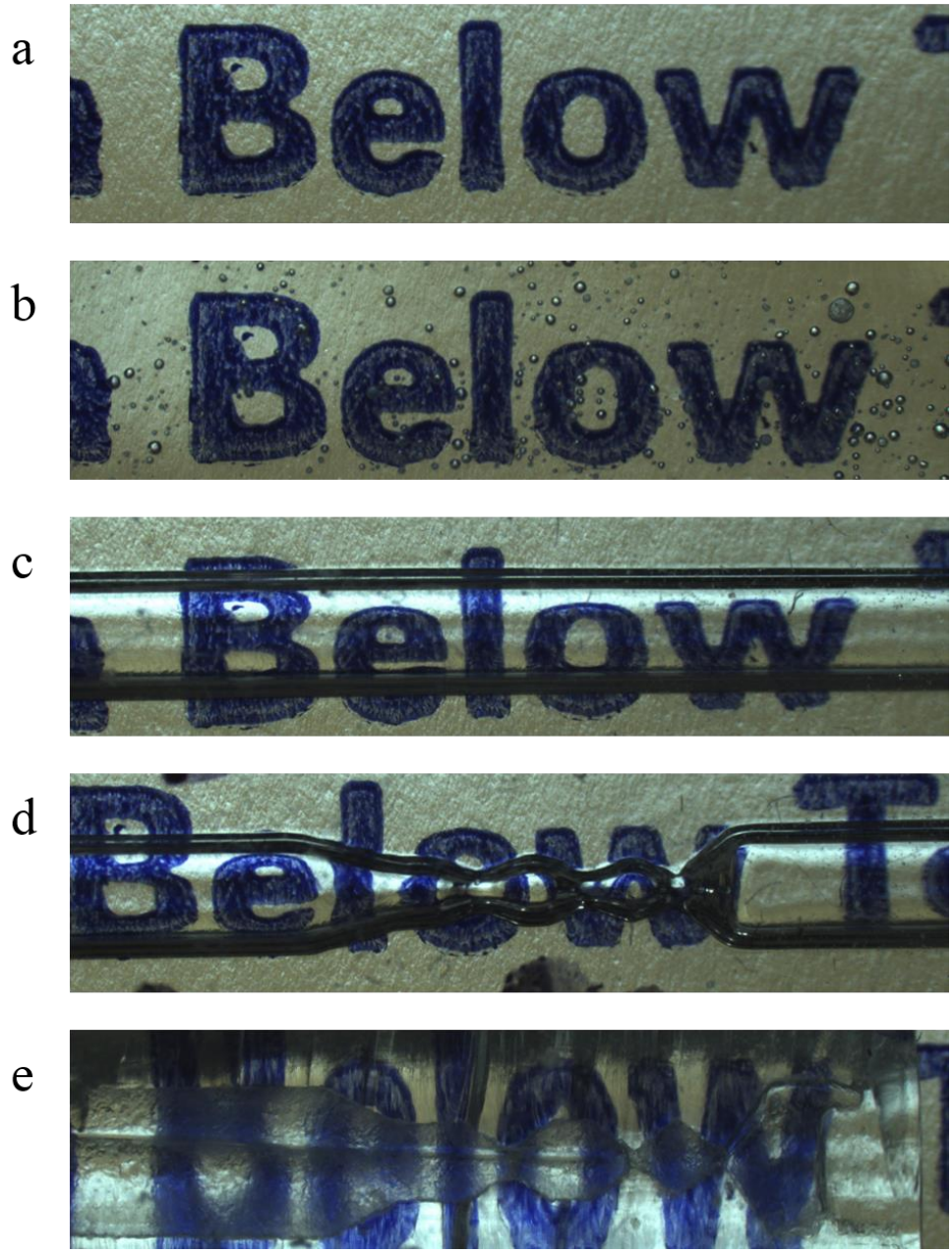

Figure 5.1 Visibility at region of interest in microfluidic channel in various device iterations. (a) Test strip of lettering with no object to view through. (b) Visibility through a 2 % w/w agar gel, approximately 2 mm in thickness. (c) Control image of visibility through a narrow channel formed from a 3D printed cast. (d) Visibility at the region of interest in a device channel formed from a 3D printed cast. (e) Visibility at the region of interest in a device channel formed using the sacrificial paraffin wax fabrication method (Iteration II). The channel was then cut in half to allow visualization through only half of the channel.

Transparency of a material indicates the optical distinctness of an object when observed through this material. In **Figure 5.1**, the object being observed through the device Iterations is the word "Below." **Figure 5.1**(a) shows the object alone, with no material placed above it, to act as a control. **Figure 5.1**(b) shows the agar gel as an example of the standard immobilization material used in LSFM. While some air bubbles can be observed, the letters remain undistorted. In **Figure 5.1**(c), a PDMS microfluidic channel is placed over the letters. There is some distortion in the regions of the edges of the channel, but ultimately the letters remain clear and the edges of the letters are sharp and distinct. **Figure 5.1**(d) shows the immobilization region of the microfluidic channel, which creates a more warped image of the letters below. This is related to the curvature of the walls of the immobilization region of the channel, as the curved surface creates a lens like effect where the object viewed changes shapes. In this case, the curved surface is convex, and the image passing through the material is expanded slightly. In **Figure 5.1**(e), the microfluidic device immobilization region created using the sacrificial template fabrication technique is shown. There is blurring of the word throughout the entire image, which is the result of residual wax lining the immobilization channel. This blurring is in addition to the same distortion due to the curvature of the channel walls. It is clear from **Figure 5.1** that the wax sacrificial template fabrication method poses some clarity problems for the device and might not be an appropriate design for the microfluidic immobilization device.

5.2.1.3 Viability of organisms following ejection

Maintaining the viability of the organisms following imaging is desired for biological applications investigating development, where behavioural observations post-neural imaging of

individual specimens may be of interest to researchers using this device. To investigate the viability of larva in the microfluidic device, larva were placed in either a separate petri dish with DI water, into a 0.9mm glass capillary tube, or into the microfluidic device. There were two immobilization durations tested in the microfluidic device, a short, 15 min interval and a more prolonged 1 hr interval. In both the DI water and the capillary tube controls, the time period was 1 hr as well. Following treatment, these animals were then moved to a dry, 6 well culture plate with food provided and observed until pupation. Successful pupation was assumed to indicate unaffected viability for the larvae. The resulting survival of the animals in each treatment group is shown in **Table 5.II**.

Table 5.II Viability of 3rd instar *Drosophila* larvae in the microfluidic device over increasing durations of immobilization

	Null Treatment (No Immobilization)	**Control Immobilization (Capillary Tube)**	**15 Minute Immobilization In Microfluidic Chip**	**60 Minute Immobilization In Microfluidic Chip**
%Survival	100% (n=5)	100% (n=5)	100% (n=5)	100% (n=5)

As shown, the immobilization in the microfluidic device for periods up to 1 hour did not affect the ability of the *Drosophila* larva to successfully pupate. This is an unusually high survival rate as compared to other immobilization devices for the larva in the literature. As discussed in Chapter 2: Literature Review, a two-layer PDMS device was used for longer duration immobilization periods, with the ability to deliver CO_2 and food to the immobilized larva [55]. The group used a periodic immobilization strategy, 30 seconds of immobilization every 5 minutes, and found that after 10 hours of this protocol 85 % of the larva survived. The group did note that 170 µm was the ideal thickness of the immobilization chamber in order to increase

survival, but increasing chamber thickness to 200 µm did not interfere with net immobilization while minimizing the detrimental effects of the mechanical immobilization [55]. Viability was also investigated by Ghaemi et al. in the 3D segmental pinning chip compared to previous, less mechanically invasive iterations of the immobilization chip [57]. It was found that the impact of the 3D segmental pinning chip was more significant on survival; after 350 s of immobilization viability was 40 % lower than the control, although the narrowed channel and 2D segmental pinning channels did not show significant changes in survival [57]. This demonstrates a trade-off between the immobilization quality and the invasive mechanical pressure required to achieve such immobilization. While the device in this thesis was modelled using the 3D segmental pinning design, there is no continuous maintenance pressure being applied to the larva during immobilization, and the entire device was composed of PDMS rather than a glass-PDMS interface as shown by Ghaemi et al. [58]. It is possible that these changes in the immobilization mechanism, while retaining the same physical dimensions, could allow for the unaffected survival of the larva during a much longer testing period of 1 hour in the current device. It is important to note that while the mechanical immobilization device described in this thesis does not use anaesthesia, mechanical pressure still has an impact on the neural activity of the larva, as the sensory responses to the constriction and inability to move will be processed in the CNS during imaging. This should be taken into account when using this device for further experiments.

5.2.1.4 Effect of Device Fabrication and Bonding Approach on Clarity of Imaging

Minimizing the thickness of PDMS surrounding the larva will improve imaging ability, as a thicker device wall can physically obstruct the movement of the sample in the z-axis. PDMS has a slightly different refractive index than the surrounding water medium (n_{PDMS} = 1.43 at 488 nm wavelength of light, and n_{water} =1.33) [85], but the slight difference should not affect clarity of the image. The image may bend slightly, but assuming there are no defects in the PDMS this bending should be uniform and minimal. The physical distance surrounding the pinning region in the various device iterations was compared to the thickness of agar that would surround a larva if imaged conventionally. A series of widefield images of larva loaded into various immobilization systems were obtained. In addition to agar embedded controls and Iteration II and III of the microfluidic devices, a PDMS tube was cast in a 1 mL syringe, forming a 4.5 mm diameter cylinder, and a hollow channel was formed in the PDMS tube with a 0.9 mm diameter glass capillary. This hollow PDMS tube acts as another control to characterize the PDMS without the pinning region of the microfluidic channel. The widefield images are shown in **Figure 5.2**.

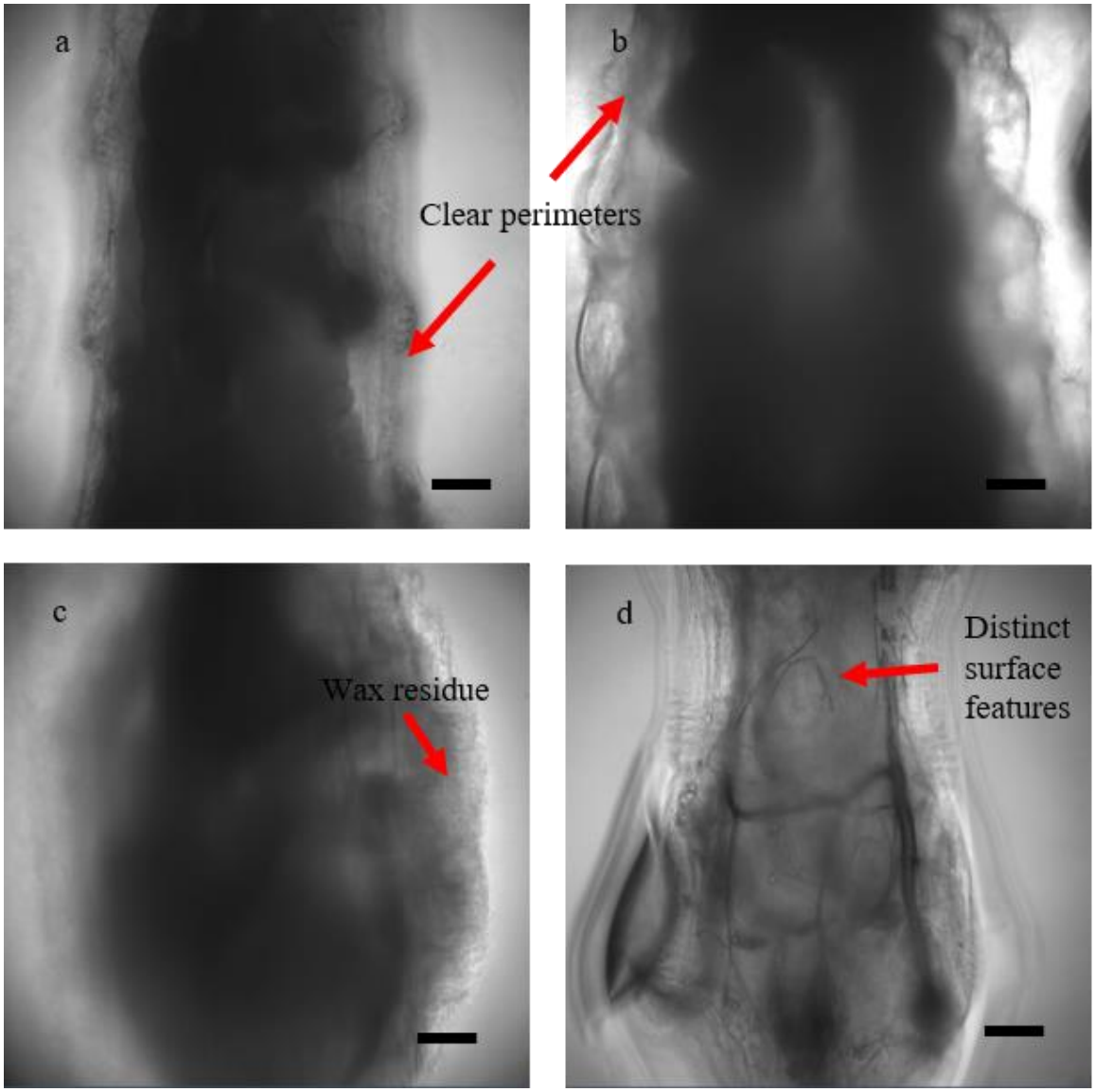

Figure 5.2 Visualization of larval body in various immobilization setups. (a) 1.5 mm diameter agar-cylinder with embedded larva (b) Hollow channel, OD 4.5 mm, ID 0.9 mm. (c) wax sacrificial temp device, OD 3.5 mm (d) sticky bonded device, with thickness of 1 mm along the objective axis and thickness of 2 mm along the illumination axis. Scale bars are 100 µm.

The ability to view the outer larval tissue is clearly impacted by the composition of the material surrounding the specimen as well as the thickness of the substrate. The agar-embedded control larva in **Figure 5.2**(a) is distinctly visible, with a clear perimeter of the larval body. The agar-

embedded larva acts as a control because the agarose is a hydrogel, and therefore 95-99 % water, and has the same refractive index as the water within the imaging chamber. The hollow channel in **Figure 5.2**(b) acts as a control for PDMS as an imaging medium without the 3D immobilization region incorporated into the channel. It is important to note that the PDMS hollow channel shares the same sharp edges of the larva as the agar cylinder in **Figure 5.2**(a), but the larva appears magnified in the hollow PDMS channel compared to the agar cylinder. All of the panels that involve PDMS as the medium, **Figure 5.2**(b)-(d), appear magnified in comparison to the agar control. As mentioned earlier, the curvature of the inner channel of the device may be causing the magnification of the image acquired by the objective lens. The Iteration II device shown in **Figure 5.2**(c) was fabricated with the sacrificial wax template. Residual wax can be observed in this widefield image, and the larva is not well defined as a result. In contrast, the Iteration III device in **Figure 5.2**(d) was created through partially-cured plasma-bonding, and provides much better visibility. Fine lines on the surface of the larva are visible in this Iteration III device. This is a much clearer device than the Iteration II because there is no wax residue interfering with the clarity of the PDMS, but it is more important to compare the Iteration III device to the hollow PDMS channel control in **Figure 5.2**(b). This improved resolution in the immobilization device is likely because the external body of the larva is fixed in place by the pinning gates in the immobilization channel, whereas the larva in the hollow channel can wiggle more freely. The most appropriate device to use for later studies is the Iteration III, partial-cured plasma-bonded PDMS device.

To examine the performance of the Iteration II device for use in this fluorescence imaging application, a comparison of the visibility of the central nervous system tissue in a dead larva

embedded in agar was compared to a larva in a 3.5 mm diameter Iteration II device created using the sacrificial wax template. The contrast between these two conditions is shown below in **Figure 5.3**.

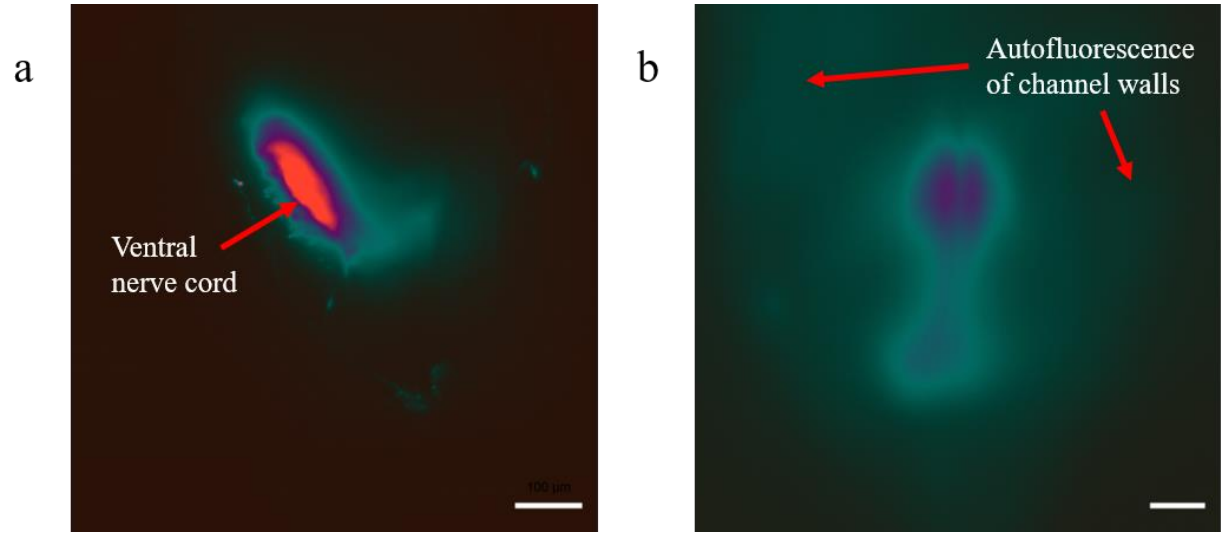

Figure 5.3 Visualization of neural tissues in the *Drosophila* central nervous system is severely reduced when using the sacrificial template device design compared to an agar-embedded control. (a) Dead larva embedded in agar imaged at laser intensity of 1.2 %. (b) Live larva within the immobilization device formed using a sacrificial template, imaged at laser intensity of 35 %. Scale bars are 100 µm.

The control larva, embedded in an agar cylinder, was imaged at a laser intensity of 1.2 % (**Figure 5.3**(a)). The larva in the device created using the wax sacrificial template was imaged at a laser intensity of 35 % (**Figure 5.3**(b)). Imaging the region of interest in the Iteration II device required a much higher laser power than agar control image did, likely due to scattering and absorption of the incident light upon contact with the wax/PDMS interface of the inner channel wall. This higher intensity of incident light produced only lower intensity of excited light and hence there was significant loss of signal. Additionally, autofluorescence of the channel itself

around the larva was observed, seen in teal surrounding the central nervous system in **Figure 5.3**(b). This autofluorescence is a material property seen in the sacrificial-template device but not in agar or the rectangular devices, indicative of residual wax within the PDMS. This higher laser power shortens the maximal duration of imaging possible due to photobleaching of the fluorophores and phototoxicity to the organism. It is clear that the Iteration II is not suitable for high-resolution whole-brain imaging of *Drosophila*.

5.2.2 *Light Sheet Imaging Capabilities*

Based on the characterization described in the previous section, the Iteration III device, fabricated through the partially-cured plasma-bonding method, was selected as the optimal device for this imaging application. This optimized device was used to perform light sheet microscopy. The light-sheet fluorescent microscope allows for illumination of an entire slice of tissue in the z-plane simultaneously, decreasing acquisition time of a full z-stack image composed of more than 600 slices of the nervous system to less than a minute. This increased acquisition time also means that time series images of a single plane can be obtained at speeds of 0.8 s/slice using this particular microscope.

5.2.2.1 Z-stack imaging

To fully demonstrate the efficacy of the final device configuration, the ability to image a live larva in the device was compared to various control imaging techniques. First, an excised brain embedded in agar is used to show the least-impeded path of light from the laser source to the neural tissue. This brain does not represent a living larva, but rather the best resolution that can

be obtained using this microscope without the hinderance of larval hemolymph and tissue. Next, both dead and live larva were embedded in agar and z-stack images were obtained. This represents the current standard for imaging a *Drosophila* larva and the resolution possible with a dead, unmoving organism versus the motion artifacts obtained when the larva is still alive and unrestrained. The final z-stack described below shows a live larva in the microfluidic device. Characterization of the visibility of the neural tissue in each of these methods is necessary to show proof of concept of effective imaging ability in the Iteration III device presented.

5.2.2.1.1 LSFM Imaging of Excised Larval Brain

To illustrate the imaging capability of the light-sheet microscope for *Drosophila* neurological study, a brain from a 3rd instar larva was excised to show how the CNS appeared unimpeded by the surrounding larval tissue. The larva was dissected according to the procedure in Chapter 3, and the brain was embedded in agarose gel for imaging. This preparation represents the best possible scenario for imaging using the light sheet microscope and the way that tissues are currently imaged using this method. There are no scattering or distorting features between the light source, the object imaged and the detector as the as the hemolymph filled body has been removed and the thickness of agar surrounding the tissue was minimized. While the neural tissue has been removed from the larva, the activity of the fluorophores does not cease immediately following death, and the brain could be imaged at low power for 30-45 minutes following excision. A z-stack of this brain is shown below in **Figure 5.4**.

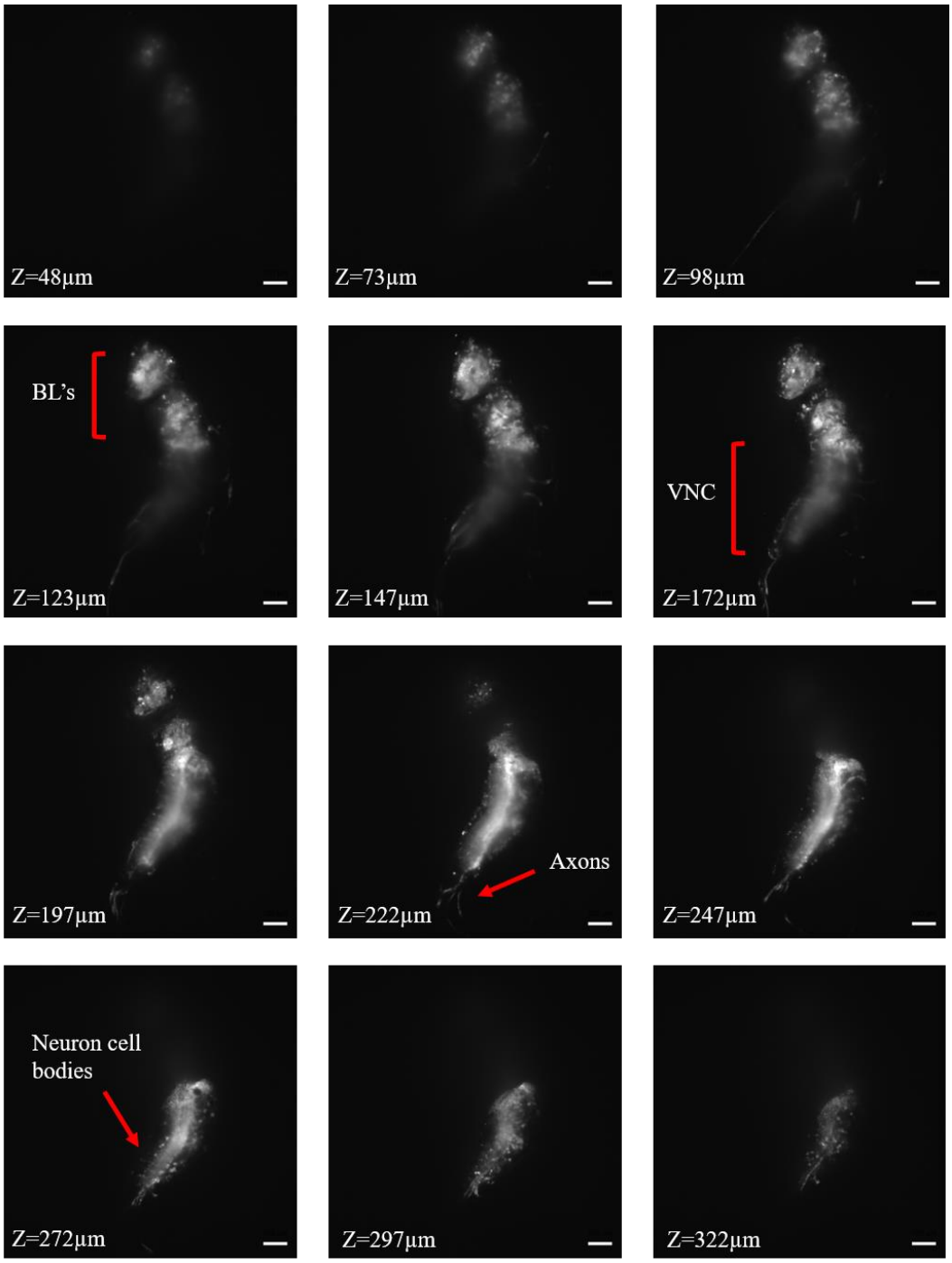

Figure 5.4 Z-stack of an excised brain embedded in agar. The volumetric image is composed of 240 slices, each 1.66 µm thick, spanning a total thickness of 397.92 µm. The laser is at 2.6 % intensity and the exposure time is 49.94 ms. Scale bar is 100 µm. BL's = brain lobes; VNC = ventral nerve cord.

There are several fine structures visible in this z-stack, such as individual neurons, which appear as distinct white dots, and axons that leave the ventral nerve cord and travel dorsally to innervate the larval body wall muscles. However, the high resolution of the excised brain comes with a caveat; this tissue, while still showing post-mortem activity in response to remaining calcium present in the neuronal cells, does not represent true physiological activity. As described in Chapter 2, in order to examine a living organism and observe a real physiological response, the tissue surrounding the central nervous system acts as a hinderance to spatial resolution. These images instead show an ideal target resolution to be achieved through the engineered design of the immobilization device. The acquisition rate of the z-stack is 7-8 slices per second. Other groups have conducted whole-brain imaging of dead, excised tissue using Gal4/UAS-GFP. Salvaterra & Kitamoto dissected larval brains in PBS and then fixed the intact tissue and mounted the brains in a solution of 50 % glycerol in PBS to conduct confocal microscopy[79]. While they observed excellent resolution, the group noted that the brain hemispheres and ventral ganglion structures were very difficult to observe through the cuticle, and thus justified the excision of the brain tissue [79]. Confocal microscopy possesses a higher spatial resolution ability than light-sheet microscopy, which contributes to the higher resolution obtained in this study. Lemon et al. also excised brains for the purpose of functional mapping of the brain tissue during fictive behaviours that were induced in the isolated brain, and recorded activity changes using the GCaMP6s GECI [73]. This group was able to map whole-CNS activity and obtain single-cell resolution throughout the dorsal regions of the suboesophageal ganglion. This resolution is very similar to the results obtained and presented above. However, the target of this project is to observe physiological responses in the CNS in an intact larva, and therefore more

appropriate, whole-larva, agar embedded controls were examined and are presented in the next section.

5.2.2.1.2 LSFM imaging of dead larva embedded in agar

The next preparation of larva presented is the agar-embedded, dead 3rd instar larva. The purpose of imaging a dead larva is to demonstrate a no-movement control, as the brain still retains some function following death but the larva will not need to be immobilized, showing the best possible resolution of the CNS with a completely still larva. Dead larvae were placed in liquid agar gel, and a 1.5 mm diameter glass capillary tube and plunger are used to draw up the larva and agar into the tube. The tube is gently rotated around the long axis to position the larva centrally within the agar as it cools, and upon gelling, the capillary tube can be placed into the microscope and the agar (with embedded larva) extruded into the imaging chamber. This preparation allows for visualization of the larva without motion of the brain tissue and with a minimized, 1.5 mm diameter agar cylinder as the immobilization medium, but also fails to meet the requirements of the project due to the altered physiology of the brain post-mortem. While the GCaMP5 GECI's still retain the ability to fluoresce for at least an hour following death of the organism, due to remaining calcium in the cells, the fluorescent responses are no longer associated with activity of the neurons and cannot be interpreted as true physiological responses. **Figure 5.5** shows a z-stack of a central nervous system of a deceased larva embedded in a 1.5 mm diameter agar cylinder.

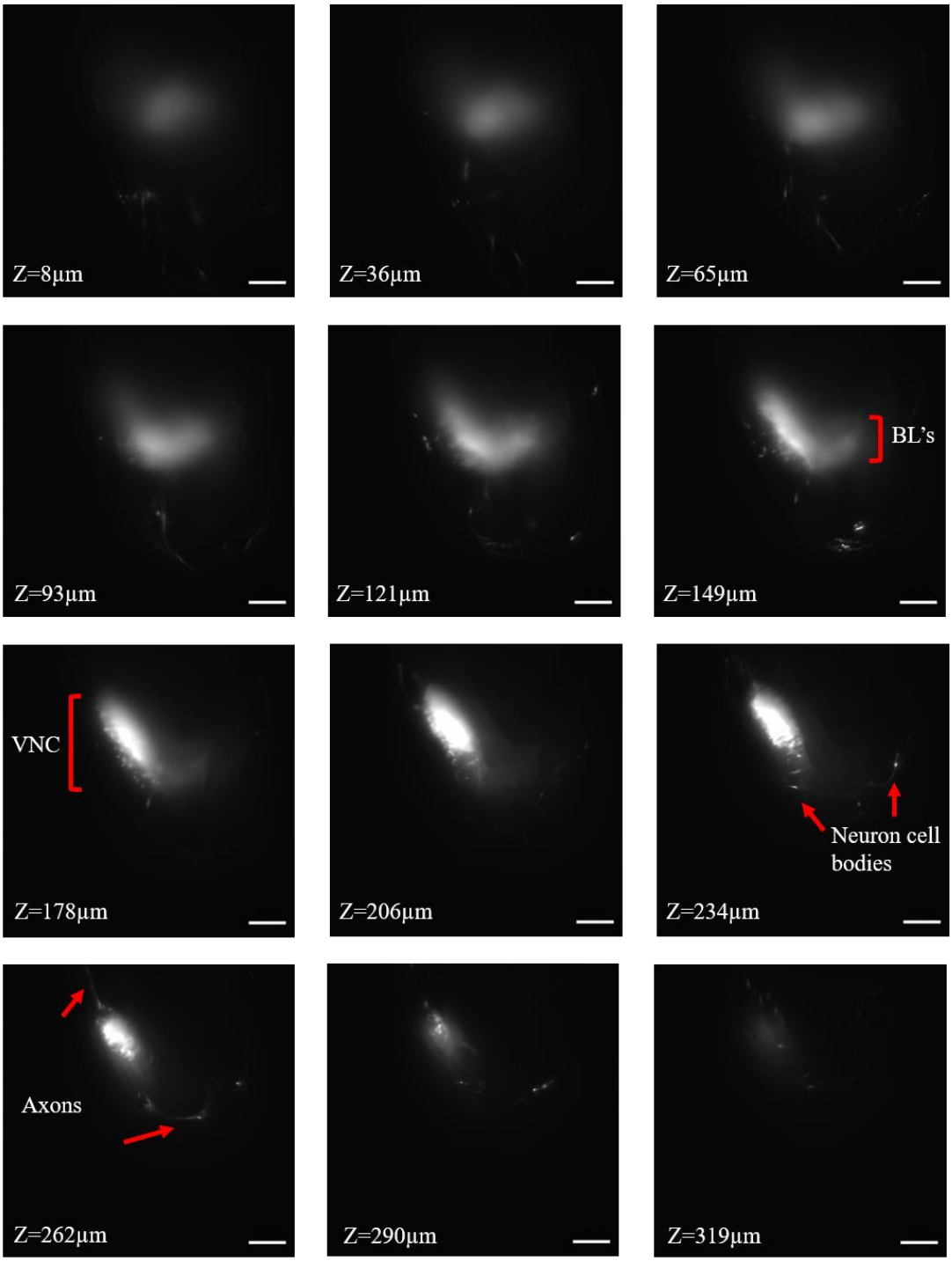

Figure 5.5 Z-stack of a dead larva embedded in agar. The volumetric image is composed of 198 slices, each 1.66 µm thick, spanning a total thickness of 328 µm. The laser is at 1.2 % intensity and the exposure time is 29.97 ms. Scale bar is 100 µm.

There are still visible cell bodies and axons at the periphery of the CNS in the dead, agar-embedded larva, but it is important to recognize the difference in observable neurons around the ventral nerve cord region. Both central nervous systems in these two conditions are no longer showing physiological responses in live larva, but there is still tissue surrounding the CNS in **Figure 5.5**. This additional tissue, composed of the outer cuticle, the surrounding organs, and hemolymph, acts as an obstruction, and though the larval body and hemolymph are relatively transparent, the extra tissue makes it difficult to view the fluorophores clearly in comparison to the excised CNS alone. This is why the slices of the image that are closer to the objective (higher z value, in µm, located in the bottom left corner of each panel of the figure) appear to be at a higher focus than the ones located furthest from the objective (low z value). The objective has a small depth of focus and the objective is scanned for the different z-position. It will only record the features that are in clear focus, but the plane that is in focus must be detected through the layers between the focal plane and the objective. Next, a comparison between a live larva and a dead larva embedded in agar must occur, to show the limitations of live imaging currently using LSFM.

5.2.2.1.3 LSFM Imaging of Live Larva in Agar

Next, a live larva was embedded in agar and imaged using the light-sheet microscope. This larva preparation illustrates that the conventional sample embedding process is inadequate when attempting to immobilize a live 3rd instar larva. The process of embedding a live larva in agar gel is the same as previously, but one must ensure the agar has cooled to a lower temperature than the hot water bath where it was being maintained in liquid form. Agar that is too hot will injure

and possibly kill the larva while drawing it up into the capillary tube, and this must be avoided. A live larva was imaged using the agar gel capillary tube to demonstrate the current state of the field for live neuronal imaging using light-sheet fluorescent microscopy and GECI's to show neural activity. A z-stack of a live larval central nervous system in an agar-embedded preparation is shown below in **Figure 5.6**.

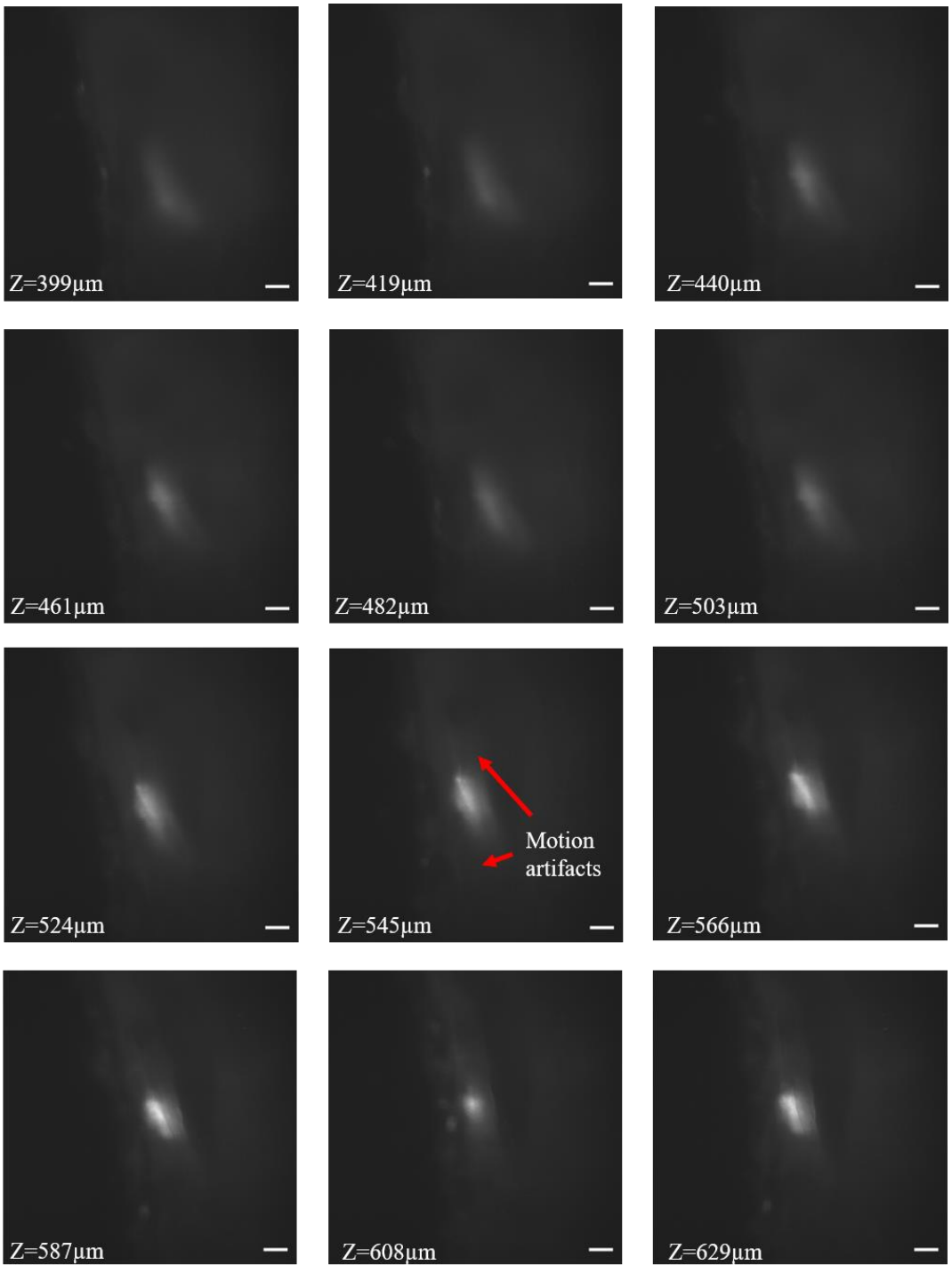

Figure 5.6 Z-stack of a live larva embedded in agar. The volumetric image is composed of 641 slices, each 1.23 µm thick, spanning a total thickness of 786 um. The laser is at 5 % intensity and the exposure time is 29.97 ms. Scale bar is 100 µm.

It is immediately clear that the CNS in the live larva embedded in agar is at a much lower resolution than the dead larva CNS shown in **Figure 5.5** or the excised brain in **Figure 5.4**. This is because of the motion of the larva, only partially restrained by the gelled agarose surrounding the outer body. During the acquisition of this image, the larva contracts its body wall muscles and pushes against the agar walls encapsulating its body. As a result, motion artifacts can be seen in the z-stack and the ventral nerve cord and brain lobes can not be identified. Individual axons and cell bodies are not visible at all when the larva is able to wiggle to such an extent. This demonstrates the need for an immobilization device: in order to study a live larva at high spatial resolution, the motion of the larva must be eliminated.

5.2.2.1.4 LSFM imaging of live larva in immobilization device

Having demonstrated the existing state of the field regarding light-sheet microscopy in dissected, deceased, and live larva embedded in agar gel, the efficacy of the novel microfluidic device for immobilizing larvae for neurological imaging was characterized. Larva were loaded into prepared microfluidic devices as described in the procedure in Chapter 3, and the device was mounted in the light sheet microscope. An acquired z-stack image is shown in **Figure 5.7**.

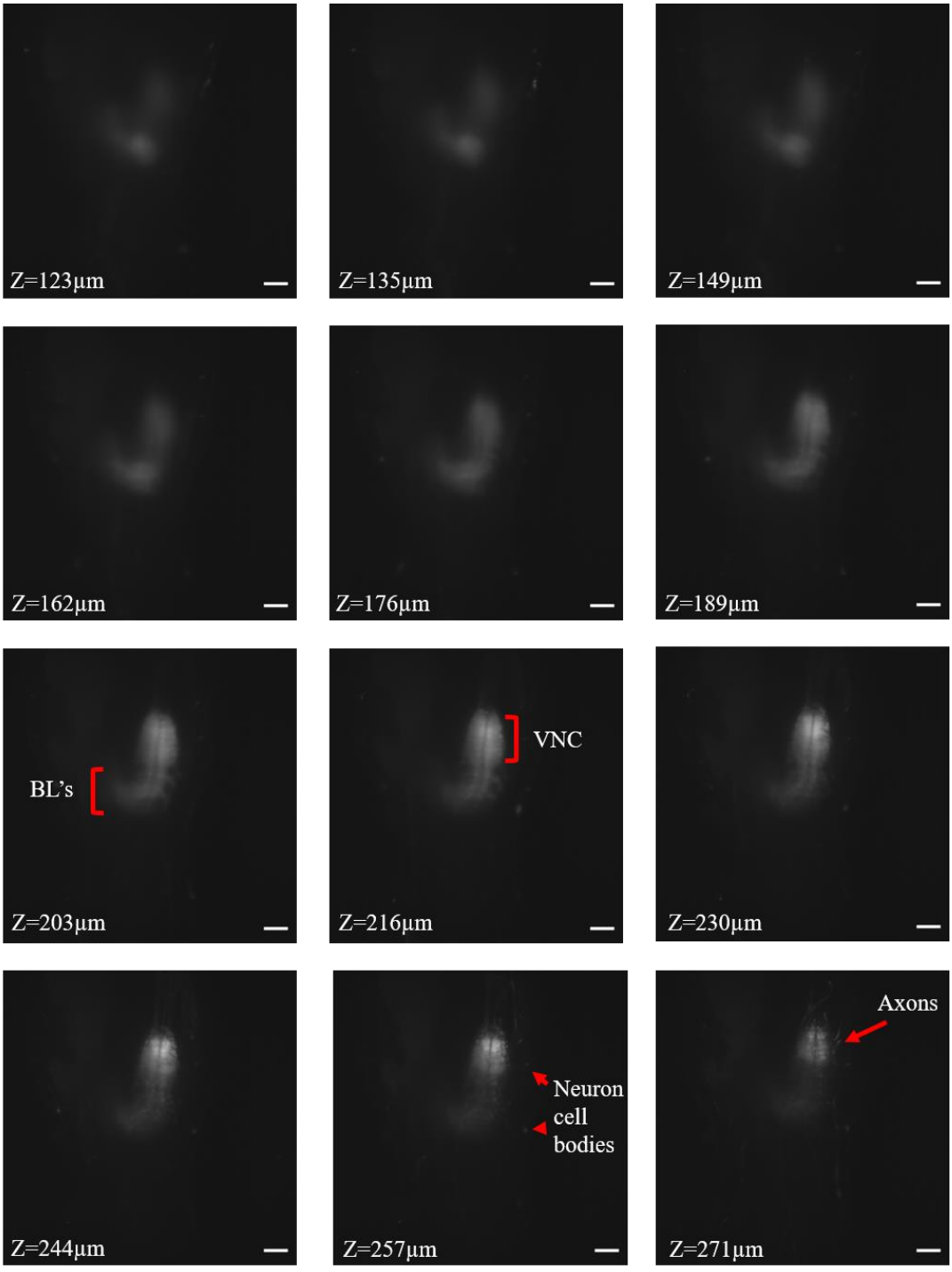

Figure 5.7 Z-stack of a live larva in the sticky bonded device iteration. The volumetric image is composed of 260 slices, each 1.23 µm thick, spanning a total thickness of 318.17 µm. The laser is at 1.5 % intensity and the exposure time is 49.94 ms. Scale bar is 100 µm.

The microfluidic device immobilized the larva much more effectively than the agar gel did, as it is clear there are fewer motion artifacts surrounding the larva immobilized above than there are in the live agar-embedded z-stack. This is primarily due to the pinning gates of the immobilization region of the channel holding the larva fixed, but the mechanical stopper inserted behind the larva to prevent escape from the channel in the y-axis also contributes to the immobilization efficacy. The intensity of illumination can also be lower in the microfluidic device in comparison to when imaging a mobile, live larva in agar, as the laser was at 1.5 % for the microfluidic device and 5 % for the live agar-embedded z-stack. This microfluidic device preparation also allows for the resolution of individual axons, something that was not possible in the live agar-embedded preparation. When compared to the dead larva in agar, the illumination is quite similar, at 1.2 % intensity, and the resolvable features of similar quality. One of the main structures that are both distinct in these two preparations is the axons leaving the dorsal part of the ventral nerve cord and travelling towards the tail of the *Drosophila* to innervate the muscles in the body wall. There is greater contrast in the visibility of the ventral nerve cord, however. In the microfluidic device, the ventral nerve cord appears to have striations, and a clear division between the left and right parts of the VNC is very distinct (**Figure 5.7**, Panel Z=216µm). In the dead larva embedded in agar, this is not possible to observe due to the over-saturation of the VNC. It is unusual that such a low intensity of the laser, just 1.2 %, could cause such saturation of the image, at a low exposure time of just 29.97 ms. This could be related to the physiological activity change in the larval brain upon death, assuming the mechanism of calcium pumps in cellular membranes is conserved between *Drosophila* and humans. The fluorophores respond to intracellular calcium, and when ATP is no longer being produced by the neurons, the ATP-

dependent membrane Ca^{2+} pumps are not able to remove calcium from the cells, causing a build up of intracellular Ca^{2+} and contributing to increased activation of the GECI's within the cells [86]. Finally, the much higher resolution seen in the excised brain preparation is due to the removal of the tissue surrounding the CNS, which is still present in the live, immobilized preparation.

A comparison of the four preparations is shown in **Figure 5.8**. A Fast Fourier Transform (FFT) was performed on a raw image slice from each of the four preparations described above. The FFT interprets the frequency of the sine and cosine waves that the image is composed of. Higher frequency waves are further from the origin, and lower frequency waves close to the origin. A greater number of high frequency waves is indicative of better resolution of an image. The images were then filtered through the imageJ "Find Edges" algorithm and the contrast enhanced to provide a more qualitative demonstration of the resolvable features in each image slice.

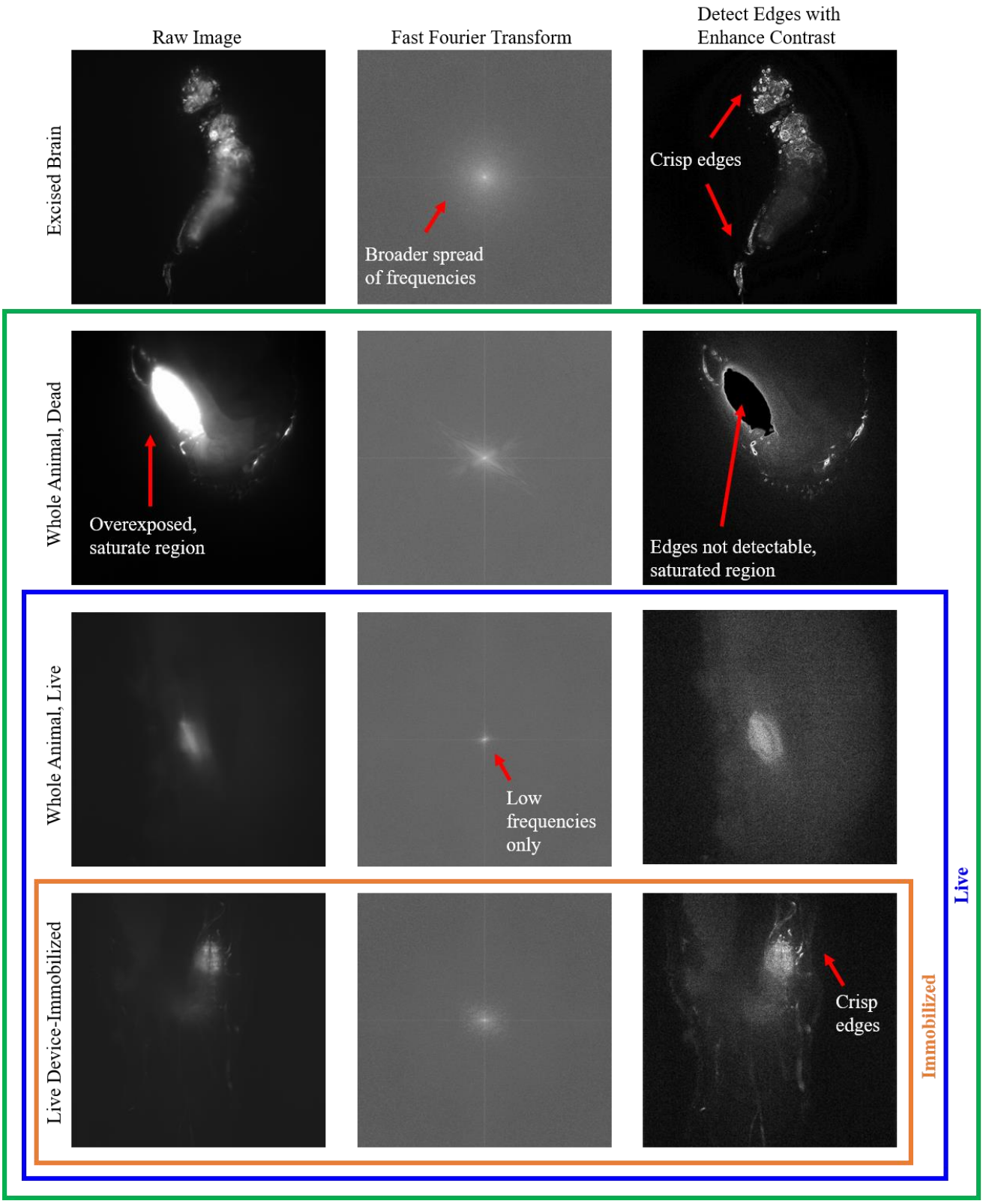
Raw Image
Fast Fourier Transform
Detect Edges with Enhance Contrast
Excised Brain
Crisp edges
Broader spread of frequencies
Whole Animal, Dead
Overexposed, saturate region
Edges not detectable, saturated region
Whole Animal, Live
Low frequencies only
Live Device-Immobilized
Crisp edges
Immobilized
Live
Whole Animal

Figure 5.8 A single z-slice of the CNS from each of the four previously discussed z-stack conditions was compared using a Fast Fourier Transform (FFT) to quantify the distribution of frequencies of sine waves composing the images. Frequencies are plotted in both the x and y axes in the FFT, with higher frequencies presented further from the origin, and lower frequencies closer to the origin. The image can be considered to be more in focus if it is composed of more higher frequency waves than another image. The raw images were also passed through the imageJ "Find Edges" algorithm, which detects significant differences in the intensity of pixels, and the resulting image was normalized to enhance the contrast using a threshold of 0.3 % saturated pixels.

The most high frequency waves are identified in the FFTs for the dead larva preparations, both the whole larva in agar and the excised brain. There is a similar distribution of waves for the immobilized larva, however, and while there are not as many high frequency waves for the immobilized larva compared to the dead larva preparations, there is a clear distinction between the immobilized larva FFT and the FFT that corresponds to the live larva in agar, indicating that the immobilization device is significantly improving the resolution of live whole brain imaging compared to what is currently possible with LSFM. The edge detection images show similar evidence that the immobilization device is coming close to matching the resolution possible with whole, dead larva, and a vast improvement to whole, live larva.

5.2.2.2 Time lapse Imaging

To demonstrate the ability to take images of the same z-plane of a live specimen with unaltered physiology over a period of time, a 3rd instar larva was pneumatically inserted into the Iteration III device, the mechanical stopper was placed in the channel to prevent escape, and images were acquired at intervals of ~0.8 s. **Figure 5.9** presents an example of a time-lapse acquired of a GCaMP5 larva over a period of ~40 s. Each panel presents a different time point within the time-lapse.

a

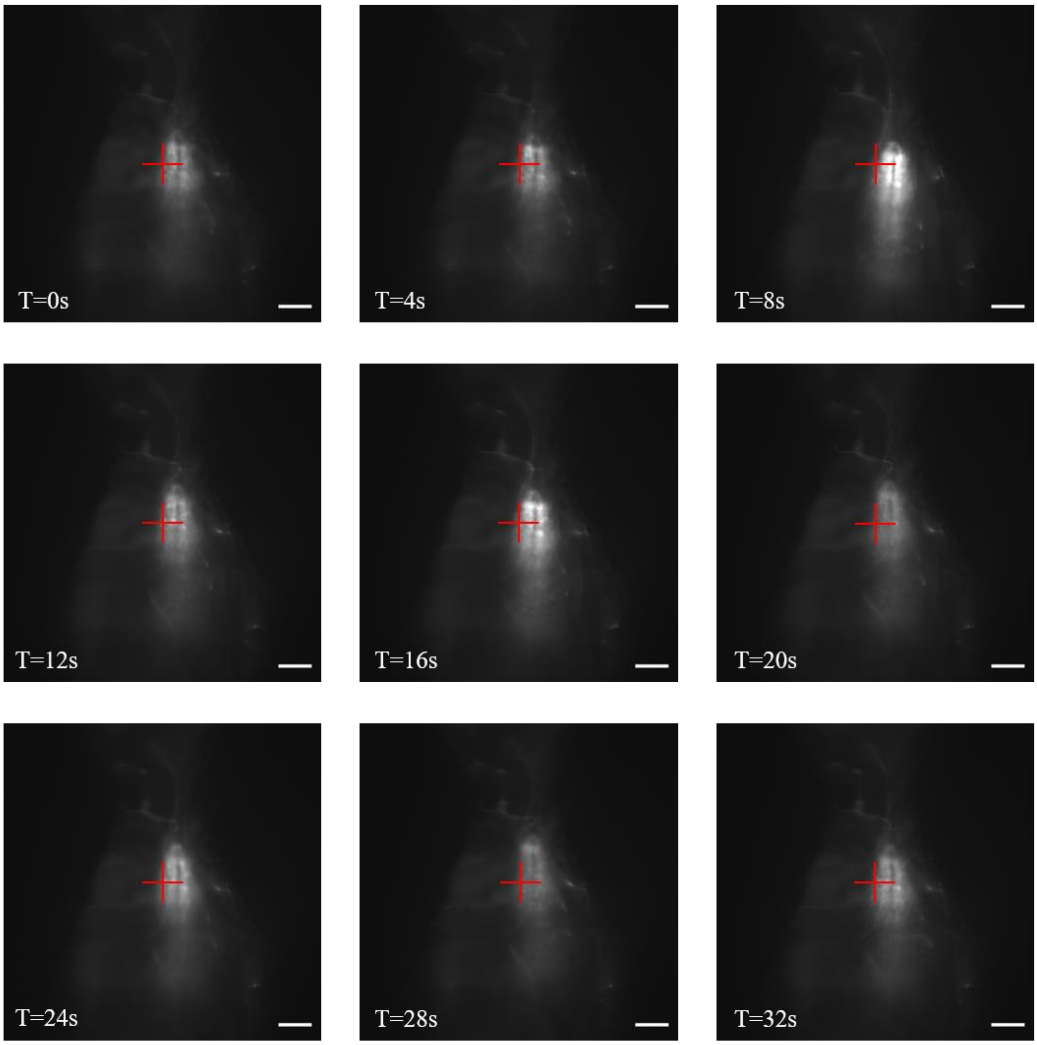
T=0s
T=4s
T=8s
T=12s
T=16s
T=20s
T=24s
T=28s
T=32s

b

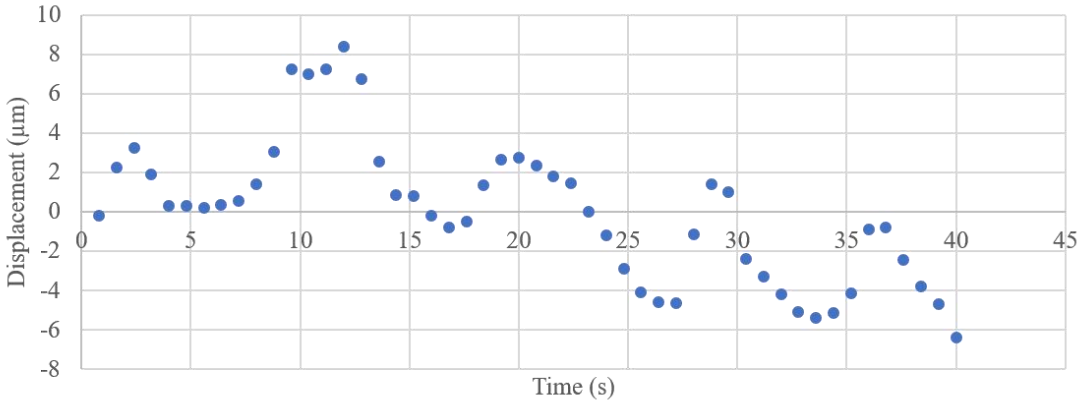
Displacement (µm)
Time (s)
10
8
6
4
2
0
-2
-4
-6
-8
0
5
10
15
20
25
30
35
40
45

Figure 5.9 (a) Time lapse images of a larva brain over a period of several seconds. Changes in intensity can be observed in addition to minor changes in position of the central nervous system in the y axis (vertical). The laser intensity is 2.2 %, the exposure time is 119.74 ms. Scale bars are 100 µm. (b) A plot showing the change in deviation of the centre of mass of the CNS over time. The blue markers represents the displacement of the CNS in the y-direction (up or down).

The motion of the central nervous system was greatly reduced compared to that of a live larva embedded in agar, but was not completely eliminated by the 3D segmental pinning chip. This was expected, as the original chip did not completely eliminate motion of the CNS, but rather reduced it to a fluctuation of ~10 µm in either direction from the set point over a period of 350 s [57]. With proper application of the mechanical stopper at the rear of the *Drosophila*, this light-sheet device showed similar results, with the deviation in the y-axis restricted to ~8 µm in either direction. However, if the mechanical stopper was not applied, much more significant deviation from the set point was observed, with the CNS moving more than the length of the CNS – approximately 500 µm – in either direction. Often, the larva would also escape from the channel and begin climbing vertically out of the device during imaging without the mechanical stopper present.

The changes in intensity shown in **Figure 5.9**(b) were not directly linked to an exposed stimulus, as this experiment was merely a proof of concept. However, the intensity is still directly linked to the activity of the neuronal cells. The periods of greater intensity throughout the time-lapse shown, such as the increased brightness at timepoints of 8 s and 16 s, could be related to neurons responding to the mechanical stimulus of the PDMS walls of the device touching the outer surface of the larva, or neurons sending motor signals to the muscles that contract to cause the motion of the hemolymph as seen in the video. There is also possibility that these changes in

activity could be related to other unpredicted stimuli, such as the sound of the sample mount moving toward and away from the objective, or the pivot scan of the lasers. Further investigation will be required to ensure the environment is completely controlled during stimulus-response testing in the future. There could also be an effect of the light of the laser on the visual receptors of the larva, triggering a response in the CNS as the laser light sheet pans past this region of the larva, similar to the source of error described in the Ahrens et al. study in larval zebrafish [70].

5.2.2.3 Stimulus Response Proof of Concept

The desired purpose of this microfluidic device was to be able to assist biologists in studying the response of the *Drosophila* brain to various sensory stimuli, including chemical, auditory, mechanical, and any others that may assist in research applications. To characterize whether different chronic sensory response states could be detected, the same larva was exposed to prolonged periods of time, ~10 minutes, at three different ambient temperatures. Acute responses to temperature change were not observed, as the rate of change for cooling the sample chamber medium was 1.0 °C/min and for heating was 0.5 °C/min. A z-slice at the same spatial position in the brain at each temperature was isolated and a horizonal line drawn through the same portion of the ventral nerve cord, as seen in **Figure 5.10(**a). The intensity of each slice was then plotted as shown in **Figure 5.10**(b) to supplement qualitative visualization of the differences across each image, at 12 °C, 25 °C, and 37 °C from left to right respectively. Finally, a plot of the pixel numbers, a representation of the intensity, of the red lines from the panels in **Figure 5.10**(a) are shown as a function of distance in panel **Figure 5.10**(c).

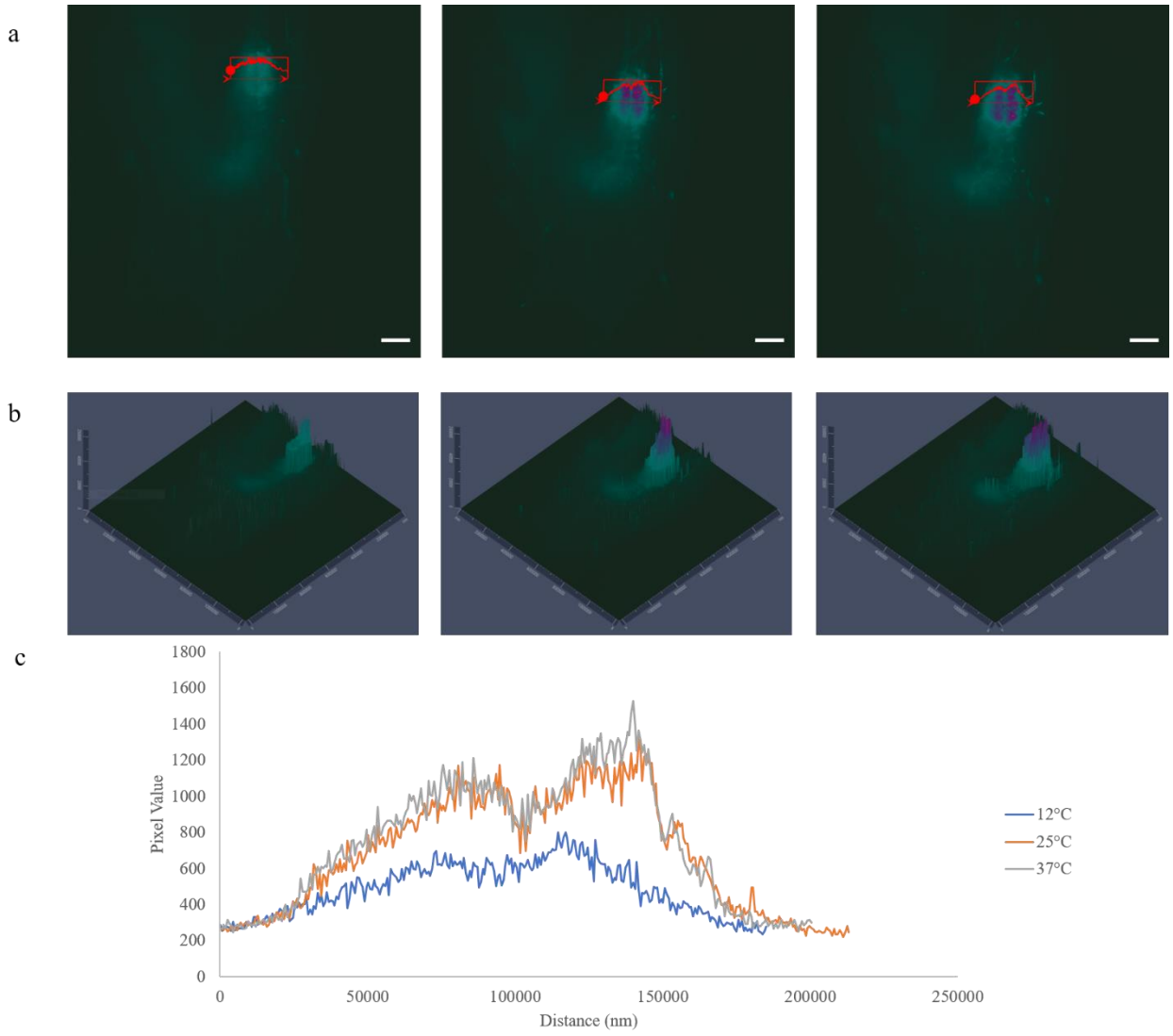

Figure 5.10 Intensity differences with change in ambient temperature. Same larval brain slice at three unique temperatures, 12, 25, and 37 ºC respectively, from left to right. (a) z-slice images of each temperature, scale bar is 100 µm. (b) plots of intensity versus spatial position of each two dimensional image in (a). (c) Intensity, expressed as pixel value versus distance plot of the line in panel (a) for each image.

It is clear that there is a much lower intensity in the *Drosophila* brain at 12 °C when comparing to the much higher peaks seen in the curves for the 25 °C and 37 °C brains. This observation could have one of two potential causes. First, the cellular activity of the neurons is altered by the

lower temperature, a tool that has been taken advantage of by *Drosophila* biologists, chilling flies on surfaces that have been pre-cooled to -1 °C to anesthetize larva for imaging applications [87]. Second, the change in activity of the fluorophore could instead be due to denaturation of the protein itself due to the decreased temperature. Akerboom et al. tested the GCaMP5 GECI in the *Drosophila* larval neuromuscular junction at a maintained physiological pH (~7.4-7.6) and room temperature (22 ± 0.5 °C) during imaging. When testing expression of the fluorophore in mice, the animal was placed on a warming blanket at 37 °C. Fish studies were conducted at 23-24 °C [63]. The fluorescence extinction was not assessed when characterizing the protein; instead, all assays were conducted at the physiological body temperature of the model organism. Despite this, it is well known that proteins and enzymes will denature when exposed to cold temperatures [88]. The majority of enzyme dimers investigated show dissociation at 0 °C, but some larger enzymes may inactivate at warmer temperatures of 10 °C, such as 17β-hydroxy-steroid dehydrogenase in the human placenta [89]. Assuming the ambient temperature of the water surrounding the microfluidic device matches the temperature of the larval body during imaging, it is very likely that the decreased activity observed is caused by the GCaMP5 protein beginning to denature.

5.3 Summary

This chapter presented the characterization and results obtained from the microfluidic 3D segmental pinning device for light-sheet fluorescence microscopy. The assays used to investigate whether the device iterations met the design criteria, the immobilization efficacy, and the ability to obtain both z-stack and time-series images were described. From these results, the loading

pressure to be tolerated was 0.86 ± 0.17, which was tolerated by iteration II and III but not by iteration I. The rectangular, adhesion-assisted bonded Iteration III was more optically transparent than the sacrificial wax template fabricated Iteration II, making it the favorable choice for high-resolution, whole-brain imaging. The chapter then described the proof of high-resolution imaging using Iteration III devices, and while complete immobilization of the CNS was not possible, variation in intensity of neurons and brain regions was still detectable using image processing software. Finally, a demonstration of the response of the GCaMP5 GECI's in the *Drosophila* brain was conducted in response to multiple ambient temperatures. These results show the capability of the immobilization chip to assist researchers in achieving high-resolution, whole-brain imaging in response to external stimuli over extended periods of time.

6 Conclusion and Future Work

6.1 Conclusion

The thesis presents a novel microfluidic device for high temporal and spatial resolution imaging of 3rd instar *Drosophila* larvae using a light-sheet fluorescent microscope. A customized chip was designed to immobilize a fully alert larva and still fit within the light-sheet microscope. Larvae were immobilized using a modified 3D-segmental pinning design and a mechanical stopper to prevent escape from the channel during imaging. Z-stack images and time-series images were captured of the larva in the microfluidic device to illustrate the imaging capabilities possible. The high spatial resolution of achieved (<5 μm) when capturing images of the immobilized larval CNS with this device was comparable to images of the CNS of whole, dead larvae embedded in agar, but the larva in these devices are live and will be a strong model for improving imaging neurotechnologies going forward.

For this device to be accessible to researchers using *Drosophila* currently, it was designed to meet several criteria. The device is simple to fabricate and operate, making use of reusable casting molds. The total fabrication cost for each device is relatively low, as PDMS is quite inexpensive and no complex equipment is required. Operation can be completely manual, minimizing additional equipment required for use beyond the light-sheet microscope.

Larvae were immobilized and imaged in the light sheet microscope for periods of 1hr consistently with no observed impact on viability. Imaging periods could be extended to 2 hours

without loss of signal from the GECI fluorophores. Larvae could be immobilized such that deviation of the CNS centre of mass was <10 μm from the centre of the field of view. Z-stack images could be acquired at a rate of 7-8 slices/s.

While this microfluidic immobilization device accomplishes the goal of high spatial resolution of the whole brain of the *Drosophila* larva at high temporal speeds of 7-8 slices/s, there are still some limitations. The device should be altered to accommodate various stimuli exposure, such as chemical or electrical. Additionally, greater speed of imaging is necessary to be able to record volumetric images of the CNS sequentially over time to be able to observe the speed of thought. Currently, this speed is not yet possible and will be one of the steps towards achieving neuronal wiring diagrams in the future.

6.2 Future Work

The first aspect to be investigated in the future is to conduct further viability testing. While there appeared to be no viability deficits following up to 60 minutes in the microfluidic devices, changing the endpoint of this assay from successful pupation to full lifespan will allow for a more in-depth investigation of whether the organisms are affected by the immobilization mechanism. While all flies were able to successfully pupate, perhaps a difference would be seen in total average lifespan of each cohort (60 minutes immobilized, 15 minutes immobilized, controls). The viability testing should be performed again, but the larvae should instead be transferred to vials following immobilization treatment, and the death of each individual fly over the course of several weeks examined.

Next, it will be useful to incorporate sensory stimuli directly into the microfluidic device. While temperature was able to be modulated in the light-sheet microscope, this was a very gradual change and not an acute stimulus. The body of any organism responds differently to acute vs. chronic stimuli, and to further understand the neuronal circuitry of the central nervous system, and be able to observe the signal transduction related to stimulus detection, acute stimuli will need to be incorporated into this device. Chemical stimuli can be delivered to the larvae through an auxillary channel, which would likely run parallel to the microfluidic device to prevent interference with the movement of the device within the microscope imaging chamber. Electrical or acoustic stimuli will also be considered, and introduced to the larvae by a mechanism that is compatible with the light-sheet microscope. These stimuli are useful for triggering a neuronal response pathway that will be used as the circuit to image at the speed of thought as the imaging technology becomes more advanced.

One of the unique features of the light-sheet microscope is the ability to move the specimen not just in the x-, y-, and z-axis, but also rotate it around the central axis of the drive shaft. The rectangular microfluidic device allows imaging from two sides of the larva, but not the sides along which the interface of the two pieces of PDMS is present. Further development of the fabrication process should be conducted to facilitate imaging from four or eight faces of the device, or even the reintroduction of a cylindrical device to allow imaging from 360 ° of rotation around the central axis. These images can then be reconstructed using the ZEN software to improve the spatial resolution of Z-sheet volumetric images following capture. Additionally, as mapping of the brain circuitry becomes possible, researchers may find it useful to examine a

specific lobe or region that is located along the side or rear of the larval CNS, and freedom to image the brain region from all sides will be useful for cases such as this.

The temporal resolution of the light-sheet microscope used in this study was fixed, but as mentioned in earlier Chapters, several groups have manipulated the microscope in such a way that the image acquisition time is reduced. It would be valuable to consider a collaboration with groups that could combine their advanced neuroimaging technology with our fabricated microfluidic device to move one step closer to recording a path of signal transduction through the neuronal circuitry of the *Drosophila* brain in high temporal resolution.

References

[1] S. Tickoo and S. Russell, “Drosophila melanogaster as a model system for drug discovery and pathway screening,” *Curr. Opin. Pharmacol.*, vol. 2, no. 5, pp. 555–560, 2002.

[2] U. B. Pandey and C. D. Nichols, “Human Disease Models in Drosophila melanogaster and the Role of the Fly in Therapeutic Drug Discovery,” *Pharmacol. Rev.*, vol. 63, no. 2, pp. 411–436, 2011.

[3] A. Jeibmann and W. Paulus, “Drosophila melanogaster as a model organism of brain diseases,” *Int. J. Mol. Sci.*, vol. 10, no. 2, pp. 407–440, 2009.

[4] E. Bier, “Drosophila, the golden bug, emerges as a tool for human genetics,” *Nat. Rev. Genet.*, vol. 6, no. 1, pp. 9–23, 2005.

[5] L. T. Reiter, L. Potocki, S. Chien, M. Gribskov, and E. Bier, “A Systematic Analysis of Human Disease-Associated Gene Sequences In,” *Genome Res.*, pp. 1114–1125, 2001.

[6] M. S. Moore, J. DeZazzo, A. Y. Luk, T. Tully, C. M. Singh, and U. Heberlein, “Ethanol intoxication in Drosophila: Genetic and pharmacological evidence for regulation by the cAMP signaling pathway,” *Cell*, vol. 93, no. 6, pp. 997–1007, 1998.

[7] R. Satta, N. Dimitrijevic, and H. Manev, “Drosophila metabolize 1,4-butanediol into γ-hydroxybutyric acid in vivo,” *Eur. J. Pharmacol.*, vol. 473, no. 2–3, pp. 149–152, 2003.

[8] J. B. Duffy, “GAL4 system in Drosophila: a fly geneticist’s Swiss army knife.,” *Genesis*, vol. 34, no. 1–2, pp. 1–15, 2002.

[9] L. Luo, L. Martin-Morris, and K. White, “Identification, secretion, and neural expression of APPL, a Drosophila protein similar to human amyloid protein precursor,” *J. Neurosci.*, vol. 10, no. 12, pp. 3849–3861, 1990.

[10] A. H. Brand and N. Perrimon, “Targeted gene expression as a means of altering cell fates and generating dominant phenotypes.,” *Development*, vol. 118, no. 2, pp. 401–15, 1993.

[11] L. Hood, “Systems biology: Integrating technology, biology, and computation,” *Mech. Ageing Dev.*, vol. 124, no. 1, pp. 9–16, 2003.

[12] S. Brenner, “The genetics of Caenorabditis elegans.,” *Genetics*, vol. 77, no. May, pp. 71–94, 1974.

[13] M. D. Adams *et al.*, “The genome sequence of Drosophila melanogaster,” *Science (80-.).*, vol. 287, no. March, pp. 2185–2195, 2000.

[14] G. M. Rubin and E. B. Lewis, “The Drosophila Genome: Viewpoint. A Brief History of Drosophila’s Contributions to Genome Research,” *Science (80-.).*, vol. 287, pp. 2216–2218, 2000.

[15] K. M. Beckingham, J. D. Armstrong, M. J. Texada, R. Munjaal, and D. A. Baker, “Drosophila melanogaster - The model organism of choice for the complex biology of multi-cellular organisms,” *Gravitational Sp. Biol.*, vol. 18, no. 2, pp. 17–29, 2005.

[16] C. Ong, L. Yung, Y. Cai, B. Bay, and G. Baeg, “Drosophila melanogaster as a model organism to study nanotoxicity,” *Nanotoxicology*, vol. 9, no. 3, pp. 396–403, 2015.

[17] Y. S. Rong and K. G. Golic, “Gene Targeting by Homologous Recombination in Drosophila,” *Science (80-.).*, vol. 288, no. June 2000, pp. 2013–2019, 2000.

[18] L. Luo, T. Tully, and K. White, “Human amyloid precursor protein ameliorates behavioral deficit of flies deleted for appl gene,” *Neuron*, vol. 9, no. 4, pp. 595–605, 1992.

[19] L. Maroteaux, J. T. Campanelli, and R. H. Scheller, “Synuclein: A Neuron-Specific Protein Localized to the Nucleus and Presynaptic Nerve Terminal,” *J. Neurosci.*, vol. 8, no. 8, pp. 2804–2815, 1988.

[20] M. B. Feany and W. W. Bender, “A Drosophila Model of Parkinson’s Disease,” *Lett. to Nat.*, vol. 404, no. March, pp. 394–398, 2000.

[21] Y. Pesah, “Drosophila parkin mutants have decreased mass and cell size and increased sensitivity to oxygen radical stress,” *Development*, vol. 131, no. 9, pp. 2183–2194, 2004.

[22] M. S. Grotewiel, I. Martin, P. Bhandari, and E. Cook-Wiens, “Functional senescence in Drosophila melanogaster,” *Ageing Res. Rev.*, vol. 4, no. 3, pp. 372–397, 2005.

[23] S. L. Helfand and B. Rogina, “ Genetics of Aging in the Fruit Fly, Drosophila melanogaster ,” *Annu. Rev. Genet.*, vol. 37, no. 1, pp. 329–348, 2003.

[24] Y. Lin, L. Seroude, and S. Benzer, “Extended life - span and stress resistance in the

Drosophila mutant methuselah," *Science (80-.).*, vol. 282, no. 5390, pp. 943–946, 1998.

[25] W. C. Orr, R. S. Sohal, W. C. Orr, and R. S. Sohal, "Extension of Life-Span by Overexpression of Superoxide Dismutase and Catalase in Drosophila melanogaster Published by : American Association for the Advancement of Science Stable URL : https://www.jstor.org/stable/2883423 digitize , preserve and extend ac," *Ext. Life-Span by Overexpression Superoxide Dismutase Catalase Drosoph. melanogaster*, vol. 263, no. 5150, pp. 1128–1130, 1994.

[26] S. Zou, S. Meadows, L. Sharp, L. Y. Jan, and Y. N. Jan, "Genome-wide study of aging and oxidative stress response in Drosophilamelanogaster," *Proc. Natl. Acad. Sci.*, vol. 97, no. 25, pp. 13726–13731, 2000.

[27] G. N. Landis *et al.*, "Similar gene expression patterns characterized aging and oxidative stress in Drosophila melanogaster," *PNAS*, vol. 101, no. 20, pp. 7663–7668, 2004.

[28] E. Le Bourg, "Aging and habituation of the tarsal response in drosophila melanogaster," *Gerontology*, vol. 29, no. 6, pp. 388–393, 1983.

[29] É. Le Bourg and N. Minois, "A mild stress, hypergravity exposure, postpones behavioral aging in Drosophila melanogaster," *Exp. Gerontol.*, vol. 34, no. 2, pp. 157–172, 1999.

[30] T. Tamura *et al.*, "Aging Specifically Impairs amnesiac-Dependent Memory in Drosophila," *Neuron*, vol. 40, no. 5, pp. 1003–1011, 2003.

[31] J. Miquel, P. R. Lundgren, K. G. Bensch, and H. Atlan, "Effects of temperature on the life span, vitality and fine structure of Drosophila melanogaster," *Mech. Ageing Dev.*, vol. 5, no. C, pp. 347–370, 1976.

[32] A. C. Economos, J. Miquel, R. Binnard, and S. Kessler, "Quantitative analysis of mating behavior in aging male drosophila melanogaster," *Mech. Ageing Dev.*, vol. 10, no. 3–4, pp. 233–240, 1979.

[33] J. David, Y. Cohet, and P. Fouillet, "The variability between individuals as a measure of senescence: A study of the number of eggs laid and the percentage of hatched eggs in the case of Drosophila melanogaster," *Exp. Gerontol.*, vol. 10, no. 1, pp. 17–25, 1975.

[34] G. Paternostro, C. Vignola, D. Bartsch, J. H. Omens, A. D. Mcculloch, and J. C. Reed, "Integrative Physiology Age-Associated Cardiac Dysfunction in," *Circ. Res.*, pp. 1053–1058, 2001.

[35] R. J. Wessels and R. Bodmer, “Screening assays for heart function mutants in Drosophila,” *Biotechniques*, vol. 37, pp. 58–66, 2004.

[36] J. Heitman, N. R. Movva, and M. N. Hall, “Targets for cell cycle arrest by the immunosuppressant Rapamycin in Yeast,” *Science (80-.).*, vol. 253, no. 5022, pp. 905–909, 1991.

[37] S. Oldham, J. Montagne, T. Radimerski, G. Thomas, and E. Hafen, “Genetic and biochemical characterization of dTOR, the Drosophila homolog of the target of rapamycin,” *Genes Dev.*, pp. 2689–2694, 2000.

[38] H. Zhang, J. P. Stallock, J. C. Ng, C. Reinhard, and T. P. Neufeld, “Regulation of cellular growth by the dTOR,” *Genes Dev.*, vol. 14, no. 21, pp. 2712–2724, 2000.

[39] S. D. Katewa and P. Kapahi, “Role of TOR signaling in aging and related biological processes in Drosophila melanogaster,” *Exp. Gerontol.*, vol. 46, no. 5, pp. 382–390, 2011.

[40] J. D. Manton, A. D. Ostrovsky, L. Goetz, M. Costa, and T. Rohlfing, “Combining genome-scale Drosophila 3D neuroanatomical data by bridging template brains,” *bioRxiv*, p. 6353, 2014.

[41] R. Tomer, K. Khairy, F. Amat, and P. J. Keller, “Quantitative high-speed imaging of entire developing embryos with simultaneous multiview light-sheet microscopy,” *Nat. Methods*, vol. 9, no. 7, pp. 755–763, 2012.

[42] P. J. Keller, A. D. Schmidt, J. Wittbrodt, and E. H. K. Stelzer, “Digital scanned laser light-sheet fluorescence microscopy (DSLM) of zebrafish and drosophila embryonic development,” *Cold Spring Harb. Protoc.*, vol. 6, no. 10, pp. 1235–1243, 2011.

[43] P. A. Sharp and P. D. Zamore, “RNA Interference,” *Science (80-.).*, vol. 287, no. 5462, pp. 2231–2233, 2000.

[44] S. Zappe, M. Fish, M. P. Scott, and O. Solgaard, “Automated MEMS-based Drosophila embryo injection system for high-throughput RNAi screens,” *Lab Chip*, vol. 6, no. 8, pp. 1012–1019, 2006.

[45] X. Zhang, M. P. Scott, C. F. Quate, and O. Solgaard, “Microoptical characterization of piezoelectric vibratory microinjections in Drosophila embryos for genome-wide RNAi screen,” *J. Microelectromechanical Syst.*, vol. 15, no. 2, pp. 277–286, 2006.

[46] D. Delubac *et al.*, “Microfluidic system with integrated microinjector for automated

Drosophila embryo injection," *Lab Chip*, vol. 12, no. 22, pp. 4911–4919, 2012.

[47] J. R. Fakhoury, J. C. Sisson, and X. Zhang, "Microsystems for controlled genetic perturbation of live Drosophila embryos: RNA interference, development robustness and drug screening," *Microfluid. Nanofluidics*, vol. 6, no. 3, pp. 299–313, 2009.

[48] J. R. Bateman, A. M. Lee, and C. T. Wu, "Site-specific transformation of Drosophila via φC31 integrase-mediated cassette exchange," *Genetics*, vol. 173, no. 2, pp. 769–777, 2006.

[49] E. M. Lucchetta, M. S. Munson, and R. F. Ismagilov, "Characterization of the local temperature in space and time around a developing Drosophila embryo in a microfluidic device," *Lab Chip*, vol. 6, no. 2, pp. 185–190, 2006.

[50] E. M. Lucchetta, J. H. Lee, L. A. Fu, N. H. Patel, and R. F. Ismagilov, "Dynamics of Drosophila embryonic patterning network perturbed in space and time using microfluidics," *Nature*, vol. 434, no. 7037, pp. 1134–1138, 2005.

[51] G. T. Dagani, K. Monzo, J. R. Fakhoury, C. C. Chen, J. C. Sisson, and X. Zhang, "Microfluidic self-assembly of live Drosophila embryos for versatile high-throughput analysis of embryonic morphogenesis," *Biomed. Microdevices*, vol. 9, no. 5, pp. 681–694, 2007.

[52] T. J. Levario, M. Zhan, B. Lim, S. Y. Shvartsman, and H. Lu, "Microfluidic trap array for massively parallel imaging of Drosophila embryos," *Nat. Protoc.*, vol. 8, no. 4, pp. 721–736, 2013.

[53] A. Schoofs, S. Niederegger, A. van Ooyen, H. G. Heinzel, and R. Spieß, "The brain can eat: Establishing the existence of a central pattern generator for feeding in third instar larvae of Drosophila virilis and Drosophila melanogaster," *J. Insect Physiol.*, vol. 56, no. 7, pp. 695–705, 2010.

[54] S. Mondal, S. Ahlawat, K. Rau, V. Venkataraman, and S. P. Koushika, "Imaging in vivo Neuronal Transport in Genetic Model Organisms Using Microfluidic Devices," *Traffic*, vol. 12, no. 4, pp. 372–385, 2011.

[55] M. Ghannad-Rezaie, X. Wang, B. Mishra, C. Collins, and N. Chronis, "Microfluidic chips for in vivo imaging of cellular responses to neural injury in Drosophila larvae," *PLoS One*, vol. 7, no. 1, 2012.

[56] R. Ardeshiri, L. Hosseini, N. Amini, and P. Rezai, "Cardiac screening of intact Drosophila

melanogaster larvae under exposure to aqueous and gaseous toxins in a microfluidic device," *RSC Adv.*, vol. 6, no. 70, pp. 65714–65724, 2016.

[57] R. Ghaemi, P. Rezai, F. R. Nejad, and P. R. Selvaganapathy, "Characterization of microfluidic clamps for immobilizing and imaging of Drosophila melanogaster larva's central nervous system," *Biomicrofluidics*, vol. 11, no. 3, 2017.

[58] R. Ghaemi, P. Rezai, B. G. Iyengar, and P. R. Selvaganapathy, "Microfluidic devices for imaging neurological response of Drosophila melanogaster larva to auditory stimulus," *Lab Chip*, vol. 15, no. 4, pp. 1116–1122, 2015.

[59] E. Rebollo, K. Karkali, F. Mangione, and E. Martín-Blanco, "Live imaging in Drosophila: The optical and genetic toolkits," *Methods*, vol. 68, no. 1, pp. 48–59, 2014.

[60] J. Nakai, M. Ohkura, and K. Imoto, "A high signal-to-noise Ca2+ probe composed of a single green fluorescent protein," vol. 3, pp. 137–141, 2001.

[61] J. Akerboom *et al.*, "Crystal structures of the GCaMP calcium sensor reveal the mechanism of fluorescence signal change and aid rational design," *J. Biol. Chem.*, vol. 284, no. 10, pp. 6455–6464, 2009.

[62] L. Tian *et al.*, "Imaging neural activity in worms, flies and mice with improved GCaMP calcium indicators," *Nat. Methods*, vol. 6, no. 12, pp. 875–881, 2009.

[63] J. Akerboom *et al.*, "Optimization of a GCaMP Calcium Indicator for Neural Activity Imaging," *J. Neurosci.*, vol. 32, no. 40, pp. 13819–13840, 2012.

[64] J. W. Lichtman and J.-A. Conchello, "Fluorescence Microscopy," *Fluoresc. Microsc. From Princ. to Biol. Appl. Second Ed.*, vol. 2, no. 12, pp. 910–919, 2005.

[65] M. Minsky, "Microscopy Apparatus," US3013467A, 1961.

[66] M. D. Egger and M. Petran, "New Reflected-Light Microscope for Viewing Unstained Brain and Ganglion Cells," *Science (80-.).*, vol. 157, no. 3786, pp. 305–307, 1967.

[67] J. G. White, W. B. Amos, and M. Fordham, "An evaluation of confocal versus conventional imaging of biological structures by fluorescence light microscopy.," *J. Cell Biol.*, vol. 105, no. 1, pp. 41–8, 1987.

[68] P. P. Laissue, R. A. Alghamdi, P. Tomancak, E. G. Reynaud, and H. Shroff, "Assessing

phototoxicity in live fluorescence imaging," *Nat. Methods*, vol. 14, no. 7, pp. 657–661, 2017.

[69] J. Huisken, J. Swoger, F. Del Bene, J. Wittbrodt, and E. H. K. Stelzer, "Optical Sectioning Deep Inside Live Embryos by Selective Plane Illumination Microscopy," *Science (80-.).*, vol. 305, no. 5686, pp. 1007–1009, 2004.

[70] M. B. Ahrens, M. B. Orger, D. N. Robson, J. M. Li, and P. J. Keller, "Whole-brain functional imaging at cellular resolution using light-sheet microscopy," *Nat. Methods*, vol. 10, no. 5, pp. 413–420, 2013.

[71] A. Kinkhabwala *et al.*, "A structural and functional ground plan for neurons in the hindbrain of zebrafish," *Proc. Natl. Acad. Sci.*, vol. 108, no. 3, pp. 1164–1169, 2011.

[72] S. L. Reidt and R. F. Bango Da Cunha Correia, "D3 . 4 : Non-diffracting LSFM in chick embryo," Dundee, Scotland, 2016.

[73] W. C. Lemon *et al.*, "Whole-central nervous system functional imaging in larval Drosophila," *Nat. Commun.*, vol. 6, no. May, 2015.

[74] M. L. Suster and M. Bate, "Embryonic assembly of a central pattern generator," *Nature*, vol. 416, no. March, pp. 174–178, 2002.

[75] B. C. Chen *et al.*, "Lattice light-sheet microscopy: Imaging molecules to embryos at high spatiotemporal resolution," *Science (80-.).*, vol. 346, no. 6208, 2014.

[76] T. C. Fadero *et al.*, "LITE microscopy: Tilted light-sheet excitation of model organisms offers high resolution and low photobleaching," *J. Cell Biol.*, vol. 217, no. 5, pp. 1869–1882, 2018.

[77] R. Ghaemi, "Microfluidics devices for Drosophila-based drug discovery assays," McMaster University, 2017.

[78] J. W. Shirley, "An Early Experimental Determination of Snell's Law," *Am. J. Phys.*, vol. 19, no. 9, pp. 507–508, Dec. 1951.

[79] P. M. Salvaterra and T. Kitamoto, "Drosophila cholinergic neurons and processes visualized with Gal4/UAS-GFP," *Gene Expr. Patterns*, vol. 1, no. 1, pp. 73–82, 2001.

[80] J. S. Miller *et al.*, "Rapid casting of patterned vascular networks for perfusable engineered

three-dimensional tissues," *Nat. Mater.*, vol. 11, no. 9, pp. 768–774, 2012.

[81] D. B. Kolesky, K. A. Homan, M. A. Skylar-Scott, and J. A. Lewis, "Three-dimensional bioprinting of thick vascularized tissues," *Proc. Natl. Acad. Sci. U. S. A.*, vol. 113, no. 12, pp. 3179–3184, 2016.

[82] D. P. Parekh, C. Ladd, L. Panich, K. Moussa, and M. D. Dickey, "3D printing of liquid metals as fugitive inks for fabrication of 3D microfluidic channels," *Lab Chip*, vol. 16, no. 10, pp. 1812–1820, 2016.

[83] J. N. Lee, C. Park, and G. M. Whitesides, "Solvent Compatibility of Poly(dimethylsiloxane)-Based Microfluidic Devices," *Anal. Chem.*, vol. 75, no. 23, pp. 6544–6554, 2003.

[84] S. Bhattacharya, A. Datta, J. M. Berg, and S. Gangopadhyay, "Studies on surface wettability of poly(dimethyl) siloxane (PDMS) and glass under oxygen-plasma treatment and correlation with bond strength," *J. Microelectromechanical Syst.*, vol. 14, no. 3, pp. 590–597, 2005.

[85] F. Schneider, J. Draheim, R. Kamberger, and U. Wallrabe, "Process and material properties of polydimethylsiloxane (PDMS) for Optical MEMS," *Sensors Actuators, A Phys.*, vol. 151, no. 2, pp. 95–99, 2009.

[86] M. Gleichmann and M. P. Mattson, "Neuronal calcium homeostasis and dysregulation," *Antioxidants Redox Signal.*, vol. 14, no. 7, pp. 1261–1273, 2011.

[87] D. M. Ratterman, "Eliminating ether by using ice for Drosophila labs," vol. 24, pp. 259–265, 2003.

[88] P. L. Privalov, "Cold Denaturation of Protein," vol. 25, no. 4, pp. 281–306, 1990.

[89] J. Jarabak, J. A. Adams, H. G. Williams-Ashman, and P. Talalay, "Purification of a 17beta-hydroxysteroid dehydrogenase of human placenta and studies on its transhydrogenase function.," *J. Biol. Chem.*, vol. 237, no. 2, pp. 345–357, 1962.